Isomer separation of multifunctional atmospheric compounds using gas chromatography and chemical ionization mass spectrometry

Thesis by
Krystal TonyBeth Vasquez

In Partial Fulfillment of the Requirements for the
Degree of
Doctor of Philosophy

CALIFORNIA INSTITUTE OF TECHNOLOGY
Pasadena, California

2022
Defended Febuary 01, 2022

Krystal TonyBeth Vasquez
ORCID: 0000-0003-4540-4212

To disabled scientists past, present, and future.

And to those who could have been with the right accommodations, but were never given the chance.

LAND ACKNOWLEDGEMENTS

Most of the research described in this work was performed at the California Institute of Technology (Caltech), which was built on Tovaangar (pronounced: To-VAA-ngar), the ancestral, and unceded, lands of the Gabrieliño-Tongva People. Tovaangar, meaning "the world," encompassed the Los Angeles Basin, the Southern Channel Islands and parts of Orange, Riverside, and San Bernardino County (Greene and Curwen, 2019). By the mid-1500s, there were an estimated 5,000 to 10,000 Tongva people living in the region (Lloyd, 2017; Greene and Curwen, 2019).

However, their community and culture rapidly disappeared upon the arrival of the Spanish due to disease, forced assimilation and, religious conversion (Los Angeles Almanac; Banta, 2021). Others fled from the area and resettled elsewhere in the state. Today, the tribe has been recognized by the California Assembly and has over 900 certified members (Cross and Day, 2020).

In addition, a small portion of the research included herein was also collected at the University of Michigan Biological Station located in Pellston, Michigan. Pellston currently occupies the land of the Odawa (Ottawa) people. It's likely that these lands were also shared with the Chippewa (Ojibwe) and Potawatomi (Bodawotomi) (Hemenway). Together with the Odawa, these three tribes make up the Anishnaabek Nation.

References

Banta, J. A timeline of Gabrieleno Tongva history, 2021. URL https://www.gabrieleno-nsn.us/timeline.

Cross, D. and Day, B. Tongva Nation continues fighting for federal recognition. *Pasadena Now*, September 2020. URL https://www.pasadenanow.com/main/tongva-nation-continues-fighting-for-federal-recognition.

Greene, S. and Curwen, T. Mapping the Tongva villages of L.A.'s past. *Los Angeles Times*, May 2019. URL https://www.latimes.com/projects/la-me-tongva-map/.

Hemenway, E. Odawa Indians. URL https://www.petoskeyarea.com/media/area-history/odawa-indians/.

Lloyd, A. A brief history of LA's Indigenous Tongva People. *LAist*, October 2017. URL https://laist.com/news/la-history/a-brief-history-of-the-tongva-people.

Los Angeles Almanac. Original people of los angeles county. URL http://www.laalmanac.com/history/hi05.php.

PERSONAL ACKNOWLEDGEMENTS

Honestly, grad school has taken enough from me over the past 6.5 years, so I'm going to make this section as short as possible to prevent it from taking any more. Regrettably, this means that I won't be able to individually list all the people that deserve to be included, but I promise I'll make it up to you later.

First, I'd like to acknowledge my advisor, Paul Wennberg. Although there were times we didn't see eye-to-eye, I can safely say that joining your lab has helped me grow as a scientist. I also want to thank John Crounse, who is truly the reason that any of my science worked in the first place.

In addition, I want to give a shout out to the members of the Wennberg and Seinfeld labs who I have had the fortune to overlap with, as well as the many other wonderful people I hung out with in the Linde Laboratory offices. You all made campus feel a little brighter.

Finally, I can't forget my chosen family. Thank you for always being so incredibly supportive over the years. To Brandon, Kelly, Jeff, Christine, and, of course, my partner Matt: I couldn't have done it without you!

ABSTRACT

Oxygenated volatile organic compounds are a group of carbon-containing species that include one or more functional groups. They are formed during oxidation of hydrocarbons in the atmosphere. Afterwards, they readily undergo atmospheric processing, which—depending on their chemical properties—can lead to the formation of harmful pollutants, such as ozone or secondary organic aerosols (SOA). Prolonged exposure to either compound can negatively impact human health.

Unfortunately, most existing analytical techniques struggle to quantify the concentrations of the majority of OVOCs due to their characteristic low abundances and high reactivities. In addition, most of these compounds are also made up of a complex mixture of isomers that few instruments are able to resolve. Since even slight changes in structure can impact an OVOC's atmospheric fate, this can lead to uncertainties when elucidating their chemical mechanisms. As a result, despite decades of research, there are still many outstanding questions pertaining to atmospheric processing of OVOCs and, by extension, their impact on air quality.

To combat this issue, novel instrumentation was developed that can provide accurate, isomer-resolved measurements of a wide variety of OVOCs, which it achieves by combining the sensitive, specific nature of gas chromatography (GC) with the equally sensitive, yet non-invasive aspects of chemical ionization mass spectrometry (CIMS). To showcase its capabilities, these new instrumental methods are applied to the study of isoprene oxidation. More specifically, we report new insights into the isomer-specific loss processes of isoprene-derived hydroxy nitrates. Inclusion of our findings into atmospheric models can greatly improve our simulations of NO_x, ozone, and nitric acid.

PUBLISHED CONTENT AND CONTRIBUTIONS

Scientific Publications

Bourgeois, I., Peischl, J., Neuman, J. A., Brown, S. S., Allen, H. M., Campuzano-Jost, P., Coggon, M. M., DiGangi, J. P., Diskin, G. S., Gilman, J. B., Gkatzelis, G. I., Guo, H., Halliday, H., Hanisco, T. F., Holmes, C. D., Huey, L. G., Jimenez, J. L., Lamplugh, A. D., Lee, Y. R., Lindaas, J., Moore, R. H., Nowak, J. B., Pagonis, D., Rickly, P. S., Robinson, M. A., Rollins, A. W., Selimovic, V., St. Clair, J. M., Tanner, D., **Vasquez, K. T.**, Veres, P. R., Warneke, C., Wennberg, P. O., Washenfelder, R. A., Wiggins, E. B., Womack, C. C., Xu, L., Zarzana, K. J., and Ryerson, T. B. Comparison of airborne measurements of NO, NO_2, HONO, NO_y, and CO during FIREX-AQ. *Atmos. Meas. Tech. Discuss.*, 2022. doi: 10.5194/amt-2021-432.

K.T.V. assisted in data collection.

Xu, L., Crounse, J. D., **Vasquez, K. T.**, Allen, H., Wennberg, P. O., Bourgeois, I., Brown, S. S., Campuzano-Jost, P., Coggon, M. M., Crawford, J. H., DiGangi, J. P., Diskin, G. S., Fried, A., Gargulinski, E. M., Gilman, J. B., Gkatzelis, G. I., Guo, H., Hair, J. W., Hall, S. R., Halliday, H. A., Hanisco, T. F., Hannun, R. A., Holmes, C. D., Huey, L. G., Jimenez, J. L., Lamplugh, A., Lee, Y. R., Liao, J., Lindaas, J., Neuman, J. A., Nowak, J. B., Peischl, J., Peterson, D. A., Piel, F., Richter, D., Rickly, P. S., Robinson, M. A., Rollins, A. W., Ryerson, T. B., Sekimoto, K., Selimovic, V., Shingler, T., Soja, A. J., Clair, J. M. S., Tanner, D. J., Ullmann, K., Veres, P. R., Walega, J., Warneke, C., Washenfelder, R. A., Weibring, P., Wisthaler, A., Wolfe, G. M., Womack, C. C., and Yokelson, R. J. Ozone chemistry in western U.S. wildfire plumes. *Sci. Adv.*, 7(50):eabl3648, 2021. doi: 10.1126/sciadv.abl3648.

K.T.V. assisted in data collection.

Wei, D., Alwe, H. D., Millet, D. B., Bottorff, B., Lew, M., Stevens, P. S., Shutter, J. D., Cox, J. L., Keutsch, F. N., Shi, Q., Kavassalis, S. C., Murphy, J. G., **Vasquez, K. T.**, Allen, H. M., Praske, E., Crounse, J. D., Wennberg, P. O., Shepson, P. B., Bui, A. A. T., Wallace, H. W., Griffin, R. J., May, N. W., Connor, M., Slade, J. H., Pratt, K. A., Wood, E. C., Rollings, M., Deming, B. L., Anderson, D. C., and Steiner, A. L. FORest Canopy Atmosphere Transfer (FORCAsT) 2.0: Model updates and evaluation with observations at a mixed forest site. *Geosci. Model. Dev.*, 14(10):6309 – 6329, 2021. doi: 10.5194/gmd-14-6309-2021.

K.T.V. assisted in data collection.

Vasquez, K. T., Crounse, J. D., Schulze, B. C., Bates, K. H., Teng, A. P., Xu, L., Allen, H. M., and Wennberg, P. O. Rapid hydrolysis of tertiary isoprene nitrate efficiently removes NOx from the atmosphere. *Proc. Natl. Acad. Sci.*, 117(52): 33011 – 33016, 2020. doi: 10.1073/pnas.2017442117.

K.T.V. performed research, analyzed data and wrote the manuscript.

Vasquez, K. T., Allen, H. M., Crounse, J. D., Praske, E., Xu, L., Noelscher, A. C., and Wennberg, P. O. Low-pressure gas chromatography with chemical ionization mass spectrometry for quantification of multifunctional organic compounds in the atmosphere. *Atmos. Meas. Tech.*, 11:6815 – 6832, 2018. doi: 10.5194/amt-11-6815-2018.

K.T.V. performed research, analyzed data and wrote the manuscript.

Field Work Contributions

Fire Influence on Regional to Global Environments and Air Quality (FIREX-AQ), 2019.

The Atmospheric Tomography Mission (ATom) 4, 2018 *(Instrument Upload)*.

Caltech Hall Rooftop Field Study, 2017.

Program for Research on Oxidants, Photochemistry, Emissions and Transport-Atmospheric Measurements of Oxidants in Summer (PROPHET-AMOS), 2016.

Select Science Communication Publications (as of December 2021)

Vasquez, K. T. Wildfires may alter the nitrogen cycle—and air pollution. *Eos*, December 2021. URL https://eos.org/articles/wildfires-may-alter-the-nitrogen-cycle-and-air-pollution.

Vasquez, K. T. Autonomous package deliveries may not reduce emissions. *Inside Science*, November 2021. URL https://insidescience.org/news/autonomous-package-deliveries-may-not-reduce-emissions.

Vasquez, K. T. Worsening heat waves are hammering the disabled community. *Environmental Health News*, November 2021. URL https://www.ehn.org/heat-waves-disabled-community-2655520353.html.

Vasquez, K. T. Diesel trucks are causing environmental injustice across US cities. *Environmental Health News*, October 2021. URL https://www.ehn.org/diesel-truck-air-pollution-2655321340.html.

Vasquez, K. T. Trees may become the biggest air pollution contributors in LA. *Inside Science*, August 2021. URL https://insidescience.org/news/trees-may-become-biggest-air-pollution-contributors-la.

Vasquez, K. T. Environmental injustice and disability: Where is the research? *Environmental Health News*, August 2021. URL https://www.ehn.org/disability-justice-2654683649.html.

Vasquez, K. T. Air pollution from household products is cutting people's lives short. *Environmental Health News*, August 2021. URL https://www.ehn.org/premature-deaths-from-air-pollution-2654630777.html.

Vasquez, K. T. How artificial intelligence can help save us from air pollution. *Environmental Health News*, August 2021. URL https://www.ehn.org/air-pollution-artificial-intelligence-2654239069.html.

Vasquez, K. T. Enjoying 4th of July fireworks? Close your windows. *Environmental Health News*, July 2021. URL https://www.ehn.org/how-do-fireworks-pollute-the-air-2653598916.html.

Vasquez, K. T. Wait, there's noise pollution at the bottom of the ocean? *JSTOR Daily*, May 2021. URL https://daily.jstor.org/noise-pollution-at-the-bottom-of-the-ocean/.

Vasquez, K. T. A disability should not be a death sentence during a natural disaster. *Environmental Health News*, July 2021. URL https://www.ehn.org/natural-disasters-disabled-community-2652503611.html.

Vasquez, K. T. Overdue? The future of large earthquakes in California. *Temblor Earthquake News*, April 2021. URL https://temblor.net/discoveries/overdue-the-future-of-large-earthquakes-in-california-12667/.

Vasquez, K. T. Measuring atmospheric trace gases using mass spectrometry. *Nature Reviews Earth & Environment*, May 2021. URL https://www.nature.com/articles/s43017-021-00163-x.

Vasquez, K. T. Air quality monitors mounted on public transit see pollution other sensors miss. *Massive Science*, March 2021. URL https://massivesci.com/articles/air-quality-pollution-trains-salt-lake-city/.

Publications on Diversity & Inclusion in STEM

Vasquez, K. T. Virtual conferences aren't as accessible as you might think. *Scientific American*, February 2021. URL https://www.scientificamerican.com/article/virtual-conferences-arent-as-accessible-as-you-might-think/.

Vasquez, K. T. Disabled scientists excluded from the lab. *Chemistry World*, December 2020. URL https://www.chemistryworld.com/opinion/disabled-scientists-excluded-from-the-lab/4012695.article.

TABLE OF CONTENTS

LIST OF ILLUSTRATIONS

Number *Page*

LIST OF TABLES

Chapter 1

INTRODUCTION

1.1 Background and motivation

Over 99.9% of our dry atmosphere is made up of three gases: nitrogen, oxygen, and argon. Yet, atmospheric chemistry research has spent decades focusing on the remaining 0.1%. Despite making up a seemingly insignificant fraction of our atmosphere, it is primarily this latter set of compounds that influences our air quality and climate (Seinfeld and Pandis, 2016). It stands to reason, then, that the accurate measurement of these gases, followed by the elucidation of their chemistry, is essential for understanding and monitoring changes to our atmosphere.

Of particular interest are a class of compounds called non-methane hydrocarbons (NMHCs), which are emitted from a variety of sources, including fossil fuel combustion, wildfires, and plants. Once released into the atmosphere, they are subsequently oxidized, usually in a matter of hours to days, by one of three trace species: the hydroxyl radical (OH), the nitrate radical (NO_3), or ozone (O_3) (Atkinson and Arey, 2003b). In the daytime, OH is the primary atmospheric oxidant, and the resulting chemistry can produce either O_3 and secondary organic aerosols (SOA). Both compounds are precursors to photochemical smog, can influence climate, and can negatively impact human health (Lelieveld et al., 2015; Monks et al., 2015; Li et al., 2016; Masson-Delmotte et al., 2021).

In the process of producing O_3 and SOA, the OH oxidation of NMHCs also forms oxygenated volatile organic compounds (OVOCs), a diverse chemical family consisting of hydrocarbons with one or more oxygen-containing functional groups (Mellouki et al., 2015). Larger NMHCs, especially, give way to a wide assortment of OVOCs. For example, the OH oxidation of methane produces 4 unique OVOCs, whereas the OH oxidation of n-butane results in 60.

The addition of functional groups on the hydrocarbon backbone make OVOCs highly reactive and, therefore, prone to additional atmospheric processing (Atkinson and Arey, 2003b; Mellouki et al., 2015). Depending on their chemical properties, this can then lead to continued production of ozone or SOA. For instance, if an OVOCs has a propensity for fragmenting upon further oxidation with OH, the reaction will typically result in the production of more ozone—typically through the initiation

of the NO_x catalytic cycle. On the other hand, if the OVOC, instead, incorporates additional functional groups into its structure, the corresponding drop in vapor pressure will force it to partition into the aerosol phase, adding to the growth and formation of the particles (Kroll and Seinfeld, 2008).

It is clear, then, that understanding the atmospheric fate of OVOCs is of the utmost importance. Unfortunately, up until now, traditional analytical techniques have struggled to accurately quantify the concentrations of trace species with such low abundances and high reactivities.

To add to the complexity, OVOCs are usually made up of multiple isomers that many instruments lump together as a singular species. Since even small changes in structure can alter an OVOC's atmospheric fate, this can result in uncertainties in the chemical mechanisms of OVOCs and their NMHC parents. Isoprene, a NMHC emitted primarily from deciduous trees, epitomizes this issue.

1.1.1 Atmospheric oxidation of isoprene

Although there are thousands of NMHCs in the atmosphere, their atmospheric impacts are small compared to isoprene. This is mainly due to the compound's atmospheric abundance—this lone biogenic species makes up approximately one-third of annual global NMHC emissions (Guenther et al., 2012). Furthermore, despite being a NMHC, isoprene's OH reactivity rivals that of many OVOCs'. In most places in the world, its two asymmetric double bonds can be rapidly oxidized in about an hour (Atkinson and Arey, 2003a), producing an isoprene peroxy radical (RO_2).

This radical can then go on and react with a number of atmospheric species (such as NO, NO_2, HO_2, etc.), marking the start of a highly complex chemical mechanism that can results in the creation of hundreds of unique OVOCs, along with their corresponding isomers (Wennberg et al., 2018). Each of these OVOCs can have a profound effect on local and regional concentrations of O_3 and SOA. That said, few are as important as the six isoprene hydroxy nitrates (IHN) isomers, which are formed in a minor pathway that occurs during the reaction of RO_2 and NO.

Whereas the primary RO_2-NO reaction produces ozone, the formation of the isoprene hydroxy nitrates (IHN) isomers can interrupt this process by trapping NO within its molecular structure, essentially serving as a reservoir. The permanence of this reservoir, however, depends on the atmospheric fate of the compound's primary isomers, 1,2-IHN and 4,3-IHN. This is especially the case in high NO environments

(with low biomolecular lifetimes), where the 1,2- and 4,3- isomers make up over 90% of the total IHN concentration (Teng et al., 2017).

Although the current understanding of the primary IHN loss pathways is still evolving, gaps in our knowledge have long led to discrepancies when comparing model simulations of ozone to ground-based measurements. In order to bring the two into better agreement, there have been several studies detailing the fate of 4,3-IHN, the second most abundant IHN isomer (Lee et al., 2014; Jacobs et al., 2014; Nguyen et al., 2015).

Following the creation of a synthesized standard, research has found that this isomer undergoes rapid OH oxidation Jacobs et al. (2014). Although ozone production does not occur immediately afterwards, it does eventually take place after a couple of generations of chemistry, following the eventual release of the NO_2 moiety downwind of its original source. 4,3-IHN can also be permanently removed from the atmosphere via deposition onto surfaces (Nguyen et al., 2015) or heterogeneous hydrolysis (Jacobs et al., 2014)—the latter is a two-step process that includes aerosol uptake followed by the reaction of water within the particle. However, the corresponding loss rates for these pathways are negligible in the atmosphere. Therefore, OH oxidation—which causes IHN to act as a temporary NO reservoir—is this isomer's dominant loss process.

There have also been attempts to study the atmospheric chemistry of 1,2-IHN, the most abundant IHN isomer, but it has proved challenging as this highly reactive compound is subject to huge instrumental losses and no pure synthetic standard currently exists. Even so, using modified measurement techniques, previous work has shown that this isomer also undergoes OH oxidation, albeit at a slightly slower pace than 4,3-IHN (Teng et al., 2017; Wennberg et al., 2018; Lee et al., 2014). Deposition is also thought to occur at a rate similar to its 4,3- counterpart (Nguyen et al., 2015) and is therefore also negligible in the context of this discussion.

Unfortunately, due to analytical challenges, researchers have yet to also constrain the condensed-phase hydrolysis loss of 1,2-IHN. However, due to the tertiary nature of its nitrate group, it is hypothesized that, unlike 4,3-IHN, this isomer can hydrolyze rapidly in clouds or in aerosol (Liu et al., 2012), as has been the case with similar organic nitrates produced from other biogenic compounds (Rindelaub et al., 2015). If true, this loss pathway could explain modeling discrepancies when simulating ozone, especially over isoprene-rich regions. It also means that IHN contributes

significantly to HNO_3 formed over continental regions (Darer et al., 2011; Browne et al., 2013; Rindelaub et al., 2015; Romer et al., 2016).

1.2 Isomer-resolved measurements of OVOCs

To produce isomer-specific measurements of OVOCs, like IHN, an instrument requires three characteristics: it should be highly sensitive, non-invasive, and highly specific (Apel et al., 2008). Techniques which are highly sensitive and non-invasive can ensure that fragile OVOCs present at low abundances can be measured quantitatively, whereas methods that boast high specificity successfully resolve the individual components present in an atmospheric sample.

Chemical ionization mass spectrometry (CIMS) meets two of these criteria (Crounse et al., 2006; Zhao, 2018). CIMS methods have been shown to be sensitive enough to detect trace gases present at mixing ratios as low as a few 10s of parts per trillion volume (pptv). Furthermore, its ionization method is non-invasive relative to the traditional electron impact mass spectrometry. Rather than bombarding an analyte with electrons, a chosen reagent ion reacts with neutral analytes, forming clusters, thereby allowing detection with minimal fragmentation.

Unfortunately, despite the fact that CIMS has been used to detect a wide range of atmospheric OVOCs, it is limited in that it cannot distinguish between isomeric compounds of the same mass. This often creates data sets that hide crucial structure-activity relationships of individual compounds, which, in turn, hinders the elucidation of their atmospheric chemistry. Gas chromatography (GC), on the other hand, has the ability to separate isomeric products (i.e.. high specificity), while simultaneously achieving reasonable signal-to-noise levels (i.e. high sensitivity), usually by preconcentrating the analytes prior to separation (Ras et al., 2009; Clemitshaw, 2004). However, contact with GC components often result in the irreversible loss, and sometimes conversion, of these highly reactive species.

Even so, it is possible to combine and modify these techniques in such a way that we achieve the trifecta of characteristics needed to detect, separate and quantify individual OVOC isomers, such as 1,2- and 4,3-IHN. Therefore, the focus of this thesis is the development of novel instrumentation that combines the sensitive, specific nature of gas chromatography, with the equally sensitive, yet non-invasive aspects of chemical ionization mass spectrometry. This instrument, dubbed the GC-CIMS, can then be used to answer outstanding questions about the atmospheric fate

of 1,2-IHN. That is, what is the relative importance of its hydrolysis loss pathway, and to what extent does it impact our air quality?

1.3 Thesis overview

The work included in this thesis details my efforts to develop the novel GC-CIMS, which is capable of collecting isomer-resolved measurements of OVOCs (Chapter 2). I then use data collected from field deployment of this instrument to place an observational constraint on the hydrolysis rate of 1,2-IHN (Chapter 3). It should be noted that Chapters 2 and 3 were originally written as standalone manuscripts, which were published in scientific journals prior to the completion of this thesis. Supplemental information pertaining to these two chapters can be found in Appendices A and B, respectively.

In addition, technical documentation and standard lab operating procedures for the GC-CIMS has been included in Appendix C and was originally written in an effort to promote knowledge transfer between existing lab members, and serve as a resource for future users. Finally, this work concludes with Chapter 4 which provides a brief overview of recent atmospheric mysteries the GC-CIMS has helped solve since its creation in 2016. This final chapter also summarizes the current state of knowledge with regards to the atmospheric fate of the isoprene hydroxy nitrate isomers, as well as provides directions for future research.

References

Apel, E. C., Brauers, T., Koppmann, R., Bandowe, B., Boßmeyer, J., Holzke, C., Tillmann, R., Wahner, A., Wegener, R., Brunner, A., Jocher, M., Ruuskanen, T., Spirig, C., Steigner, D., Steinbrecher, R., Gomez Alvarez, E., Müller, K., Burrows, J. P., Schade, G., Solomon, S. J., Ladstätter-Weißenmayer, A., Simmonds, P., Young, D., Hopkins, J. R., Lewis, A. C., Legreid, G., Reimann, S., Hansel, A., Wisthaler, A., Blake, R. S., Ellis, A. M., Monks, P. S., and Wyche, K. P. Intercomparison of oxygenated volatile organic compound measurements at the saphir atmosphere simulation chamber. *J. Geophys. Res.: Atmos.*, 113(D20), 2008. doi: 10.1029/2008JD009865.

Atkinson, R. and Arey, J. Gas-phase tropospheric chemistry of biogenic volatile organic compounds: A review. *Atmos. Environ.*, 37:197 – 219, 2003a. doi: 10.1016/S1352-2310(03)00391-1.

Atkinson, R. and Arey, J. Atmospheric degradation of volatile organic compounds. *Chem. Rev.*, 103(12):4605 – 4638, 2003b. doi: 10.1021/cr0206420.

Browne, E. C., Min, K.-E., Wooldridge, P. J., Apel, E., Blake, D. R., Brune, W. H., Cantrell, C. A., Cubison, M. J., Diskin, G. S., Jimenez, J. L., Weinheimer, A. J., Wennberg, P. O., Wisthaler, A., and Cohen, R. C. Observations of total $RONO_2$ over the boreal forest: NOx sinks and HNO_3 sources. *Atmos. Chem. Phys.*, 13 (9):4543 – 4562, 2013. doi: 10.5194/acp-13-4543-2013.

Clemitshaw, K. A review of instrumentation and measurement techniques for ground-based and airborne field studies of gas-phase tropospheric chemistry. *Crit. Rev. Environ. Sci. Technol.*, 34(1):1 – 108, 2004. doi: 10.1080/10643380490265117.

Crounse, J. D., McKinney, K. A., Kwan, A. J., and Wennberg, P. O. Measurement of gas-phase hydroperoxides by chemical ionization mass spectrometry. *Anal. Chem.*, 78(19):6726 – 6732, 2006. doi: 10.1021/ac0604235.

Darer, A. I., Cole-Filipiak, N. C., O'Connor, A. E., and Elrod, M. J. Formation and stability of atmospherically relevant isoprene-derived organosulfates and organonitrates. *Environ. Sci. Technol.*, 45:1895 – 1902, 2011. doi: 10.1021/es103797z.

Guenther, A. B., Jiang, X., Heald, C. L., Sakulyanontvittaya, T., Duhl, T., Emmons, L. K., and Wang, X. The model of emissions of gases and aerosols from nature version 2.1 (MEGAN2.1): An extended and updated framework for modeling biogenic emissions. *Geosci. Model Dev.*, 5(6):1471 – 1492, 2012. doi: 10.5194/gmd-5-1471-2012.

Jacobs, M. I., Burke, W. J., and Elrod, M. J. Kinetics of the reactions of isoprene-derived hydroxynitrates: Gas phase epoxide formation and solution phase hydrolysis. *Atmos. Chem. Phys.*, 14(17):8933 – 8946, 2014. doi: 10.5194/acp-14-8933-2014.

Kroll, J. H. and Seinfeld, J. H. Chemistry of secondary organic aerosol: Formation and evolution of low-volatility organics in the atmosphere. *Atmos. Environ.*, 42 (16):3593 – 3624, 2008. doi: 10.1016/j.atmosenv.2008.01.003.

Lee, L., Teng, A. P., Wennberg, P. O., Crounse, J. D., and Cohen, R. C. On rates and mechanisms of oh and o3 reactions with isoprene-derived hydroxy nitrates. *J. Phys. Chem. A*, 118(9):1622 – 37, 2014. doi: 10.1021/jp4107603.

Lelieveld, J., Evans, J. S., Fnais, M., Giannadaki, D., and Pozzer, A. The contribution of outdoor air pollution sources to premature mortality on a global scale. *Nature*, 525(7569):367 – 371, 2015. doi: 10.1038/nature15371.

Li, C., Balluz, L. S., Vaidyanathan, A., Wen, X.-J., Hao, Y., and Qualters, J. R. Long-term exposure to ozone and life expectancy in the United States, 2002 to 2008. *Medicine*, 95(7), 2016. doi: 10.1097/MD.0000000000002474.

Liu, S., Shilling, J. E., Song, C., Hiranuma, N., Zaveri, R. A., and Russell, L. M. Hydrolysis of organonitrate functional groups in aerosol particles. *Aerosol Sci. Technol.*, 46(12):1359 – 1369, 2012. doi: 10.1080/02786826.2012.716175.

Masson-Delmotte, V., Zhai, P. Pirani, A., Connors, S. L., Péan, C., Berger, S., Caud, N., Chen, Y., Goldfarb, L., Gomis, M., Huang, M., Leitzell, K., Lonnoy, E., Matthews, J., Maycock, T., Waterfield, T., Yelekçi, O., Yu, R., and Zhou, B., editors. *The Physical Science Basis. Contribution of Working Group I to the Sixth Assessment Report of the Intergovernmental Panel on Climate Change*, 2021. IPCC, Cambridge University Press.

Mellouki, A., Wallington, T. J., and Chen, J. Atmospheric chemistry of oxygenated volatile organic compounds: Impacts on air quality and climate. *Chem Rev*, 115 (10):3984 – 4014, 2015. doi: 10.1021/cr500549n.

Monks, P. S., Archibald, A. T., Colette, A., Cooper, O., Coyle, M., Derwent, R., Fowler, D., Granier, C., Law, K. S., Mills, G. E., Stevenson, D. S., Tarasova, O., Thouret, V., von Schneidemesser, E., Sommariva, R., Wild, O., and Williams, M. L. Tropospheric ozone and its precursors from the urban to the global scale from air quality to short-lived climate forcer. *Atmos. Chem. Phys.*, 15(15):8889 – 8973, 2015. doi: 10.5194/acp-15-8889-2015.

Nguyen, T. B., Crounse, J. D., Teng, A. P., St. Clair, J. M., Paulot, F., Wolfe, G. M., and Wennberg, P. O. Rapid deposition of oxidized biogenic compounds to a temperate forest. *P. Natl. Acad. Sci.*, 112(5):E392 – E401, 2015. doi: 10.1073/pnas.1418702112.

Ras, M. R., Borrull, F., and Marcé, R. M. Sampling and preconcentration techniques for determination of volatile organic compounds in air samples. *Trends Analyt. Chem*, 28(3):347–361, 2009. doi: 10.1016/j.trac.2008.10.009.

Rindelaub, J. D., McAvey, K. M., and Shepson, P. B. The photochemical production of organic nitrates from α-pinene and loss via acid-dependent particle phase hydrolysis. *Atmos. Environ.*, 100:193 – 201, 2015. doi: 10.1016/j.atmosenv.2014.11.010.

Romer, P. S., Duffey, K. C., Wooldridge, P. J., Allen, H. M., Ayres, B. R., Brown, S. S., Brune, W. H., Crounse, J. D., de Gouw, J., Draper, D. C., Feiner, P. A., Fry, J. L., Goldstein, A. H., Koss, A., Misztal, P. K., Nguyen, T. B., Olson, K., Teng, A. P., Wennberg, P. O., Wild, R. J., Zhang, L., and Cohen, R. C. The lifetime of nitrogen oxides in an isoprene-dominated forest. *Atmos. Chem. Phys.*, 16(12): 7623 – 7637, 2016. doi: 10.5194/acp-16-7623-2016.

Seinfeld, J. H. and Pandis, S. N. *Atmospheric Chemistry and Physics: From Air Pollution to Climate Change*. Wiley, 3rd ed edition, 2016.

Teng, A. P., Crounse, J. D., and Wennberg, P. O. Isoprene peroxy radical dynamics. *J. Am. Chem. Soc.*, 139(15):5367 – 5377, 2017. doi: 10.1021/jacs.6b12838.

Wennberg, P. O., Bates, K. H., Crounse, J. D., Dodson, L. G., McVay, R. C., Mertens, L. A., Nguyen, T. B., Praske, E., Schwantes, R. H., Smarte, M. D., St Clair, J. M., Teng, A. P., Zhang, X., and Seinfeld, J. H. Gas-phase reactions of isoprene and its major oxidation products. *Chem. Rev.*, 2018. doi: 10.1021/acs.chemrev.7b00439.

Zhao, R. *The Recent Development and Application of Chemical Ionization Mass Spectrometry in Atmospheric Chemistry*, pages 1 – 33. John Wiley & Sons, Ltd, 2018. ISBN 9780470027318. doi: 10.1002/9780470027318.a9655.

Chapter 2

LOW-PRESSURE GAS CHROMATOGRAPHY WITH CHEMICAL IONIZATION MASS SPECTROMETRY FOR QUANTIFICATION OF MULTIFUNCTIONAL ORGANIC COMPOUNDS IN THE ATMOSPHERE

Vasquez, K. T., Allen, H. M., Crounse, J. D., Praske, E., Xu, L., Noelscher, A. C., and Wennberg, P. O. Low-pressure gas chromatography with chemical ionization mass spectrometry for quantification of multifunctional organic compounds in the atmosphere. *Atmos. Meas. Tech.*, 11:6815 – 6832, 2018. doi: 10.5194/amt-11-6815-2018.

Abstract

Oxygenated volatile organic compounds (OVOCs) are formed during the oxidation of gas phase hydrocarbons in the atmosphere. However, analytical challenges have hampered ambient measurements for many of these species, leaving unanswered questions regarding their atmospheric fate. We present the development of an *in situ* gas chromatography (GC) technique that, when combined with the sensitive and specific detection of chemical ionization mass spectrometry (CIMS), is capable of the isomer-resolved detection of a wide range of OVOCs. The instrument addresses many of the issues typically associated with chromatographic separation of such compounds (e.g., analyte degradation). The performance of the instrumentation is assessed through data obtained in the laboratory and during two field studies. We show that this instrument is able to successfully measure otherwise difficult-to-quantify compounds (e.g., organic hydroperoxides and organic nitrates) and observe the diurnal variations of a number of their isomers.

2.1 Introduction

The composition of the atmosphere is determined through a dynamic array of chemical emission, transport, deposition and photochemical processing. Our ability to accurately predict future trends of both air quality and climate change depends on understanding these processes. Of particular interest is the photooxidation of non-methane hydrocarbons (NMHCs), which influence the distributions of key atmospheric constituents such as ozone (O_3) and secondary organic aerosol (SOA). While decades of research have provided much insight into the link between atmo-

spheric composition and chemistry, significant knowledge gaps still persist and the atmospheric degradation pathways of many NMHCs remain poorly understood.

The gas-phase oxidation of NMHCs is typically initiated by one of several atmospheric oxidants (i.e., OH, NO_3, or O_3) converting these hydrocarbons into oxygen-containing, often multifunctional, intermediates. These first-generation oxygenated volatile organic compounds, or OVOCs, can undergo further transformations through a number of competing physical and photochemical sinks (Atkinson and Arey, 2003; Mellouki et al., 2015), each of which can have a unique effect on the atmosphere. Some OVOCs can undergo photochemical fragmentation to smaller species, often through conversion of NO to NO_2 leading to local ozone formation, while others (such as those with longer atmospheric lifetimes) can be transported downwind prior to oxidation, extending their effects to regional and global scales. Chemical oxidation can also cause OVOCs to increase their functionality, creating large low-volatility, multifunctional products that partition into the particle phase and contribute to the formation and growth of aerosol. In addition, it has been shown that significant portions of OVOCs can be removed from the atmosphere through fast deposition processes (Nguyen et al., 2015), which can greatly affect the chemical cycling of many important compounds.

It is the relative importance of each possible sink that establishes the dominant tropospheric fate of these compounds and thereby the impact of their hydrocarbon precursors (Koppmann and Wildt, 2008). This seemingly straightforward relationship can quickly become complicated, however, especially for larger compounds ($>C_3$). A prime example of this can be seen during the OH oxidation of isoprene, a highly abundant and reactive biogenic VOC, which produces six isomeric peroxy radicals (RO_2). Changes in the relative abundance of these radicals can result in vastly different ratios of its OVOC products (Orlando and Tyndall, 2012; Teng et al., 2017; Wennberg et al., 2018), allowing isoprene to have a profound effect on ozone or SOA through its bimolecular reaction products—isoprene hydroxy nitrates (IHNs) and isoprene hydroxy hydroperoxides (ISOPOOHs), respectively—or the OH radical which is recycled during the subsequent chemistry of products formed from the unimolecular RO_2 reaction channel (e.g. hydroperoxy aldehydes or HPALDs; Peeters et al., 2014). These structural effects are also apparent throughout the later-generation chemistry of isoprene and other NMHCs and the outputs of global chemistry transport models can be quite sensitive to this isomer-specific chemistry. For example, ozone production, in particular, has been shown to be highly dependent

on the assumed yields and reaction rates of specific organic nitrate isomers (Squire et al., 2015), which together determine the net NO_x recycling capabilities of each compound.

Despite its importance, our understanding of this intricate chemistry has been hindered by the lack of instrumentation capable of providing isomer-resolved measurements of important OVOCs. Recent progress has been made in this respect for laboratory studies (e.g., Bates et al., 2014, 2016; Lee et al., 2014; Teng et al., 2015, 2017; Schwantes et al., 2015; Praske et al., 2015, 2018). Analytical techniques for ambient measurements, however, suffer from high detection limits and/or large instrumental losses of these reactive analytes (Vairavamurthy et al., 1992; Apel et al., 2003, 2008; Clemitshaw, 2004), and so the focus has typically been on smaller, more abundant compounds (Mellouki et al., 2003; Goldan et al., 2004; Koppmann and Wildt, 2008; Hellén et al., 2017).

Gas chromatography (GC) can reach the detection limits needed to measure a variety of larger OVOCs by preconcentrating analytes prior to separation and utilizing detection methods such as flame ionization detection (FID) or electron impact mass spectrometry (EI-MS) (Ras et al., 2009). As a result, this technique is increasingly popular and has been or is currently being developed for the *in situ* detection of carbonyls (Apel et al., 2003; Zhao et al., 2013), organic acids (Hellén et al., 2017), organic nitrates (Mills et al., 2016), and other oxygenated organic compounds (e.g., Clemitshaw, 2004; Millet et al., 2005; Goldan et al., 2004; Koppmann and Wildt, 2008; Roukos et al., 2009; Lerner et al., 2017). Nevertheless, these field-deployable GC techniques come with their own analytical challenges as the non-specificity of common detectors such as GC–FID and overall difficulty in differentiating fragmentation patterns of isobaric and isomeric species with GC–MS can create data sets that hide the intricacies of crucial structure–activity relationships of individual compounds. In addition, the multifunctional nature of these compounds makes them highly reactive, increasing the likelihood that they will be lost or converted into different species through surface-enhanced reactions that can occur at various stages of GC analysis. Converted species can be subsequently detected (e.g., Rivera-Rios et al., 2014), thus identifying such artifacts necessitates authentic calibrations even for species not being targeted. Due to the lack of commercially available standards for many species of interest, this can quickly become labor intensive or simply not feasible, leading to large uncertainties in these types of measurements and much confusion regarding chemical mechanism elucidation.

Table 2.1: Examples of OVOCs measured in this study.

Compound	Abbreviation	Example structure
Isoprene hydroxy nitrate	IHN	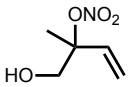
Isoprene hydroxy hydroperoxide	ISOPOOH	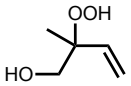
Isoprene epoxydiol	IEPOX	 (cis)
Isoprene hydroperoxy aldehyde	HPALD	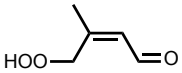
Isoprene carbonyl nitrate	ICN	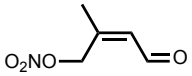
Propene hydroxy nitrate	Propene HN	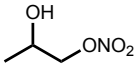
Butene hydroxy nitrate	Butene HN	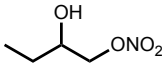
Propanone nitrate	PROPNN	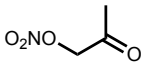
Hydroxymethyl hydroperoxide	HMHP	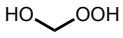

Here, we present the development and deployment of a new GC method that uses the highly sensitive detection of chemical ionization mass spectrometry (CIMS) for the near-real-time detection of a number of OVOCs. With this instrumentation, we address many of the historical issues associated with the use of GC for atmospheric field sampling, allowing for the preservation of difficult-to-measure compounds and enabling isomer-resolved measurements of a wide array of compounds. Compounds discussed in this study are shown in Table 2.1. To distinguish among isomers of hydroxynitrates, ISOPOOH, HPALD, and isoprene carbonyl nitrates (ICNs), we employ an abbreviated naming scheme in which the first number denotes the carbon position where the oxidant originally adds to the parent alkene and the second denotes the position of the additional functional group (e.g., for 1,2-IHN the hydroxy group

is located on the first carbon of the isoprene backbone (C1), followed by a nitrooxy group at C2).

2.2 Instrument description

The GC high-resolution time-of-flight (HRToF) CIMS integrates the use of a metal-free, low-pressure gas chromatography (LP-GC) instrument positioned upstream of a HRToF-CIMS (TofWerk/Caltech). This combination allows for two main sampling modes: (1) direct atmospheric sampling for the real-time quantification of gas-phase species (hereafter, direct CIMS sampling) and (2) GC–CIMS analysis for the collection, separation, and quantification of ambient isomer distributions of select OVOCs. The overall design of this instrumentation is based upon an existing test bed that has been used in previous laboratory studies (e.g., Bates et al., 2014; Lee et al., 2014; Teng et al., 2015, 2017; Schwantes et al., 2015). However, in those studies, the GC prototype required a short length of the column to be manually submerged into a chilled isopropanol bath, a setup that is cumbersome, if not impossible, to use outside of a laboratory setting. These studies were also performed under very low humidities. Here, we have field-hardened this design such that GC operation is automated and chromatography is reproducible under a variety of field conditions. A simplified schematic of the GC-HRToF-CIMS is shown in Fig. 2.1, highlighting the main flow paths of direct CIMS sampling (orange) as well as GC trapping (blue and purple) and eluting (red and purple). Details of the GC automation are discussed in Sect. 2.2.2.

2.2.1 HRToF-CIMS

The HRToF-CIMS builds upon methods developed with a previous custom-built quadrupole CIMS (Crounse et al., 2006, later upgraded to a cToF-CIMS). Ambient air is drawn at high flow rate (~2000 slm, P ~1 atm) through a custom Teflon-coated glass inlet (3.81 cm I.D x 76.2 cm long; Fig. 2.1B). A small fraction of this flow is subsampled perpendicular to the main flow in order to discriminate against large particles and debris, and directed to the CIMS, the GC, or a zeroing system through short lengths of 6.35 mm O.D. PFA tubing. When measured directly by the CIMS, ambient air, diluted with dry N_2, flows through a fluoropolymer-coated (Cytonix PFC801A) glass flow tube (Fig. 2.1F) to ensure a well-mixed gas stream prior to chemical ionization by CF_3O^- reagent ions (*m/z* 85). The flow tube pressure is held at 35 mbar and samples ambient air at a constant flow rate of 180 sccm as regulated by a critical orifice (Fig. 2.1G). This ambient air is then diluted by a

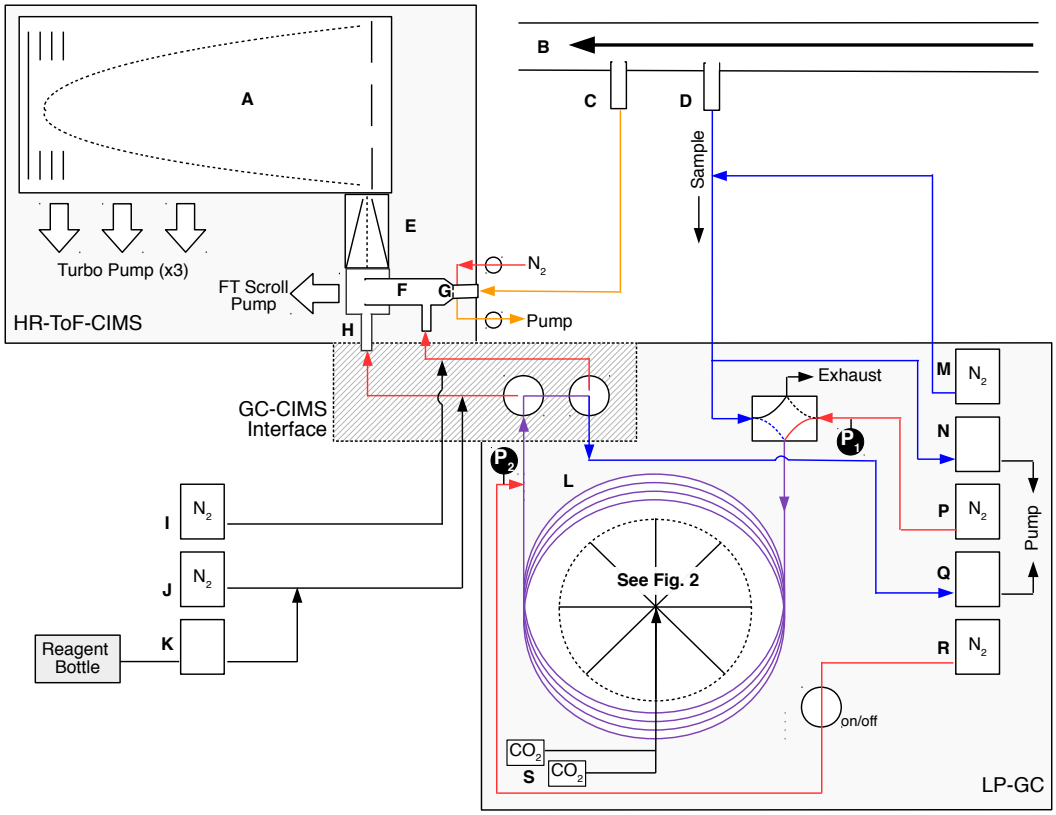

Figure 2.1: A simplified instrument schematic of GC-HRToF-CIMS showing the HRToF-CIMS, the LP-GC, and the interface between the two systems. The main components are (A) time-of-flight mass spectrometer, (B) Teflon-coated glass inlet, (C) CIMS sampling port, (D) GC-CIMS sampling port, (E) hexapole ion guide, (F) Teflon-coated glass flow tube, (G) critical orifice, (H) 210-Po ionization source, (I) CIMS dilution flow, (J) CIMS ion source dilution flow, (K) CF_3OOCF_3 reagent flow, (L) GC column and cryotrap, (M) GC dilution flow, (N) GC sample intake pump, (P) GC column flow, (Q) GC bypass pump, (R) GC N_2 pickup flow, and (S) CO_2 solenoid valves. Pressure gauges at the head and tail of the column are denoted by P_1 and P_2, respectively. Select instrument flow states are differentiated by the various line colors, for which orange represents the flow path during direct CIMS sampling, blue represents the path GC trapping, and red represents the path during GC elution. Analytical lines that are used during both GC trapping and eluting are purple. Diagram is not to scale.

factor of 10 with dry N_2 (Fig. 2.1I). Two valves located upstream of this orifice ensure a constant mass flow through the flow tube by pumping on the inlet (~0.5 slm). When the instrument switches to a different analysis mode (e.g., performs a GC or zeroes), these valves are toggled to overfill the flow tube with dry nitrogen and prevent ambient air from being sampled through this flow path.

The CF_3O^- ion chemistry has been described in detail elsewhere (Huey et al., 1996; Amelynck et al., 2000a,b; Crounse et al., 2006; Paulot et al., 2009a,b; St. Clair

et al., 2010; Hyttinen et al., 2018). Briefly, CF_3O^- is formed by passing 380 sccm of 1 ppmv CF_3OOCF_3 in N_2 through a cylindrical tube (Fig. 2.1H) containing a layer of polonium-210 (NRD LLC P-2021, initial activity: 10 mCi). Alpha particles produced from the radioactive decay of the polonium react with the N_2 gas to produce electrons that react rapidly with CF_3OOCF_3 to produce CF_3O^- ions, which, in turn, react with analytes by forming clusters (*m/z* = analyte mass + 85) or fluoride-transfer (*m/z* = analyte mass + 19) product ions. This method allows for the detection of small organic acids and other oxygenated multifunctional compounds with high sensitivity (LOD $\approx$ 10 pptv during direct sampling for 1 s integration period) and minimal fragmentation.

Following ionization, the ions are directed via a conical hexapole ion guide into the high-resolution mass spectrometer (Tofwerk), which collects data for masses between *m/z* 19 and *m/z* 396 at 10 Hz time resolution. The HRToF-CIMS has a mass resolving power of ~3000 $m/\Delta m$, allowing for the separation of some ions with different elemental composition but the same nominal mass.

2.2.2 GC

2.2.2.1 Design and automation

Chromatographic separation of analytes is achieved on a short (1-m) megabore column encased between two aluminum plates. These plates measure 130 mm x 130 mm x 5 mm (total mass = 466 g), creating the compact design shown in Fig. 2.2. The column is housed within a rectangular groove (0.8 mm wide x 2.4 mm deep) machined into the bottom plate, which serves to hold the column in place, and provides good thermal contact with the metal as it loops 2.5 times around the plate. The temperature of the metal assembly can be controlled over a large range (-60^o C to 200^oC); maximum heating rate of 42^oC min^{-1}) using a combination of CO_2 coolant and an electrical heating system that consists of a temperature ramping controller (Watlow F4 series), heaters (~400 W; KH series, Omega; Fig. 2.2A), and three resistance temperature detectors (RTDs, F3102, Omega; Fig. 2.2B, numbered). Sample collection and elution are controlled using automated solenoid valves (NResearch, Inc.) to direct gas to one of a number of vacuum outlets (Fig. 2.1F, H, and Q). These processes occur in parallel with direct CIMS sampling to minimize interruptions in data collection.

The GC is cooled through the evaporation and expansion of liquid CO_2, which enters from the center of each plate and flows along eight radial grooves. An

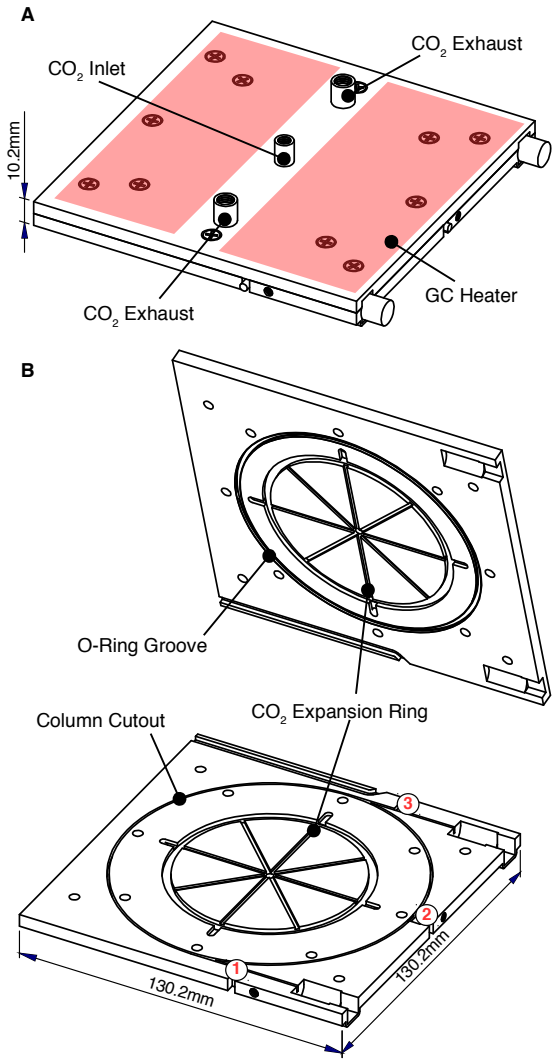

Figure 2.2: Schematic of the GC cryotrap and heating unit. Column sits in a groove machined into one plate, providing good thermal contact. CO_2 enters from the center of both plates and expands in the eight radial spokes before exiting through four exhaust ports. Heaters are adhered to the outside of the GC assembly; two of these heaters are shown above in red. The temperature is measured at three locations near the column: (1) near the inlet of the column, (2) on the column ring, and (3) near the outlet of the column.

O-ring seal forces the CO_2 to exit through ports located near the radius of the column. The movement of the CO_2 from the center to the outside of the plate establishes a temperature gradient in the same direction. Symmetry enables the entire column to remain at a similar temperature, in spite of this gradient. In contrast, a previous version of this GC assembly used during this instrument's first deployment allowed CO_2 to enter from a single point along the column diameter

(See Fig. A.1), resulting in large temperature gradients across the column and degradation of the chromatography (e.g. irregular peak shapes).

The CO_2 flow is controlled by two solenoid valves (Series 9, Parker; Fig. 2.1S) connected to ~29 cm x 0.25 mm ID and ~35 cm x 0.15 mm I.D. PEEK restrictors. With both valves open, a total CO_2 flow rate of 25 slm (as gas) is admitted to cool the GC assembly to -20^{o}C within the allotted 10 minute period. During trapping, only the solenoid valve connected to the 0.15 mm I.D. restrictor remains open to minimize CO_2 usage. Fine control over the GC temperature was accomplished by utilizing a proportional-integral-derivative (PID) control loop with the heaters and the RTD located on the column ring (Fig. 2.2, red no. 2 on the diagram). Additional efficiency was gained by insulating the GC assembly with Nomex™ felt and wrapping the felt with Kapton tape to prevent water vapor from diffusing to and condensing on the cold plates, as well as placing the entire instrument in a temperature-controlled, weatherproofed enclosure (see Sect. 2.2.4). Altogether, this resulted in reproducible temperature profiles with minimal temperature gradients across the column (less than 2^{o}C) during field operation (See Fig. A.2).

2.2.2.2 Operating parameters

To initiate sample collection, ambient air is subsampled from the main instrument inlet (1 slm; Fig. 2.1N) and diluted by a factor of 15 to 30 (Fig. 2.1M), depending on the relative humidity (RH) of the sample. The diluted air is pulled through the pre-cooled 0.53 mm I.D. RTX-1701 megabore column (Restek) by a flow-controlled pump (220 sccm; Fig. 2.1Q) and targeted compounds are cryofocused on the head of the column over a 10-minute period at -20^oC (as discussed in later sections, the choice of the dilution and trapping temperature is a compromise between adequately cryofocusing the maximum amount of analyte while avoiding the collection of water). Following collection, a four-port Teflon solenoid valve (SH360T042, NResearch) is switched, allowing N_2 carrier gas to enter the column at a constant flow rate of 5 sccm (Horiba Z512, Fig. 2.1P), and two three-way valves (225T032, NResearch) are toggled to direct the column effluent to either the flow tube (Fig. 2.1F) or the ion source (Fig. 2.1H) of the mass spectrometer—in both configurations, the entire length of column is held under low-pressure conditions ($<$ 260 mbar at P_1 [Fig. 2.1]). Compounds are then separated on the column using the following automated temperature program: a 3 minute temperature ramp to 20^{o}C (~13^{o}C min^{-1}), followed by a 3^{o}C min^{-1} ramp to 50^{o}C, followed by a

10^{o}C min^{-1} increase to 120^{o}C for a total temperature ramping time of 20 minutes. Following completion of the temperature program, the column is baked at 120^{o}C for an additional 2 min to remove remaining analytes.

As mentioned above, connecting the GC outlet directly to the mass spectrometer allows the entire column to remain at sub-ambient pressures during elution (180 mbar (into ion source) or 260 mbar (into flow tube) at P_1). This allows for low-pressure chromatography which provides several advantages over conventional GC methods (Sapozhnikova and Lehotay, 2015). For instance, low pressures support the use of short, large bore columns without significant loss in peak separation. This becomes especially advantageous during cryotrapping as this larger I.D. column allows for a greater volume of analytes to be sampled, beneficially impacting the instrument signal-to-noise ratio. In addition, low-pressure conditions also allow for faster analysis times at lower elution temperatures (Table 2.2). The decrease in analysis time provides this instrument with sufficient time resolution to capture diurnal variations in measured species (one GC cycle per hour), while lower elution temperatures allow this method to be applied for analysis of thermally labile species, as discussed in later sections.

2.2.3 GC-CIMS interface

Following the column, a 100 - 200 sccm N_2 pickup flow (Fig. 2.1R) is added to the 5 sccm column flow to decrease the residence time in the PFA tubing connecting the GC to the mass spectrometer. As mentioned above, solenoid valves direct the analytes into the CIMS instrument, either through the flow tube (similar to direct CIMS sampling) or directly into the ion source. Unlike direct ambient sampling, it is possible to pass the GC flow through the ion source as oxygen is not retained on the column during trapping. In other cases, oxygen that enters the ion source is ionized (O_2^-) and causes interferences at many *m/z* values.

Figure 2.3 shows a comparison of two chromatograms obtained by these different analysis modes. Introduction via the flow tube (hereafter FT mode; Fig. 2.3, blue) allows for interaction of analytes with only CF_3O^- (and CF_3O^--derived) reagent ions, providing a straightforward comparison to the direct CIMS samples as well as quantification of the GC transmission of analytes. However, due to tubing and gas flow configurations, the pressure within the column is greater under FT mode than when directed to the ion source region. Therefore, compounds tend to elute later and at higher temperatures, making introduction into the ion source (hereafter IS

Table 2.2: Comparison of elution temperature (^{o}C) and retention time (minutes, in parentheses) for isoprene nitrates.

Study	Column	1-OH 2-N	4-OH 3-N	*Z* 4-OH 1-N	*E* 4-OH 1-N	*Z* 1-OH 4-N	*E* 1-OH 4-N
Mills et al. (2016)	Rtx-1701[a]	N/A	110 (26.1)	119.2 (36.5)	133.7 (39.3)	133.2 (39.4)	142.7 (41.2)
Mills et al. (2016)	Rtx-200[a]	N/A	101.1 (16.7)	110 (22.4)	110 (25.1)	110 (23.3)	110 (26.5)
This study	Rtx-1701[b]	42.4 (10.5)	45.1 (11.4)	63.2 (14.5)	71.3 (15.3)	71.3 (15.3)	76.4 (15.8)

[a] Column is 30 m, 0.32 mm ID, 1 μm phase thickness

[b] Column is 1 m, 0.53 mm ID, 3 μm phase thickness

mode; Fig. 2.3, black) the preferred analysis mode when separating more thermally labile compounds in the current instrument configuration.

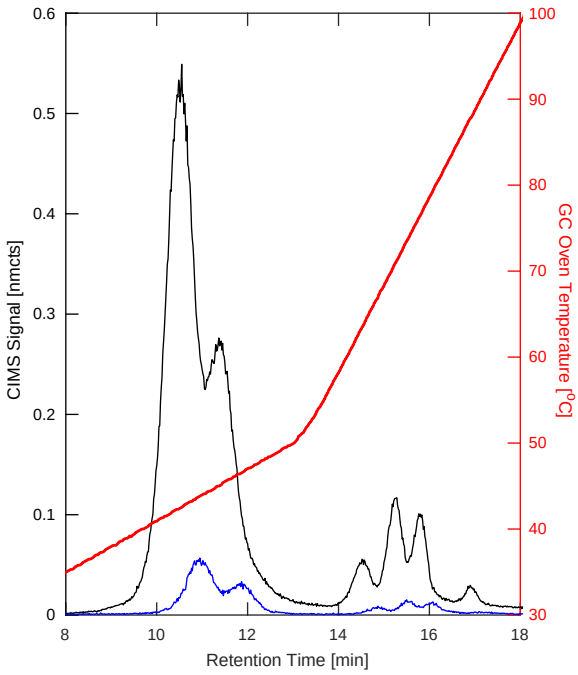

Figure 2.3: Comparison of chromatograms of the IHN isomers obtained from the two different GC analysis modes in which the same amount of analyte is collected on the column but is directed into either the ion source (black) or flow tube (blue). GCs that are directed into the ion source result in approximately a 10-fold signal increase compared to flow tube GC analysis. In addition, compounds analyzed via the ion source typically elute at lower temperatures compared to flow tube analysis, an advantage for sampling fragile, multifunctional compounds.

IS mode also creates an enhancement in instrument sensitivity due to the increase in analyte–reagent ion interaction time (as the analytes can interact with CF_3O^- as soon as it forms, rather than mixing with the ions downstream) and overall drier conditions. The enhancement in sensitivity is quantified through comparison to the direct CIMS measurements, which show a multiplicative enhancement factor that is nonlinearly dependent on the gas flow entering the ion source. For the instrument flows used in this work, the ion source enhancement was determined to be 9.8 ± 0.8, which was determined by comparing peak areas produced when operating in FT vs. IS mode (see Appenxid A). Additional discrepancies between IS mode and direct CIMS measurements may result from analyte interactions with the metal walls of the ionizer. In addition, direct electron attachment to analytes (often followed by

fragmentation) can occur in the ion source, though differences between the two GC modes are typically explained within error by the enhancement factor. These fragment ions, however, provide additional structural information. For example, different fragment ions may arise from the fragmentation of a primary nitrate versus a tertiary nitrate (See Fig. A.6).

2.2.4 Instrument housing and supporting equipment

The GC-HRToF-CIMS was placed in a weatherproofed, temperature-controlled enclosure during field sampling to protect the instrument electronics and allow for efficient GC cooling. In total, the instrument enclosure measured 1.1 m x 1.7 m x 0.9 m (W x H x D), taking up a footprint of approximately 1 m^2 (Fig. 2.4). Weatherproofing was created by using Thermolite™ insulated paneling (Laminators, Inc.) that covered the aluminum instrument rack (80/20, Inc.) and was aided by weather stripping placed between the panels and the rack. For temperature control, two Ice Qube HVAC units (IQ1700B and IQ2700B, Blade series, cooling power = 498 and 791 W, respectively) were attached to one side of the enclosure to remove the heat produced by the instrument. During the range of ambient temperatures experienced during these studies (8.7^{o}C –37.8^{o}C), the internal temperature of the enclosure remained at or below 30^{o}C under normal operating conditions.

Along with the instrument enclosure, two scroll pumps (nXDS 20i, Edwards) were located separately from the instrument in their own weather-resistant container and were used to back the three turbomolecular pumps (TwisTorr 304 FS, Agilent) and the flow tube attached to the mass spectrometer. A weather station was also co-located with the instrument during the two field studies. It included sensors for air temperature, RH, solar irradiance, wind direction, wind speed, and atmospheric pressure.

2.2.5 Instrument calibration

Instrument sensitivity was assessed in the laboratory using a select number of commercially available compounds. These experiments were performed using authentic standards for hydrogen cyanide (HCN), sulfur dioxide (SO_2), hydroxyacetone (HAc), and glycolaldehyde (GLYC). The absolute concentrations of these compounds were quantitatively determined by Fourier transform infrared spectroscopy (FTIR) before undergoing dilution and CIMS sampling (see Appendix A for additional details regarding calibration procedures). However, because many compounds of interest are not commercially available and difficult to synthesize and purify, these four standard

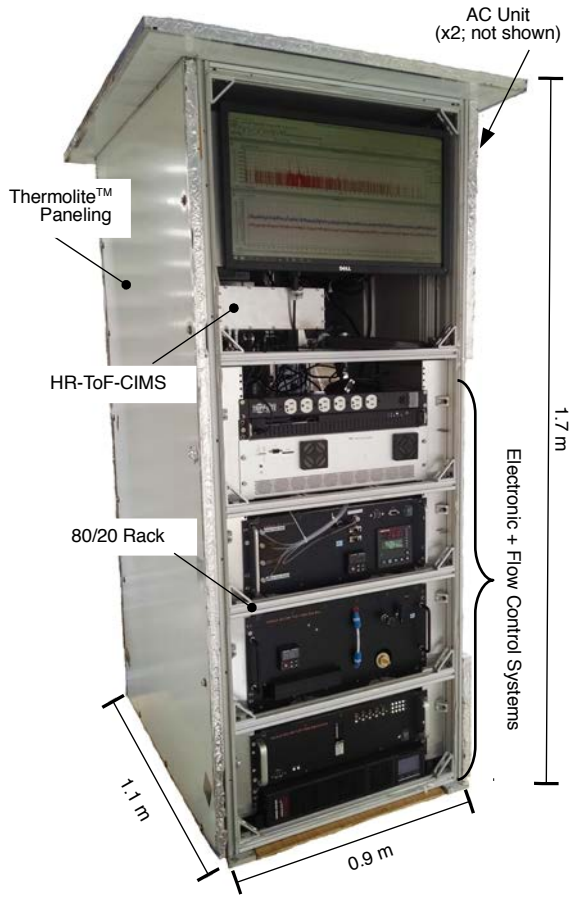

Figure 2.4: The weatherproofed and temperature-controlled enclosure in which the instrument resides during field sampling. The front panel of the enclosure is removed in this photo.

gases were simultaneously sampled on the cToF-CIMS (which uses the same chemical ionization technique) to directly compare the compound sensitivities between these two instruments. On average, the cToF-CIMS was observed to be 1.4 times more sensitive than the HRToF-CIMS for the four gases tested. We used this factor to proxy sensitivities for other compounds that had been previously determined for the cToF-CIMS through calibrations or estimated using ion–molecule collision rates as described in Paulot et al. (2009a), Garden et al. (2009), Crounse et al. (2011), Schwantes et al. (2015), and Teng et al. (2017).

For the chromatography, preliminary peak assignment was based on previous laboratory studies that were performed on the test bed this field deployable system was based upon (Bates et al., 2014; Nguyen et al., 2014; Lee et al., 2014; Praske et al., 2015; Teng et al., 2015), as detailed in the supplementary material of Teng et al. (2017). Many of these studies used synthesized standards that had been de-

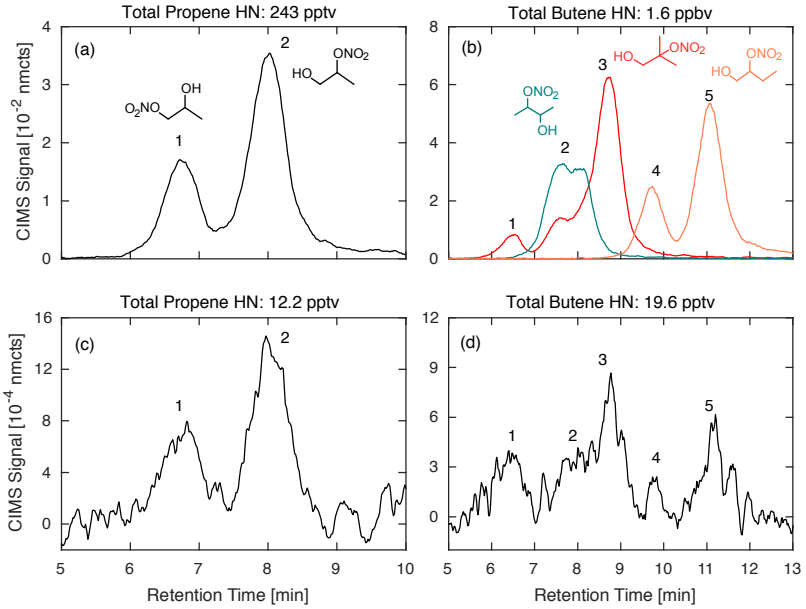

Figure 2.5: Comparison of hydroxy nitrates formed during chamber experiments (A-B) from propene (left) and three structural isomers of butene (right; 1-butene (orange), 2-butene (teal), and 2-methyl-propene (red); dominant hydroxynitrate structures shown) with the corresponding *m/z* signal observed during a 2017 field study in Pasadena, CA (C-D). Data shown are a 10-second average.

veloped for compounds such as ISOPOOH (Rivera-Rios et al., 2014; St Clair et al., 2016), IEPOX (Bates et al., 2014), and IHN (Teng et al., 2017), while others oxidized parent hydrocarbons in a chamber and determined elution orders based on assumptions regarding physical chemistry of reaction intermediates, as in Teng et al. (2015). However, due to differences in the analytical setups, verification of these assignments and their retention times have also been made for a number of targeted compounds through laboratory experiments described in more detail in Appendix A. The results from one of these studies is shown in Fig. 2.5, which compares the retention times for alkyl hydroxy nitrates derived from propene (propene HN) and three structural isomers of butene (butene HN) created in the chamber bag with chromatograms gathered in the field.

2.2.6 Instrumental backgrounds

In the field, we use two methods to quantify the instrumental background signals caused by interfering ions present at targeted analyte masses. In the first method, the instrument undergoes a "dry zero" at which the CIMS flow tube is overfilled with dry nitrogen so that no ambient air is sampled during this time. In this method,

the humidity within the instrument changes substantially compared with ambient measurements. The second method, an "ambient zero," passes air from the main inlet through a zeroing assembly, which includes a sodium bicarbonate denuder and a scrubber filled with Pd-coated alumina pellets. The scrubbed air then enters the flow tube after instrument flows are adjusted to mimic near-ambient humidity levels. During field sampling, both zeroing methods occur twice each hour during a 6 min period that separates the CIMS and GC–CIMS measurements. The dry zero is most similar to the GC measurements and can assess the health of the instrument over the course of a campaign as these backgrounds should not change over time, while the ambient zero captures background signals that are adjusted for the water-dependent sensitivity of the compounds measured during direct CIMS sampling.

2.2.7 Data processing

Data from the mass spectrometer are collected using data acquisition software provided by Tofwerk (TofDaq). These data are later combined with the instrument component read-backs collected using single-board computers (Diamond Systems) and converted into a MATLAB file using in-house-developed scripts. To account for fluctuations in the reagent ion, observed mass signals are normalized to the signal associated with the isotope of the reagent ion ($^{13}CF_3O^-$, *m/z* 86) and its cluster with water ($[H_2O \cdot {}^{13}CF_3O]^-$, *m/z* 104). The analyte signal is defined as this normalized absolute number of counts (nmcts) recorded at *m/z*.

For the chromatography, we modified an open-source MATLAB peakfit function (O'Haver, 2017). Peak areas are determined for desired masses by subtracting a baseline and fitting the chromatograms with the appropriate peak shapes as shown in Fig. 2.6 for ISOPOOH and its isobaric oxidation product, isoprene epoxydiol (IEPOX, *m/z* 203; St Clair et al., 2016). These areas are then scaled by the relative CIMS sensitives of each isomer (see Appendix A), ion source enhancement (if applicable) and a transmission factor. The resulting values are then normalized by volume of air collected on the column in order to obtain the corresponding ambient mixing ratios.

2.3 Discussion

2.3.1 Sample collection

Due to their lower volatility and highly reactive nature, the accuracy and precision of ambient OVOC measurements can be greatly limited by the sample collection method. GC sampling techniques often used in atmospheric chemistry collect gas-

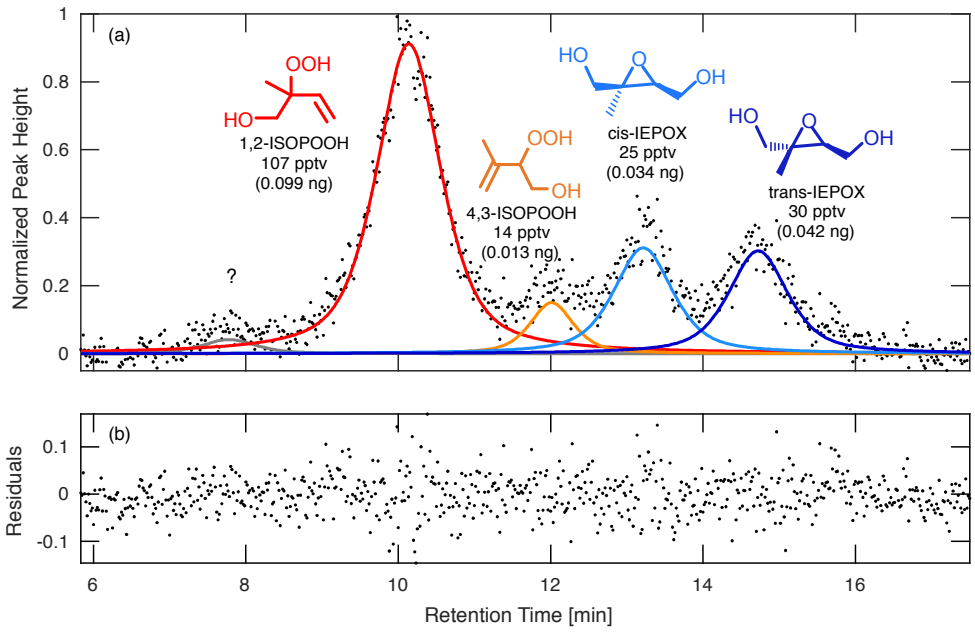

Figure 2.6: Sample chromatogram of ISOPOOH and IEPOX observed during the PROPHET 2016 field study. (A) The chromatogram, peak fits, and (B) resulting fit residuals were obtained from the peakfit MATLAB function for the deconvolution and integration the four isomers. The isomers observed during this study were 1,2-ISOPOOH (red), 4,3-ISOPOOH (orange), cis-IEPOX (light blue) and trans-IEPOX (dark blue). In addition, an unknown peak (gray) can be seen eluting at 7.8 minutes prior to the ISOPOOH and IEPOX isomer species. To obtain the ambient mixing ratios, peaks are deconvoluted and integrated using an appropriate peak shape (in this case, a Gaussian-Lorentzian blend), scaled by the relative CIMS sensitivities of each isomer (see Appendix A), ion source enhancement (if applicable), and estimated transmission factor, and then normalized by volume of air collected on the column. The GC signal shown here has been normalized to the largest peak height. Amounts shown in parentheses correspond to the amount of analyte trapped in the column.

phase compounds on solid adsorbents (e.g., TENAX®) that have been developed to combat some of the aforementioned issues (such as preventing the co-collection of water by trapping analytes at higher temperatures; Demeestere et al., 2007; Ras et al., 2009). However, the use of OVOC-specific adsorbents has shown problems with the formation of artifacts caused by the reaction of ozone, NO_2, and other compounds trapped on the sorbent surfaces (Klenø et al., 2002; Noziére et al., 2015; Mills et al., 2016) and can lead to significant analyte loss, especially for polar and/or labile compounds such as tertiary organic nitrates (as suggested in Mills et al. (2016)), organic hydroperoxides, and other highly functionalized compounds. In addition, high humidity can result in increased water uptake into the sorbent materials during ambient sampling (Ras et al., 2009) requiring additional water removal steps such

as the utilization of chemical scrubbers, which can react with compounds of interest (Koppmann and Wildt, 2008; Roukos et al., 2009), or trapping at above optimal temperatures, which may result in the loss of more volatile compounds (Vairavamurthy et al., 1992; Roukos et al., 2009). These issues motivate our use of dilution and cryotrapping on the column to transmit a wider range of analytes through our system.

Trapping efficiency was assessed by cryofocusing a mixture of propene HN and IHN for varying amounts of time (and thus sample volumes) in order to test for linearity of the cryotrap. Results provided in the Appendix A show that the GC peak area was linearly proportional to the volumes sampled, suggesting that compounds are preserved on the column during trapping (Fig. A.3). Analyte breakthrough has been monitored in the laboratory by directing the GC flow into the CIMS during trapping to monitor analyte signals. For most compounds of interest (>C_3), there has been no evidence of breakthrough under typical trapping conditions (-20^{o}C) when this procedure has been performed for a trapping period of up to 12 minutes, though we note chromatography can be significantly degraded prior to breakthrough, as the analytes spread to larger bands on the column.

Experiments were performed to determine if oxidants such as ozone and NO_2 can interfere with targeted compounds trapped on the column. We oxidized isoprene under high-NO_x conditions to produce IHN, as its isomer-specific reaction rate with ozone would make it apparent whether certain isomers were affected more than others. When we attempted to co-trap 100 ppb of NO_2 and 200 ppb of ozone, our results show no evidence that either oxidant affects the IHN trapped on the column, even at lower dilutions (15x) and lower trapping temperatures (-50^{o}C).

2.3.1.1 Trapping temperature and column humidity

Our trapping temperature (-20^{o}C) was optimized on the original laboratory prototype and was chosen as a compromise between analyte retention and avoidance of water retention. We find that trapping above -20^{o}C results in degradation of the chromatography for several species, examples of which can be seen in Appendix A (Fig. A.4). However, at -20^{o}C some higher-volatility compounds are not trapped efficiently, resulting in irregular peak shapes (Fig. A.5). Further optimization of trapping conditions is needed in order to improve the chromatography for these species and further reduce the likelihood of water retention.

Because compounds are trapped at sub-ambient temperatures, unless special care is taken, relative humidity inside the column can easily reach 100% during ambient sampling. This is problematic because co-trapped water and ice clog the column, and many species of interest are highly soluble and reactive and readily hydrolyze (Koppmann and Wildt, 2008; Roukos et al., 2009; Lee et al., 2014; Teng et al., 2017). We address this issue by diluting the ambient air with dry N_2 prior to cryotrapping to reduce the RH below the ice point at -20^{o}C (1.3 hPa water vapor). This is illustrated in Fig. 2.7 during GC analysis of IHN at high RH (~50%) with three different sample dilutions. When water is trapped during the lowest dilution (5x), the column flow is observed to decrease over time (Fig. 2.7A), indicating the formation of an ice blockage. In addition, the isomer distribution of IHN is dramatically altered, as seen by the loss of 1,2-IHN (first peak, Fig. 2.7D) and the corresponding formation of an isoprene diol, its hydrolysis product (Fig. 2.7G). However, at the two higher dilutions (15x and 20x), the column flow remains stable throughout the trapping period (Fig. 2.7B-C)—consistent with minimal ice formation—and the isomer distribution of IHN is preserved between the two runs (Fig. 2.7E-F). Though some water is retained on the column even at these higher dilutions, it was likely trapped downstream of the analytes, limiting its interactions with IHN.

During sampling, the operating dilution is chosen based on ambient RH measurements. The effectiveness of the dilution is verified by monitoring the water signal ($[H_2O \cdot {}^{13}CF_3O]^-$, *m/z* 104), which should quickly fall to background levels during elution when minimal water is retained (as seen in Fig. 2.7E-F). For the data shown here, we diluted the samples by a factor of 15 during laboratory studies and by a factor of 20 to 30 in the field studies. The high sample dilution demands a very high sensitivity to be able to adequately quantify many of the compounds of interest, which is achievable on this instrument when operating in IS mode (discussed in Sect. 2.2.3). Even so, ambient mixing ratios of several of the targeted analytes described here pushed the detection limits of the instrumentation, leading to increased uncertainty, especially when deconvolution was required prior to integration of chromatographic peaks.

2.3.2 Analyte transmission

In addition to rapid hydrolysis, many targeted OVOCs are highly susceptible to irreversible losses or chemical conversion upon contact with surfaces (Grossenbacher et al., 2001, 2004; Giacopelli et al., 2005; Rivera-Rios et al., 2014; Xiong et al., 2015; Mills et al., 2016; Hellén et al., 2017). We addressed this issue

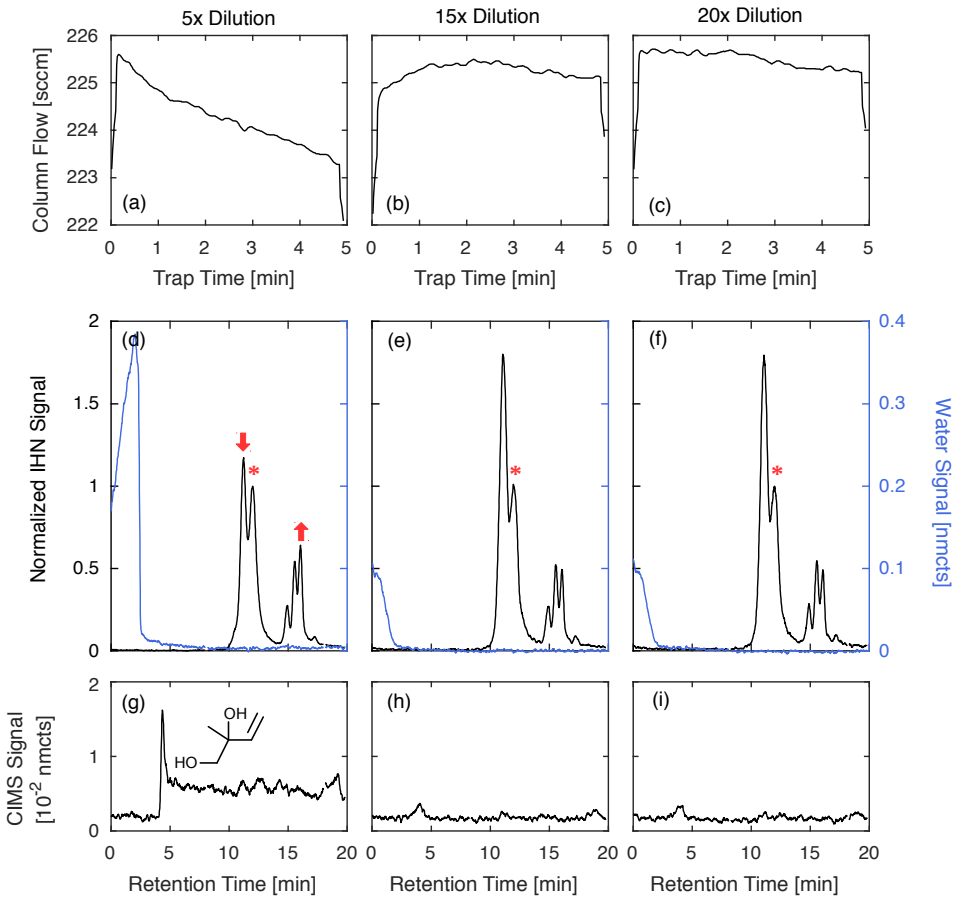

Figure 2.7: Comparison of GC column flow (A-C) and three chromatograms (D-F) of IHN (*m/z* 232, black) and water (*m/z* 104, blue) at three different dilutions from a high RH chamber experiment. The beginning of a chromatogram is marked when the temperature program initiates. When water is trapped during the lowest dilution (5x), column flow decreases (indicating an ice blockage) and the isomer distribution of IHN is dramatically altered as noted by a loss in the first peak (1,2-IHN) and increase in the last peak (*E* 1,4-IHN). These peak changes are marked by arrows and described relative to 4,3-IHN (*). The 1,2-isoprene diol (*m/z* 187, G), an expected product of 1,2-IHN hydrolysis, is also observed in this scenario. However, when the sample is sufficiently diluted prior to trapping, the water signal quickly falls to background levels and isomer distribution is preserved with minimal diol formation. Column flow also remains relatively stable throughout the trapping period when minimal water is retained.

through the utilization of metal-free LP-GC. As mentioned above, this technique holds several known advantages over traditional GC methods, including elution at lower temperatures (Table 2.2), that make it possible to better preserve thermally

labile species. In addition, all wetted instrument surfaces (with the exception of the ion source) are composed of inert materials such as PFA/PTFE Teflon, PEEK and column-phase materials. This reduces unwanted reactions on surfaces, most notably the metal-catalyzed decomposition of compounds such as hydroxyperoxides and organic nitrates (Rivera-Rios et al., 2014; Mills et al., 2016).

Despite measures taken to improve analyte transmission, losses are still observed for some species such as hydroperoxides and epoxides. This highlights the importance of accurately quantifying analyte transmission through the GC column. Yet, for traditional GC-based measurements, transmission typically remains unknown which can be detrimental when there is a lack of available standards and GC response factors must be based on another compound that has a similar chemical makeup but may interact differently with the column phase. However, the combination of our LP-GC system with the high sensitivity of the CIMS provides two sampling modes (direct CIMS and GC–CIMS) that automatically alternate between each other in half-hour increments. This allows us to compare individual chromatograms to CIMS measurements taken simultaneously with cryotrapping in order to assess GC transmission efficiency under field conditions, without the need for external standards. This is carried out by comparing mixing ratios calculated from direct CIMS sampling measurements and the sum of the entire chromatogram signal (normalized by the amount of air trapped), which is best performed when concentrations are high, and thus, measurement error is minimized. Using this method, we assess the transmission efficiency of IHN, which has been shown to have 100% transmission through a similar system (Lee et al., 2014). In the field, the percent difference of IHN mixing ratios calculated from these two measurement modes was typically less than 5%. We note that transmission less than unity can be the result of incomplete transmission of a single isomer (rather than the sum of all isomers). An example of this is in the case of ISOPOOH and IEPOX—IEPOX is transmitted more poorly through this column than ISOPOOH (Bates et al., 2014). In these cases, we use laboratory experiments to monitor discrepancies between mixing ratios obtained from direct CIMS sampling and GC–CIMS analysis and observe how these discrepancies change as we alter the isomer distribution (such as through additional oxidation of ISOPOOH). Using this method, we determine that ISOPOOH transmission is nearly 100%, while IEPOX has a transmission of about 67%.

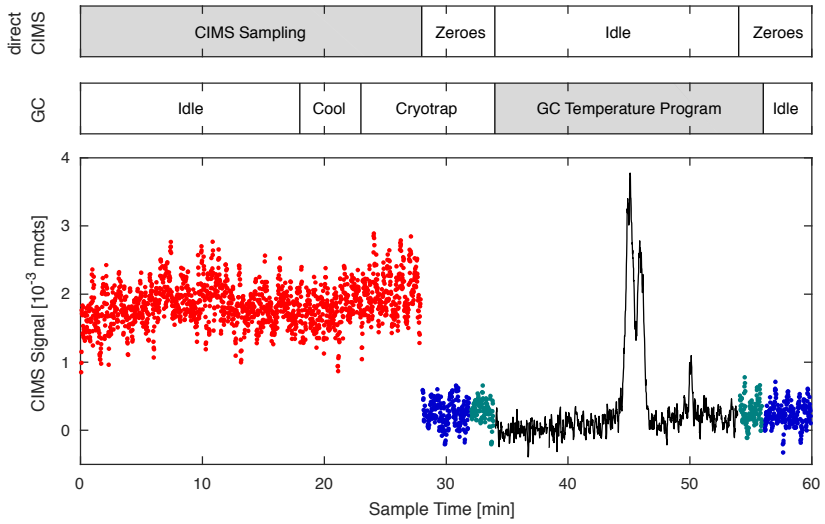

Figure 2.8: Typical GC–CIMS sampling cycle during the 2017 field study in Pasadena, CA. Data shown for *m/z* 232. Cycle has a period of 1 hour in which the first half is dedicated to direct CIMS measurements (red), and the latter half measures compound signals that have undergone chromatographic separation (black). The two sampling modes are separated by a zeroing period comprised of a 4 min ambient zero (blue) and a 2 min dry zero (green). Most GC processes occur in the background during direct sampling, so as not to interrupt data collection. Data shown here are a 2 s average. Changes in the amount of flow entering the ion source during direct CIMS and GC–CIMS sampling directly correlate with the signal-to-noise ratio seen during each operating mode. The increased flow rate through the ion source during the GC sampling mode results in higher ion counts and an increased signal-to-noise ratio.

2.4 Field performance and ambient air measurements

The GC-HRToF-CIMS has participated in two field studies that served as a test for this analytical method. Its first deployment occurred as part of the Program for Research on Oxidants, Photochemistry, Emissions and Transport (PROPHET) campaign that occurred between 1 and 31 July, 2016, when it was placed on the top of a 30 m research tower surrounded by the dense forests of rural, northern Michigan. The following summer, the instrument underwent a second deployment at the California Institute of Technology (Caltech) campus in Pasadena, CA, where measurements were taken from the roof of the 44 m tall Millikan Library between 15 July and 17 August, 2017. In contrast to PROPHET, Pasadena is typically characterized as a high-NO_x urban environment due to its proximity to Los Angeles, though biogenic emissions have also been known to influence the area (Arey et al., 1995; Pollack et al., 2013). During both deployments, the instrument provided a

near-continuous measure of OVOC concentrations, through either direct sampling or GC analysis. Interruptions in the GC measurements were primarily due to required maintenance of the cooling system (e.g. changing CO_2 tanks). When the GC was operational, data were captured during 1 h cycles in which the first half was dedicated to direct CIMS measurements and the latter half measured analytes after chromatographic separation, with the collection of ambient and dry zeros interlaced between operational modes. This sampling routine is shown in Fig. 2.8 for a single mass (*m/z* 232) collected during the 2017 Caltech field study.

At PROPHET, the low-NO_x environment (Millet et al., 2018) provided ideal conditions for measuring several organic peroxides, such as ISOPOOH. However, because ISOPOOH and its oxidation product, IEPOX, are isobaric, other analytical techniques are either unable to separate these two species or rely on the relative abundances of fragment ions to determine the relative contribution of each to the observed signal (Paulot et al., 2009b). With the GC–CIMS, we were able to physically separate the isomers prior to quantification (Fig. 2.6), allowing real-time information regarding the distribution of these two species (Fig. 2.9). As such, we observed that IEPOX comprised about half of the total daytime signal (07:00 - 22:00 local time; Fig. 2.9E), a fraction that is typically estimated through models when assessing IEPOX aerosol uptake (as in Budisulistiorini et al. (2017)). In addition, we are also able to differentiate the isomers that make up ISOPOOH and IEPOX, which can serve to highlight the isomer-specific chemistry of these compounds. A prime example is the observed daytime ratio of 1,2-ISOPOOH to 4,3-ISOPOOH. This ratio (~7.6) is higher than expected when accounting only for the isomer-specific bimolecular reaction rates of the isoprene peroxy radicals (Wennberg et al., 2018). Thus, these measurements allow us to conclude that there was competitive RO_2 isomerization of the 4-OH isoprene peroxy radicals (Peeters et al., 2009; Crounse et al., 2011; Teng et al., 2017) during the course of this campaign.

Other multifunctional organic peroxides were also observed during this campaign, such as those seen at *m/z* 201 (Fig. 2.10). Though the CIMS signal at *m/z* 201 has previously been assigned to the HPALDs (Crounse et al., 2011), a product of isoprene RO_2 isomerization, laboratory GC studies have determined that this signal is actually composed of several compounds (Teng et al., 2017). This is consistent with field chromatograms obtained at PROPHET, which show up to five individual peaks at this mass-to-charge ratio. Using the peak assignment discussed in Teng et al. (2017), we assign the last two peaks in Fig. 2.10 as the 1-HPALD (purple)

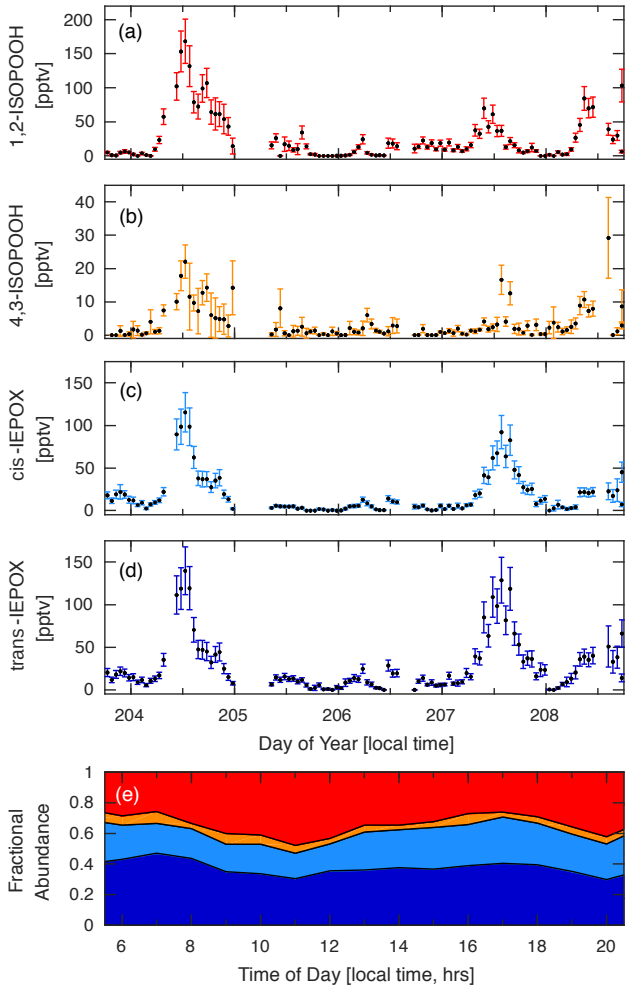

Figure 2.9: Time series for the four isobaric species: (A) 1,2-ISOPOOH, (B) 4,3-ISOPOOH, (C) *cis*-IEPOX, and (D) *trans*-IEPOX. Data were collected during the PROPHET campaign between 22 and 27 July, 2016. (E) Diurnal profile of the fractional abundance of each of these four isomers based on their hourly mean values calculated from the time series data shown here. Shaded areas correspond to 1,2-ISOPOOH (red), 4,3-ISOPOOH (orange), *cis*-IEPOX (light blue), and *trans*-IEPOX (dark blue).

and 4-HPALD (gray), which together compose ~38% of the total GC peak area. The second peak (green) is likely the same unidentified early eluting peak seen in the Teng et al. (2017) study (which also results from isoprene RO_2 isomerization). The two other peaks (red and orange) are unidentified and may result from different chemistry.

The GC-HRToF-CIMS has also demonstrated its ability to measure individual isomers of organic nitrates during its two deployments, as showcased by our IHN

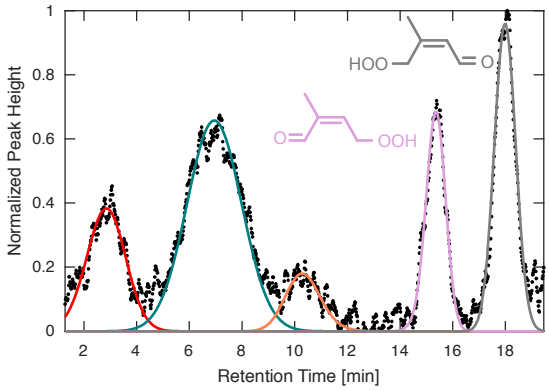

Figure 2.10: Chromatogram obtained during the PROPHET campaign for *m/z* 201. The latter two peaks have been identified previously as the two HPALD isomers (Teng et al., 2017). The three early peaks remain unidentified. GC signal has been normalized to the largest peak height.

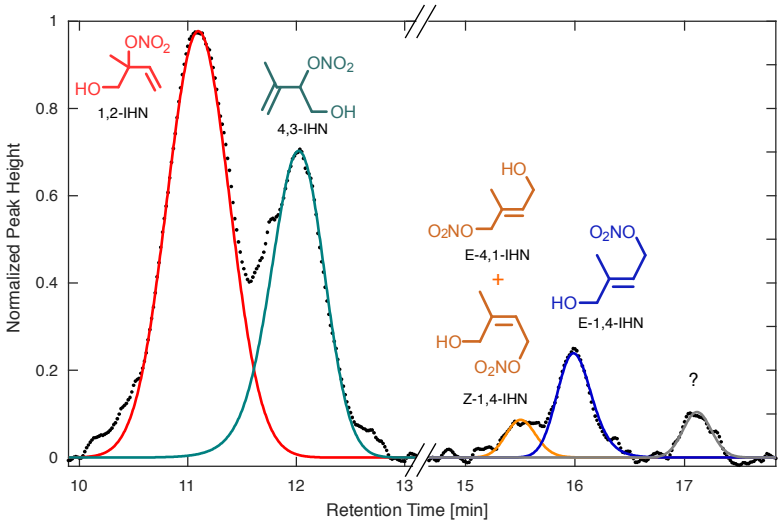

Figure 2.11: Chromatogram obtained during the Caltech field study for *m/z* 232, attributed to the IHN isomers, normalized to the largest peak height. At least four isomers of IHN were observed: 1,2-IHN (red), 4,3-IHN (green), *E*-4,1- and *Z*-1,4-IHN (coelute, orange), and *E*-1,4-IHN (blue). *Z*-4,1-IHN was not present above the instrument detection limit. An unidentified component, which likely corresponds to a species observed in laboratory isoprene oxidation studies, is present near the end of the chromatogram (gray, see Teng et al. (2017)).

measurements. The two dominant isomers of IHN (1,2-IHN and 4,3-IHN) were observed at both PROPHET (with an average daytime ratio of ~2.6) and at Caltech (with an average daytime ratio of ~1.4). At Caltech, other IHN isomers (Fig. 2.11),

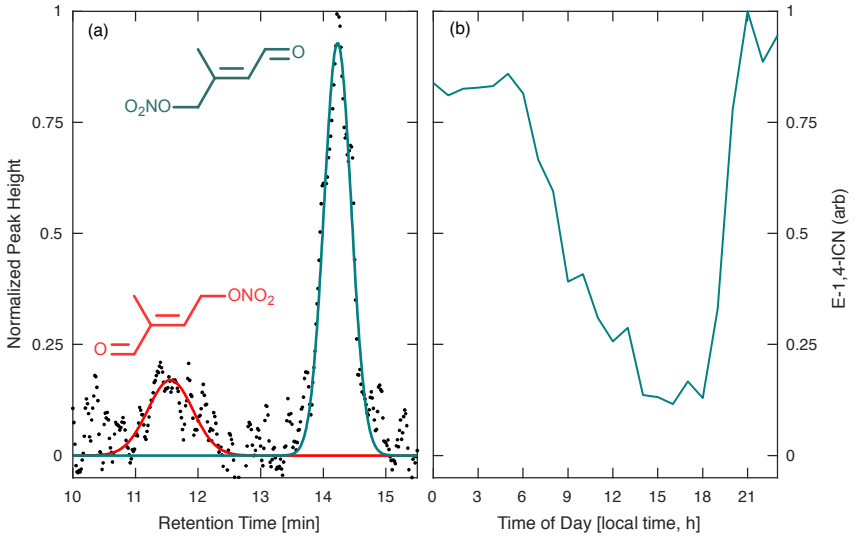

Figure 2.12: Data obtained during the Caltech field study provided (A) chromatograms for the two isoprene carbonyl nitrate isomers (4,1-ICN in red and 1,4-ICN in green, *m/z* 230) produced by isoprene + NO_3 chemistry, normalized to the largest peak height. Peak assignment is based on results from Schwantes et al. (2015). (B) Average diurnal profile was obtained for the most abundant ICN isomer, 1,4-ICN, via chromatograms collected between August 1–16, 2017. This profile appears to correspond with the expected formation of ICN from NO_3 oxidation of isoprene in dark/dim conditions and the rapid loss in light periods.

as well as an unidentified component that has been previously observed during laboratory studies (Teng et al., 2017), were also quantified. Comparison of isomer ratios obtained from each site was used to assess the isoprene RO_2 chemistry and is consistent with competitive unimolecular reaction pathways at PROPHET. Interestingly, the IHN ratio at PROPHET differed significantly from the corresponding ISOPOOH ratio despite the similar formation pathways of each pair of oxidation products. We suspect this reflects differences in their loss pathways which will be discussed further in an upcoming paper.

In addition to IHN, the GC–CIMS also observed other large (>C_3) organic nitrates. For example, evidence of isoprene + NO_3 chemistry during the Caltech experiment is indicated by the nighttime increase in the signal at *m/z* 230, which is assigned to the ICNs (Schwantes et al., 2015). Though only two isomers were observed during this study (Fig. 2.12), the distribution of these species (assigned as 4,1-ICN and 1,4-ICN) matches results from Schwantes et al. (2015) and may confirm the hypothesis that NO_3 addition to the C1 carbon if isoprene is favored (Suh et al., 2001). As the distribution of the isoprene nitroxy peroxy radical (INO_2) is less constrained than

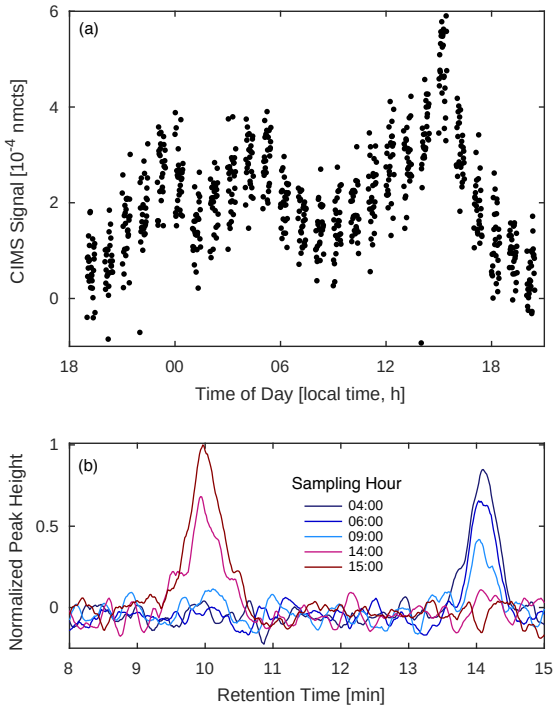

Figure 2.13: Data collected between August 11–12, 2017 during the Caltech field study. (A) Diurnal profile of unidentified compounds observed at *m/z* 236 (MW 151). (B) Select field chromatograms from the same sampling period. The GC shows at least two compounds contribute to the signal, one more abundant at night (blue) and the other more abundant in the late afternoon (red).

the OH-derived RO_2 counterpart, further observations of ambient ICN isomers with the GC–CIMS may lead to improved understanding of the impact of nighttime NO_3 chemistry (Schwantes et al., 2015). In addition, a suspected nitrogen-containing compound was observed at Caltech at *m/z* 236 (MW 151; Fig. 2.13). Data obtained from direct CIMS sampling showed at least two local maxima, one occurring before sunrise and the other shortly after noon. With the addition of the GC, we find that two distinct species contribute to this instrument signal with varying contributions over the course of a day. That is, the first compound (eluting at 9.8 minutes) is responsible for the majority of the signal in the early afternoon, possibly indicative of production via photooxidation, whereas the second compound (eluting at 13.8 minutes) is most abundant between sunset and sunrise, possibly due to production from nighttime NO_3 chemistry, high photolability, a short lifetime against the OH radical, or some combination thereof.

2.5 Summary

We have developed an automated GC–CIMS system that captures diurnal changes in the isomer distributions of a wide range of important OVOCs. This novel method addresses common issues typically associated with ambient GC measurements, allowing observations of compounds that have previously proven difficult to measure. We use a combination of sample dilution and temperature control to avoid the adverse effects caused by high column humidity (e.g. hydrolysis of reactive compounds). This, along with the use of LP-GC methodology, cryotrapping directly on the column and the creation of a near-metal-free GC design, reduces analyte degradation upon contact with the instrument surfaces.

Analytical performance was assessed through a combination of laboratory studies and field campaigns. GC-HRToF-CIMS has demonstrated its ability to provide continuous, reproducible measurements, effectively trapping tested species with no observable breakthrough and providing a quantitative measurement of GC transmission by utilizing its two sampling modes (direct CIMS and GC–CIMS sampling). Though additional optimization is needed to expand the number of species that can be measured using this technique, its participation in future field studies will help enable the elucidation of the chemical mechanisms of a number of species, such as the isoprene oxidation products, by providing information that will help assess how compound structure impacts its formation or atmospheric fate and thereby its effect on the global atmosphere.

Acknowledgements

We would like to thank Steve Bertman, Phil Stevens, and the University of Michigan Biological Station (UMBS) for organizing the PROPHET 2016 campaign. We are indebted to the many PROPHET participants who helped us move the instrument to and from the top of the tower safely. We also thank the Caltech campus and affiliated staff for accommodating the summer 2017 study. The construction of the GC-HRToF-CIMS instrument was supported by the National Science Foundation (AGS-1428482), with additional NSF support (AGS-1240604) provided for the instrument field deployments. Work performed by K. T. Vasquez and H. M. Allen was supported by the National Science Foundation Graduate Research Fellowship (NSF GRFP). K. T. Vasquez also acknowledges support from an Earl C. Anthony Fellowship in chemistry during an early portion of this study.

References

Amelynck, C., Schoon, N., and Arijs, E. Gas phase reactions of CF_3O^- and $CF_3O^-H_2O$ with nitric, formic, and acetic acid. *Int. J. Mass Spectrom.*, 203(1): 165–175, 2000a. doi: 10.1016/S1387-3806(00)00321-3.

Amelynck, C., Van, A.-M., Schoon, B. N., and Arijs, E. Gas phase reactions of CF_3O^- and $CF_3O^-H_2O$ and their relevance to the detection of stratospheric hcl. *Int. J. Mass Spectrom.*, 202(1):207–216, 2000b. doi: 10.1016/S1387-3806(00)00244-X.

Apel, E. C., Hills, A. J., Lueb, R., Zindel, S., Eisele, S., and Riemer, D. D. A fast-GC/MS system to measure C_2 to C_4 carbonyls and methanol aboard aircraft. *J. Geophys. Res. Atmos.*, 108(D20), 2003. doi: 10.1029/2002JD003199.

Apel, E. C., Brauers, T., Koppmann, R., Bandowe, B., Boßmeyer, J., Holzke, C., Tillmann, R., Wahner, A., Wegener, R., Brunner, A., Jocher, M., Ruuskanen, T., Spirig, C., Steigner, D., Steinbrecher, R., Gomez Alvarez, E., Müller, K., Burrows, J. P., Schade, G., Solomon, S. J., Ladstätter-Weißenmayer, A., Simmonds, P., Young, D., Hopkins, J. R., Lewis, A. C., Legreid, G., Reimann, S., Hansel, A., Wisthaler, A., Blake, R. S., Ellis, A. M., Monks, P. S., and Wyche, K. P. Intercomparison of oxygenated volatile organic compound measurements at the saphir atmosphere simulation chamber. *J. Geophys. Res. Atmos.*, 113(D20), 2008. doi: 10.1029/2008JD009865.

Arey, J., Crowley, D. E., Crowley, M., Resketo, M., and Lester, J. Hydrocarbon emissions from natural vegetation in California's South Coast Air Basin. *Atmos. Environ.*, 29(21):2977–2988, 1995. doi: 10.1016/1352-2310(95)00137-N.

Atkinson, R. and Arey, J. Atmospheric degradation of volatile organic compounds. *Chem. Rev.*, 103(12):4605–4638, 2003. doi: 10.1021/cr0206420.

Bates, K. H., Crounse, J. D., St Clair, J. M., Bennett, N. B., Nguyen, T. B., Seinfeld, J. H., Stoltz, B. M., and Wennberg, P. O. Gas phase production and loss of isoprene epoxydiols. *J. Phys. Chem. A*, 118(7):1237–46, 2014. doi: 10.1021/jp4107958.

Bates, K. H., Nguyen, T. B., Teng, A. P., Crounse, J. D., Kjaergaard, H. G., Stoltz, B. M., Seinfeld, J. H., and Wennberg, P. O. Production and fate of C_4 dihydroxycarbonyl compounds from isoprene oxidation. *J. Phys. Chem. A*, 120 (1):106–117, 2016. doi: 10.1021/acs.jpca.5b10335.

Budisulistiorini, S. H., Nenes, A., Carlton, A. G., Surratt, J. D., McNeill, V. F., and Pye, H. O. T. Simulating aqueous-phase isoprene-epoxydiol (IEPOX) secondary organic aerosol production during the 2013 Southern Oxidant and Aerosol Study (SOAS). *Environ. Sci. Tech.*, 51(9):5026–5034, 2017. doi: 10.1021/acs.est.6b05750. PMID: 28394569.

Clemitshaw, K. A review of instrumentation and measurement techniques for ground-based and airborne field studies of gas-phase tropospheric chemistry. *Crit. Rev. Env. Sci. Tec.*, 34(1):1–108, 2004. doi: 10.1080/10643380490265117.

Crounse, J. D., McKinney, K. A., Kwan, A. J., and Wennberg, P. O. Measurement of gas-phase hydroperoxides by chemical ionization mass spectrometry. *Anal. Chem.*, 78(19):6726–6732, 2006. doi: 10.1021/ac0604235.

Crounse, J. D., Paulot, F., Kjaergaard, H. G., and Wennberg, P. O. Peroxy radical isomerization in the oxidation of isoprene. *Phys. Chem. Chem. Phys.*, 13:13607–13613, 2011. doi: 10.1039/C1CP21330J.

Demeestere, K., Dewulf, J., De Witte, B., and Van Langenhove, H. Sample preparation for the analysis of volatile organic compounds in air and water matrices. *J. Chromatogr. A*, 1153(1):130–144, 2007. doi: 10.1016/j.chroma.2007.01.012.

Garden, A. L., Paulot, F., Crounse, J. D., Maxwell-Cameron, I. J., Wennberg, P. O., and Kjaergaard, H. G. Calculation of conformationally weighted dipole moments useful in ion-molecule collision rate estimates. *Chem. Phys. Lett.*, 474(1):45–50, 2009. doi: 10.1016/j.cplett.2009.04.038.

Giacopelli, P., Ford, K., Espada, C., and Shepson, P. B. Comparison of the measured and simulated isoprene nitrate distributions above a forest canopy. *J. Geophys. Res. Atmos.*, 110(D1), 2005. doi: 10.1029/2004JD005123.

Goldan, P. D., Kuster, W. C., Williams, E., Murphy, P. C., Fehsenfeld, F. C., and Meagher, J. Nonmethane hydrocarbon and oxy hydrocarbon measurements during the 2002 New England air quality study. *J Geosphys Res-Atmos*, 109(D21), 2004. doi: 10.1029/2003JD004455.

Grossenbacher, J. W., Couch, T., Shepson, P. B., Thornberry, T., Witmer-Rich, M., Carroll, M. A., Faloona, I., Tan, D., Brune, W., Ostling, K., and Bertman, S. Measurements of isoprene nitrates above a forest canopy. *J. Geophys. Res. Atmos.*, 106(D20):24429–24438, 2001. doi: 10.1029/2001JD900029.

Grossenbacher, J. W., Barket Jr., D. J., Shepson, P. B., Carroll, M. A., Olszyna, K., and Apel, E. A comparison of isoprene nitrate concentrations at two forest-impacted sites. *J. Geophys. Res. Atmos.*, 109(D11), 2004. doi: 10.1029/2003JD003966.

Hellén, H., Schallhart, S., Praplan, A. P., Petäjä, T., and Hakola, H. Using in situ gc-ms for analysis of C_2–C_7 volatile organic acids in ambient air of a boreal forest site. *Atmos. Meas. Tech.*, 10(1):281–289, 2017. doi: 10.5194/amt-10-281-2017.

Huey, L. G., Villalta, P. W., Dunlea, E. J., Hanson, D. R., and Howard, C. J. Reactions of CF_3O^- with atmospheric trace gases. *J. Phys. Chem.*, 100(1):190–194, 1996. doi: 10.1021/jp951928u.

Hyttinen, N., Otkjær, R. V., Iyer, S., Kjaergaard, H. G., Rissanen, M. P., Wennberg, P. O., and Kurtén, T. Computational comparison of different reagent ions in the chemical ionization of oxidized multifunctional compounds. *J. Phys. Chem. A*, 122(1):269–279, 2018. doi: 10.1021/acs.jpca.7b10015.

Klenø, J. G., Wolkoff, P., Clausen, P. A., Wilkins, C. K., and Pedersen, T. Degradation of the adsorbent Tenax TA by nitrogen oxides, ozone, hydrogen peroxide, oh radical, and limonene oxidation products. *Environ. Sci. Technol.*, 36(19): 4121–4126, 2002. doi: 10.1021/es025680f.

Koppmann, R. and Wildt, J. *Oxygenated Volatile Organic Compounds*, pages 129–172. John Wiley & Sons, 2008.

Lee, L., Teng, A. P., Wennberg, P. O., Crounse, J. D., and Cohen, R. C. On rates and mechanisms of OH and O_3 reactions with isoprene-derived hydroxy nitrates. *J. Phys. Chem. A*, 118(9):1622–37, 2014. doi: 10.1021/jp4107603.

Lerner, B. M., Gilman, J. B., Aikin, K. C., Atlas, E. L., Goldan, P. D., Graus, M., Hendershot, R., Isaacman-VanWertz, G. A., Koss, A., Kuster, W. C., Lueb, R. A., McLaughlin, R. J., Peischl, J., Sueper, D., Ryerson, T. B., Tokarek, T. W., Warneke, C., Yuan, B., and de Gouw, J. A. An improved, automated whole air sampler and gas chromatography mass spectrometry analysis system for volatile organic compounds in the atmosphere. *Atmos. Meas. Tech.*, 10(1):291–313, 2017. doi: 10.5194/amt-10-291-2017.

Mellouki, A., Le Bras, G., and Sidebottom, H. Kinetics and mechanisms of the oxidation of oxygenated organic compounds in the gas phase. *Chem. Rev.*, 103 (12):5077–5096, 2003. doi: 10.1021/cr020526x.

Mellouki, A., Wallington, T. J., and Chen, J. Atmospheric chemistry of oxygenated volatile organic compounds: Impacts on air quality and climate. *Chem. Rev.*, 115 (10):3984–4014, 2015. doi: 10.1021/cr500549n.

Millet, D. B., Donahue, N. M., Pandis, S. N., Polidori, A., Stanier, C. O., Turpin, B. J., and Goldstein, A. H. Atmospheric volatile organic compound measurements during the pittsburgh air quality study: Results, interpretation, and quantification of primary and secondary contributions. *J. Geophys. Res. Atmos.*, 110(D7), 2005. doi: 10.1029/2004JD004601.

Millet, D. B., Alwe, H. D., Chen, X., Deventer, M. J., Griffis, T. J., Holzinger, R., Bertman, S. B., Rickly, P. S., Stevens, P. S., Léonardis, T., Locoge, N., Dusanter, S., Tyndall, G. S., Alvarez, S. L., Erickson, M. H., and Flynn, J. H. Bidirectional ecosystem–atmosphere fluxes of volatile organic compounds across the mass spectrum: How many matter? *ACS Earth and Space Chem.*, 2(8):764–777, 2018. doi: 10.1021/acsearthspacechem.8b00061.

Mills, G. P., Hiatt-Gipson, G. D., Bew, S. P., and Reeves, C. E. Measurement of isoprene nitrates by GCMS. *Atmos. Meas. Tech.*, 9(9):4533–4545, 2016. doi: 10.5194/amt-9-4533-2016.

Nguyen, T. B., Crounse, J. D., Schwantes, R. H., Teng, A. P., Bates, K. H., Zhang, X., St. Clair, J. M., Brune, W. H., Tyndall, G. S., Keutsch, F. N., Seinfeld, J. H., and Wennberg, P. O. Overview of the focused Isoprene eXperiment at the California Institute of Technology (FIXCIT): Mechanistic chamber studies on the oxidation of biogenic compounds. *Atmos. Chem. Phys.*, 14(24):13531–13549, 2014. doi: 10.5194/acp-14-13531-2014.

Nguyen, T. B., Crounse, J. D., Teng, A. P., St. Clair, J. M., Paulot, F., Wolfe, G. M., and Wennberg, P. O. Rapid deposition of oxidized biogenic compounds to a temperate forest. *P. Natl. Acad. Sci.*, 112(5):E392–E401, 2015. doi: 10.1073/pnas.1418702112.

Noziére, B., Kalberer, M., Claeys, M., Allan, J., D'Anna, B., Decesari, S., Finessi, E., Glasius, M., Grgić, I., Hamilton, J. F., Hoffmann, T., Iinuma, Y., Jaoui, M., Kahnt, A., Kampf, C. J., Kourtchev, I., Maenhaut, W., Marsden, N., Saarikoski, S., Schnelle-Kreis, J., Surratt, J. D., Szidat, S., Szmigielski, R., and Wisthaler, A. The molecular identification of organic compounds in the atmosphere: State of the art and challenges. *Chem. Rev.*, 115(10):3919–3983, 2015. doi: 10.1021/cr5003485.

O'Haver, T. Peak fitters, Aug 2017. URL https://terpconnect.umd.edu/~toh/spectrum/InteractivePeakFitter.htm.

Orlando, J. J. and Tyndall, G. S. Laboratory studies of organic peroxy radical chemistry: An overview with emphasis on recent issues of atmospheric significance. *Chem. Soc. Rev.*, 41:6294–6317, 2012. doi: 10.1039/C2CS35166H.

Paulot, F., Crounse, J. D., Kjaergaard, H. G., Kroll, J. H., Seinfeld, J. H., and Wennberg, P. O. Isoprene photooxidation: New insights into the production of acids and organic nitrates. *Atmos. Chem. Phys.*, 9(4):1479–1501, 2009a. doi: 10.5194/acp-9-1479-2009.

Paulot, F., Crounse, J. D., Kjaergaard, H. G., Kürten, A., St. Clair, J. M., Seinfeld, J. H., and Wennberg, P. O. Unexpected epoxide formation in the gas-phase photooxidation of isoprene. *Science*, 325(5941):730–733, 2009b. doi: 10.1126/science.1172910.

Peeters, J., Nguyen, T. L., and Vereecken, L. HO_x radical regeneration in the oxidation of isoprene. *Phys. Chem. Chem. Phys.*, 11:5935–5939, 2009. doi: 10.1039/B908511D.

Peeters, J., Müller, J.-F., Stavrakou, T., and Nguyen, V. S. Hydroxyl radical recycling in isoprene oxidation driven by hydrogen bonding and hydrogen tunneling: The upgraded LIM1 mechanism. *J. Phys. Chem. A*, 118(38):8625–8643, 2014. doi: 10.1021/jp5033146. PMID: 25010574.

Pollack, I. B., Ryerson, T. B., Trainer, M., Neuman, J. A., Roberts, J. M., and Parrish, D. D. Trends in ozone, its precursors, and related secondary oxidation products in los angeles, california: A synthesis of measurements from 1960 to 2010. *J. Geophys. Res. Atmos.*, 118(11):5893–5911, 2013. doi: 10.1002/jgrd.50472.

Praske, E., Crounse, J. D., Bates, K. H., Kurten, T., Kjaergaard, H. G., and Wennberg, P. O. Atmospheric fate of methyl vinyl ketone: Peroxy radical reactions with NO and HO_2. *J. Phys. Chem. A*, 119(19):4562–4572, 2015. doi: 10.1021/jp5107058.

Praske, E., Otkjær, R. V., Crounse, J. D., Hethcox, J. C., Stoltz, B. M., Kjaergaard, H. G., and Wennberg, P. O. Atmospheric autoxidation is increasingly important in urban and suburban north america. *P. Natl. Acad. Sci.*, 115(1):64–69, 2018. doi: 10.1073/pnas.1715540115.

Ras, M. R., Borrull, F., and Marcé, R. M. Sampling and preconcentration techniques for determination of volatile organic compounds in air samples. *Trends Anal. Chem.*, 28(3):347–361, 2009. doi: 10.1016/j.trac.2008.10.009.

Rivera-Rios, J. C., Nguyen, T. B., Crounse, J. D., Jud, W., St. Clair, J. M., Mikoviny, T., Gilman, J. B., Lerner, B. M., Kaiser, J. B., de Gouw, J., Wisthaler, A., Hansel, A., Wennberg, P. O., Seinfeld, J. H., and Keutsch, F. N. Conversion of hydroperoxides to carbonyls in field and laboratory instrumentation: Observational bias in diagnosing pristine versus anthropogenically controlled atmospheric chemistry. *Geophys. Res. Lett.*, 41(23):8645–8651, 2014. doi: 10.1002/2014GL061919.

Roukos, J., Plaisance, H., Leonardis, T., Bates, M., and Locoge, N. Development and validation of an automated monitoring system for oxygenated volatile organic compounds and nitrile compounds in ambient air. *J. Chromatogr. A*, 1216(49): 8642–8651, 2009. ISSN 0021-9673. doi: 10.1016/j.chroma.2009.10.018.

Sapozhnikova, Y. and Lehotay, S. J. Review of recent developments and applications in low-pressure (vacuum outlet) gas chromatography. *Anal. Chim. Acta.*, 899:13–22, 2015. doi: 10.1016/j.aca.2015.10.003.

Schwantes, R. H., Teng, A. P., Nguyen, T. B., Coggon, M. M., Crounse, J. D., St Clair, J. M., Zhang, X., Schilling, K. A., Seinfeld, J. H., and Wennberg, P. O. Isoprene NO_3 oxidation products from the RO_2 + HO_2 pathway. *J. Phys. Chem. A*, 119(40):10158–10171, 2015. doi: 10.1021/acs.jpca.5b06355.

Squire, O. J., Archibald, A. T., Griffiths, P. T., Jenkin, M. E., Smith, D., and Pyle, J. A. Influence of isoprene chemical mechanism on modelled changes in tropospheric ozone due to climate and land use over the 21st century. *Atmos. Chem. Phys.*, 15(9):5123–5143, 2015. doi: 10.5194/acp-15-5123-2015.

St. Clair, J. M., McCabe, D. C., Crounse, J. D., Steiner, U., and Wennberg, P. O. Chemical ionization tandem mass spectrometer for the in situ measurement of methyl hydrogen peroxide. *Rev. Sci. Instrum.*, 81(9), 2010. doi: 10.1063/1.3480552.

St Clair, J. M., Rivera-Rios, J. C., Crounse, J. D., Knap, H. C., Bates, K. H., Teng, A. P., Jorgensen, S., Kjaergaard, H. G., Keutsch, F. N., and Wennberg, P. O. Kinetics and products of the reaction of the first-generation isoprene hydroxy hydroperoxide (ISOPOOH) with OH. *J. Phys. Chem. A*, 120(9):1441–51, 2016. doi: 10.1021/acs.jpca.5b06532.

Suh, I., Lei, W., and Zhang, R. Experimental and theoretical studies of isoprene reaction with NO_3. *J. Phys. Chem. A*, 105(26):6471–6478, 2001. doi: 10.1021/jp0105950.

Teng, A. P., Crounse, J. D., Lee, L., St. Clair, J. M., Cohen, R. C., and Wennberg, P. O. Hydroxy nitrate production in the OH-initiated oxidation of alkenes. *Atmos. Chem. Phys.*, 15(8):4297–4316, 2015. doi: 10.5194/acp-15-4297-2015.

Teng, A. P., Crounse, J. D., and Wennberg, P. O. Isoprene peroxy radical dynamics. *J. Am. Chem. Soc.*, 139(15):5367–5377, 2017. doi: 10.1021/jacs.6b12838.

Vairavamurthy, A., Roberts, J. M., and Newman, L. Methods for determination of low molecular weight carbonyl compounds in the atmosphere: A review. *Atmos. Enviro. Part A*, 26(11):1965–1993, 1992. doi: 10.1016/0960-1686(92)90083-W.

Wennberg, P. O., Bates, K. H., Crounse, J. D., Dodson, L. G., McVay, R. C., Mertens, L. A., Nguyen, T. B., Praske, E., Schwantes, R. H., Smarte, M. D., St Clair, J. M., Teng, A. P., Zhang, X., and Seinfeld, J. H. Gas-phase reactions of isoprene and its major oxidation products. *Chem. Rev.*, 2018. doi: 10.1021/acs.chemrev.7b00439.

Xiong, F., McAvey, K. M., Pratt, K. A., Groff, C. J., Hostetler, M. A., Lipton, M. A., Starn, T. K., Seeley, J. V., Bertman, S. B., Teng, A. P., Crounse, J. D., Nguyen, T. B., Wennberg, P. O., Misztal, P. K., Goldstein, A. H., Guenther, A. B., Koss, A. R., Olson, K. F., de Gouw, J. A., Baumann, K., Edgerton, E. S., Feiner, P. A., Zhang, L., Miller, D. O., Brune, W. H., and Shepson, P. B. Observation of isoprene hydroxynitrates in the southeastern United States and implications for the fate of NOx. *Atmos. Chem. Phys.*, 15(19):11257–11272, 2015. doi: 10.5194/acp-15-11257-2015.

Zhao, Y., Kreisberg, N. M., Worton, D. R., Teng, A. P., Hering, S. V., and Goldstein, A. H. Development of an in situ thermal desorption gas chromatography instrument for quantifying atmospheric semi-volatile organic compounds. *Aerosol Sci. Technol.*, 47(3):258–266, 2013. doi: 10.1080/02786826.2012.747673.

Chapter 3

RAPID HYDROLYSIS OF TERTIARY ISOPRENE NITRATE EFFICIENTLY REMOVES NOX FROM THE ATMOSPHERE

Vasquez, K. T., Crounse, J. D., Schulze, B. C., Bates, K. H., Teng, A. P., Xu, L., Allen, H. M., and Wennberg, P. O. Rapid hydrolysis of tertiary isoprene nitrate efficiently removes NOx from the atmosphere. *Proc. Natl. Acad. Sci.*, 117(52): 33011 – 33016, 2020. doi: 10.1073/pnas.2017442117.

Abstract

The formation of a suite of hydroxy nitrate (IHN) isomers during the OH-initiated oxidation of isoprene affects both the concentration and distribution of nitrogen oxide free radicals (NO_x). Experiments performed in an atmospheric simulation chamber suggest that the lifetime of the most abundant isomer, 1,2-IHN, is shortened significantly by a water-mediated process (leading to nitric acid formation) while the lifetime of a similar isomer, 4,3-IHN, is not. Consistent with these chamber studies, NMR kinetic experiments constrain the 1,2-IHN hydrolysis lifetime to less than 10 s in D_2O at 298 K, whereas the 4,3-IHN isomer has been observed to hydrolyze much less efficiently. These laboratory findings are used to interpret observations of the IHN isomer distribution in ambient air. The IHN isomer ratio (1,2-IHN to 4,3-IHN) in a high NO_x environment decrease rapidly in the afternoon, which is not explained using known gas-phase chemistry. When simulated with an observationally-constrained model, we find that an additional loss process for the 1,2-IHN isomer with a time constant of about 6 hours best explains our atmospheric measurements. Using estimates for 1,2-IHN Henry's law constant and atmospheric liquid water volume, we show that condensed-phase hydrolysis of 1,2-IHN can account for this loss process. Simulations from a global chemistry transport model show that the hydrolysis of 1,2-IHN accounts for a substantial fraction of NO_x lost (and HNO_3 produced), resulting in large impacts on oxidant formation, especially over forested regions.

3.1 Introduction

The formation of organic nitrates during the oxidation of volatile organic compounds (VOCs) serves to sequester nitrogen oxides (NO_x = NO + NO_2). This chemistry is

expected to become increasingly important as NO_x levels decline (Browne and Cohen, 2012), as has been occuring in the United States (Simon et al., 2015). Because the formation and subsequent fate of organic nitrates alters the concentrations and distributions of NO_x in the atmosphere, they, by extension, also significantly impact the production of tropospheric ozone and organic aerosols (Perring et al., 2013; Mao et al., 2018; Xu et al., 2015; Rollins et al., 2012), which have known impacts on the environment and human health.

Due to the sheer abundance and reactivity of isoprene in the boundary layer, organic nitrates created from its oxidation are believed to greatly affect the atmospheric NO_x lifetime (Trainer et al., 1991; Wu et al., 2007; Horowitz et al., 2007; Beaver et al., 2012; Paulot et al., 2012; Mao et al., 2013; Squire et al., 2015; Carlton et al., 2018; Li et al., 2018). Isoprene-derived hydroxy nitrates (IHN) are formed primarily during the OH oxidation of isoprene in the presence of NO (Paulot et al., 2009) (Fig. 3.1). Recent laboratory measurements suggest the branching ratio for this pathway (α) is approximately 13% (Teng et al., 2017), which is higher than many previous estimates (Wennberg et al., 2018). While eight IHN isomers can form (Teng et al., 2017), two of these isomers (1,2-IHN and 4,3-IHN; Fig. 3.1) make up the majority of the total IHN yield at atmospherically relevant conditions. Once formed, current understanding suggests that IHN are primarily lost from the atmosphere through deposition and chemical oxidation (Perring et al., 2013; Wennberg et al., 2018; Fisher et al., 2016).

The relative importance of the IHN loss pathways determines the extent to which NO_x is recycled back into the atmosphere. For instance, deposition results in the permanent removal of NO_x, but the IHN lifetime against deposition under typical atmospheric conditions is relatively long ($\tau_{dep} \approx 24$ h for $v_{dep} = 1.7$ cm s^{-1} (Nguyen et al., 2015) and boundary layer height (BLH) = 1.5 km). On the other hand, chemical oxidation by OH is more important, providing a lifetime of 9.3 and 6.9 h (assuming [OH] = 1×10^6 molecules cm^{-3}) for 1,2-IHN and 4,3-IHN, respectively (Wennberg et al., 2018). Though studies have shown that the nitrate moiety typically remains attached to these molecules following this chemistry (particularly for 4,3-IHN), subsequent photooxidation of second-generation products can still contribute to significant NO_x recycling (Lee et al., 2014; Müller et al., 2014).

Model simulations of field measurements tend to overestimate daytime concentrations of IHN (Giacopelli et al., 2005; Liu et al., 2012; Xiong et al., 2015; Wolfe et al., 2015; Fisher et al., 2016). While this might be partially due to assumptions

made regarding the isomer distribution of isoprene RO_2 and α, this discrepancy has also been attributed to a missing IHN sink. Several possible sinks have been hypothesized. It has been suggested that the tertiary nitrate group on 1,2-IHN allows this molecule to hydrolyze rapidly in clouds or in aerosol (Liu et al., 2012; Boyd et al., 2015; Rindelaub et al., 2015; Bean and Hildebrandt Ruiz, 2016; Day et al., 2010). This loss pathway could contribute significantly to HNO_3 formed over continental regions (Darer et al., 2011; Hu et al., 2011; Browne et al., 2013; Rindelaub et al., 2015; Romer et al., 2016; Zare et al., 2018). Photolysis has also been proposed (Xiong et al., 2015). Unlike hydrolysis, photolysis of organic nitrates is expected to release NO_2 back into the atmosphere, contributing to tropospheric ozone production downwind of sources (Müller et al., 2014; Zare et al., 2018).

Here, we used newly-developed instrumentation (Vasquez et al., 2018) to monitor changes in the isomer distribution of IHN during a 2017 summer field study conducted in Pasadena, CA. These ambient observations are interpreted using a combination of laboratory chamber experiments, aqueous hydrolysis experiments, and observationally-constrained model simulations. We focus our analysis on the two most abundant isomers, 1,2-IHN and 4,3-IHN. Since 1,2-IHN and 4,3-IHN are thought to undergo similar atmospheric fates (Fig. 3.1), we use the ratio of their concentrations (1,2-IHN to 4,3-IHN, hereafter referred to as "IHN isomer ratio", for simplicity) as a proxy for differences in their non-photochemical loss.

This novel data set suggests the 1,2-IHN isomer is rapidly lost via hydrolysis in the atmosphere at a rate competitive with other oxidation and deposition pathways. In addition, global simulations suggest that this loss pathway greatly impacts the global concentration of NO_x, ozone and nitric acid.

3.2 Methods

3.2.1 Description of field site

Measurements described here were collected from a field site located at the Caltech campus in Pasadena, CA which is located in the Los Angeles metropolitan area approximately 18 km northeast of downtown Los Angeles (DTLA) and 7 km south of the San Gabriel Mountains. The instrument was located on the southwest corner of the roof of the 44 m tall Millikan Library (Lat: 34.137; Lon: -118.126) from 01–17 August 2017, sampling into the daytime prevailing winds which arrived predominantly from the south. Because of its proximity to DTLA, the site experienced high levels of anthropogenic pollution ($[NO]_{avg,\ daytime}$ = 2.5 ppbv). In addition, local

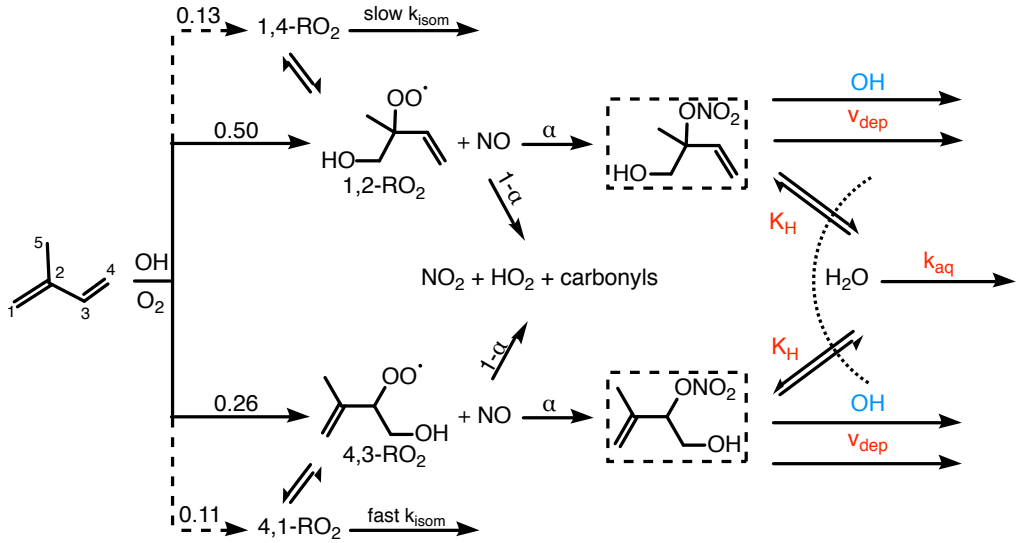

Figure 3.1: Isoprene hydroxy nitrates (IHN) are formed through a small, but important pathway (α) present in the reaction of isoprene and OH ($+O_2$) in the presence of NO. The dominant pathway ($1-\alpha$) forms NO_2 and promotes ozone production. The formation of the two IHN isomers shown here (1,2-IHN and 4,3-IHN, dashed boxes) represent the majority of the IHN formed under atmospherically relevant RO_2 lifetimes. Once formed, 1,2-IHN and 4,3-IHN can undergo deposition, oxidation or incorporation into aerosol where they can hydrolyze. The branching between IHN loss pathways directly affects isoprene's impact on NO_x and oxidant levels. IHN loss pathways that result in NO_x recycling are highlighted in blue, while those that result in the permanent loss of NO_x are red.

vegetation is made up of known isoprene emitters (Guenther et al., 1994), allowing for local biogenic emissions to influence the site.

In addition, a weather station was co-located with our main GC-CIMS instrument to monitor relative humidity (%), air temperature (°C), barometric pressure (mbar), solar radiation (W/m^2), wind speed (m/s) and wind direction. Additional details regarding this field site are provided in Appendix B.

3.2.2 Isomer measurements

The GC-CIMS instrumentation, and details of its field operation, has been described previously in the literature (Vasquez et al., 2018). Briefly, ambient air was pulled at a high flow rate (~2000 slm) through a Teflon-coated glass inlet (3.8 cm I.D, 76.2 cm long). A subsampled portion of this gas stream was then directed into the CIMS, either directly or after analytes are separated on a 1-m GC column. Analyte concentrations were quantified using a CF_3O^- reagent ion which is sensitive towards the detection of oxygenated multifunctional compounds such as organic peroxides

and nitrates (Crounse et al., 2006; Paulot et al., 2009; St. Clair et al., 2010; Hyttinen et al., 2018). In the field, the instrument collected data in automated 1 hour cycles with GC separation occuring in the latter half hour.

Laboratory experiments were performed on a prototype version of the GC-CIMS field instrument. Analytes were trapped on a portion of a 1-m column that was submerged in an isopropanol bath chilled to approximately -20^{o}C. The column was then held inside a Varian CP-3800 GC oven and heated. The column effluent was then directed into a CF_3O^- CIMS.

Measurement uncertainty from field data arose from low analyte signal, caused by a combination of low ambient concentrations and the high instrument dilution needed to prevent simultaneous trapping of water (Vasquez et al., 2018). Additional details regarding data processing and measurement uncertainties can be found in Appendix B.

3.2.3 1-D atmospheric model

A 1-D atmospheric model was used to interpret ambient measurements collected during the Caltech field study. The model simulates the emission, deposition, vertical transport and photochemical oxidation of 250 species in an atmospheric column tuned to replicate conditions observed during the 2010 CalNex-LA campaign which also took place on the Caltech campus. The model combines the RACM2 chemical mechanism (Goliff et al., 2013) with the condensed isoprene oxidation mechanisms described in Wennberg et al. (2018) and IHN deposition rates based on measurements made by Nguyen et al. (2015). Vertical transport is simulated in the model using K-theory (Wolfe and Thornton, 2011) and its implementation in the model is described in more detail in Appendix B.

Given the uncertainty in local isoprene emissions due to vegetation heterogeneity in and around the Pasadena area, sensitivity tests were performed to determine a reasonable emission rate that produced agreement between measured and modeled isoprene concentrations. Aerosol liquid water concentrations (ALWC) used to model IHN partitioning were calculated using ISORROPIA-II (Fountoukis and Nenes, 2007) using inputs of temperature, RH, and inorganic aerosol components measured during CalNex-LA and compared with results presented in Guo et al. (2017).

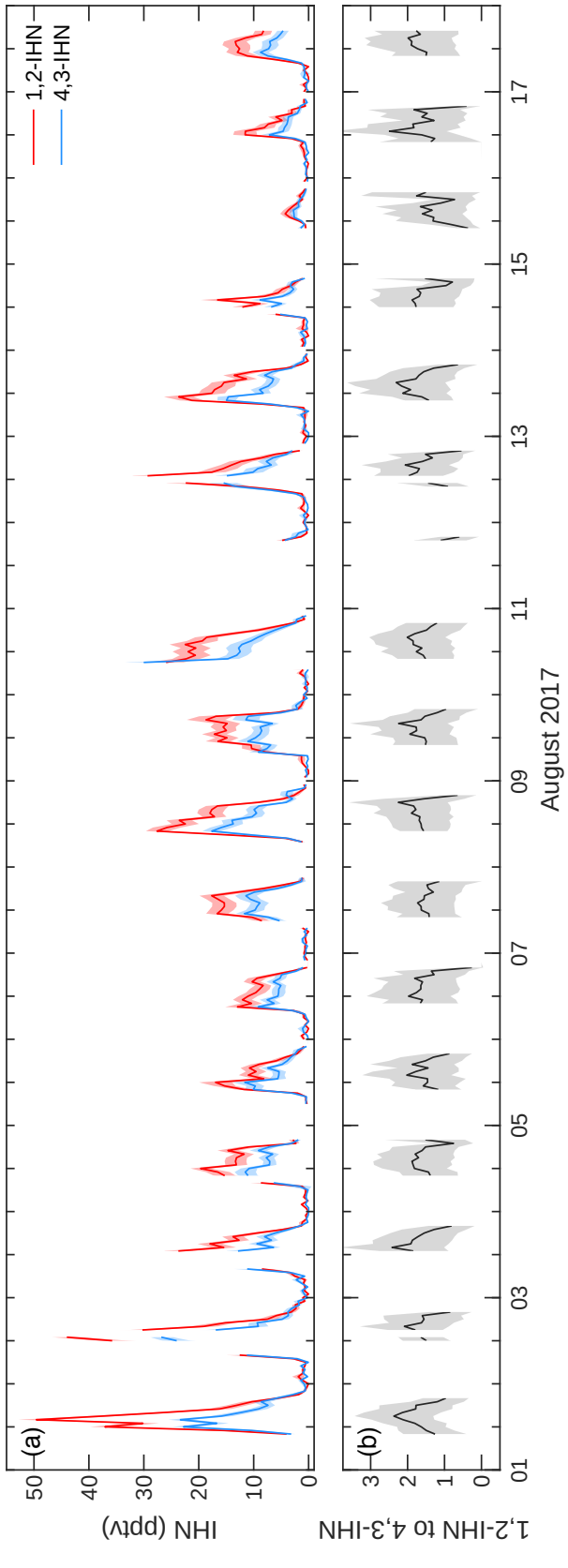

Figure 3.1: Data obtained by the GC-CIMS during the Caltech field study shown as a (A) time series of 1,2-IHN (red) and 4,3-IHN (blue). Solid lines represent the hourly GC measurements and the shaded regions encompass the error of those measurements. Also shown is the (B) observed daytime (10:00–20:00 local time) isomer ratio of 1,2-IHN to 4,3-IHN during the Caltech field study.

3.3 Results and discussion

3.3.1 Field observations

Hourly measurements of the ambient concentrations of the IHN isomers were obtained between 1 –17 August, 2017 using a gas chromatography chemical ionization mass spectrometer (GC-CIMS) deployed atop the Millikan Library (44 m AGL) which is located on the California Institute of Technology (Caltech) campus in Pasadena, CA ($[OH]_{avg,\ peak} = 5 \times 10^6$ molecules cm^{-3} (Griffith et al., 2016); $[NO]_{avg,\ daytime} = 2.5$ ppbv). Details of the field site, measurement technique, and data processing are provided in the *Materials and Methods* and Appendix B.

Daytime observations (10:00–20:00 local time) of 1,2-IHN and 4,3-IHN from Caltech (Fig. 3.1) suggest an additional IHN sink is present in the atmosphere that disproportionately affects the 1,2-IHN isomer. We observed a daily, rapid decline of the IHN isomer ratio starting in the mid-afternoon (around 15:00 local time). Chromatograms collected at this site (Fig 3.2) illustrate that this was caused by a drop in the concentration of 1,2-IHN relative to 4,3-IHN. However, these observations are not explained using known gas-phase chemistry as the gas-phase lifetime of 1,2-IHN is expected to be longer than 4,3-IHN due to its slower reaction rate with OH (Lee et al., 2014). This is verified in Fig. 3.3 where the IHN isomer ratio simulated with a 1-D atmospheric model (red) consistently overpredicts the observed ratio (black), with the largest discrepancies occurring in the evening. The model shows that when considering only the gas-phase isoprene chemistry (Wennberg et al., 2018) and dry deposition (Nguyen et al., 2015), the IHN isomer ratio should steadily increase during this time (in response to faster 4,3-IHN loss via OH), in contrast with observations.

3.3.2 Laboratory evidence for IHN hydrolysis

Chamber studies

Isoprene oxidation experiments performed in a 24 m^3 chamber (see Appendix B) suggest that 1,2-IHN is hydrolyzed much faster than 4,3-IHN, lending one possible explanation to the observed trend of the ambient IHN isomer ratio measured at Caltech. In the dark chamber, the lifetime of the 1,2-IHN isomer decreased from 45 min at 50% RH to 15 min at 90% RH—whereas no change in the 4,3-IHN lifetime was observed. In addition, chromatograms obtained from these experiments (see Fig. B.2) mirrored those collected in the field (Fig. 3.2) and accompanying signals

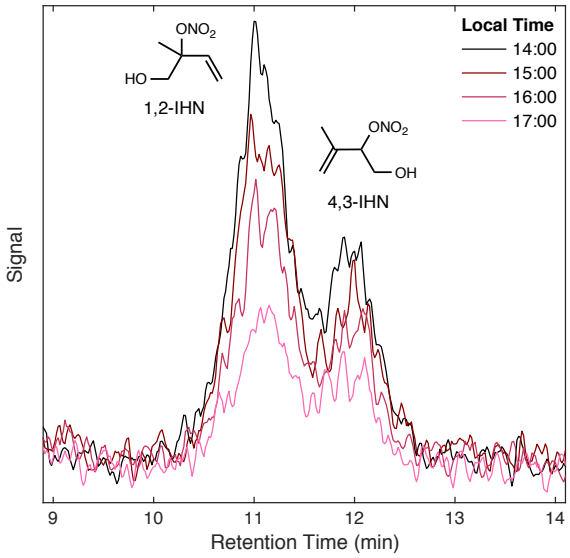

Figure 3.2: Four chromatograms of IHN collected during the Caltech field study on August 1, 2017 show that the peak area of 1,2-IHN declines more rapidly than 4,3-IHN in the late afternoon.

of IHN hydrolysis products, such as the isoprene diol and a small yield of 1,4-IHN (Teng et al., 2017), were observed.

During these experiments, it is likely that IHN hydrolysis was occurring within a condensed-phase reservoir formed by the uptake of water at high RH by salts that had been previously deposited on the chamber walls. Similar experiments with high levels of added ammonium sulfate seed (up to 500 μg m^{-3}) did not measurably alter the decay rate. In addition, gas-phase experiments performed in a clean 1 m^3 Teflon chamber bag did not show any decay of 1,2-IHN at high RH (>80%) over a 12 hour period. Unfortunately, this complicates interpretation of the loss rates observed in the 24 m^3 chamber, as they are likely dependent on the volume of liquid material on the walls, as well as the mixing and transport processes.

3.3.2.1 ^{1}H NMR

As we were unable to provide a quantitative constraint on the hydrolysis loss through the chamber experiments, we use a newly-developed synthetic route to 1,2-IHN (see Appendix B) with ^{1}H NMR to probe the kinetics of the 1,2-IHN hydrolysis loss (Darer et al., 2011). For this experiment, a known volume of synthesized 1,2-IHN was added to a known volume of CD_3Cl, rapidly mixed, and quickly analyzed using

^{1}H NMR (see Fig. B.3). In a similar fashion, 1,2-IHN was added to D_2O, mixed and analyzed. No 1,2-IHN ^{1}H NMR signals remained in the D_2O sample (elapsed time from mixing to completion of analysis <1 minute). Based on the signal-to-noise ratio of the 1,2-IHN ^{1}H NMR signals in the CD_3Cl sample, we assign an upper limit of 10 s for the aqueous hydrolysis lifetime of 1,2-IHN in D_2O (see Appendix B). For comparison, Jacobs et al. (2014) measured the 4,3-IHN hydrolysis lifetime to be approximately 17.5 h in D_2O. The large difference in the hydrolysis lifetimes of these two isomers is consistent with both our chamber and field observations.

3.3.3 Model simulations of IHN hydrolysis

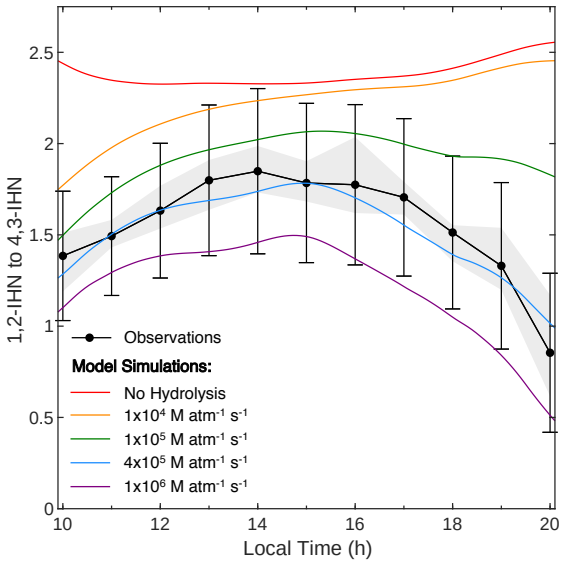

Figure 3.3: Comparison of observed (black) and modeled (colored lines) diurnal profiles of the IHN isomer ratio from the Caltech field study. Each black dot represents the median of the hourly IHN isomer ratios, while the gray region encompasses the 25th and 75th percentile values, and the error bars represent the error in the study-averaged results. The model simulation that includes dry deposition and gas-phase chemistry only (red) overpredicted the IHN ratio, particularly in the afternoon when 4,3-IHN loss should be faster than that of 1,2-IHN due to OH oxidation. Inclusion of a condensed-phase hydrolysis loss coefficient of 1,2-IHN (defined as, k^*_{hydro}, a product of Henry's law constant and aqueous hydrolysis rate ($K_H \times k_{aq}$)), enables the model to reproduce the observed IHN isomer ratio using $k^*_{hydro} = 4 \times 10^5$ M atm^{-1} s^{-1} (blue).

Based on laboratory evidence, we incorporated condensed-phase hydrolysis into a 1-D box model to test whether this loss is consistent with the observed diurnal profile of the IHN isomer ratio observed at Caltech. Details of this model are provided in the *Materials and Methods* and Appendix B. Briefly, the model uses

the recently developed condensed isoprene mechanism (Wennberg et al., 2018) and K-theory (Wolfe and Thornton, 2011) to simulate the formation, oxidation, and mixing of IHN isomers in an atmospheric column representative of conditions observed during CalNex-LA (Ryerson et al., 2013), which took place on the Caltech campus in 2010. Aerosol liquid water (ALW) concentrations used in the model were calculated with ISOROPPIA-II, (Fountoukis and Nenes, 2007) using aerosol measurements obtained from CalNex-LA. Our calculated ALW was compared with results presented in Guo et al. (2017). We assume that IHN uptake into the particle is reversible and in instantaneous equilibrium with gas-phase concentrations (Pye et al., 2010).

The Henry's law constant (K_H) and aqueous hydrolysis rate ($k_{(aq)}$) of 1,2-IHN is unknown. For K_H, we incorporate a temperature-dependent estimate of this parameter, based on the findings of Shepson et al. (1996) and as described in more detail in Appendix B. Constrained by the temperatures used in the model (8.4–23.2°C), this gives an estimated K_H range of 1.08 –1.97×10^5 M atm^{-1}. For $k_{(aq)}$, we vary this value for each simulation and assume the rate doubles for each 10°C increase in temperature (see Appendix B). We then determine what the product of these two parameters, referred to here as the hydrolysis loss coefficient (k^*_{hydro} = $K_H \times k_{(aq)}$) must be to explain the observed diurnal dependence on the IHN isotope ratio.

Figure 3.3 shows how modeled IHN isomer ratios compare to observations over a range of hydrolysis loss coefficients, with the best agreement occurring when $k^*_{hydro} = 4 \times 10^5$ M atm^{-1} s^{-1} (blue). Given the estimated range of K_H, this implies a $k_{(aq)}$ of 2.0–3.7 s^{-1}, a range not inconsistent with our NMR study. At this rate, the heterogenous lifetime of 1,2-IHN against hydrolysis ranges between 4–7 h in the daytime driven by changes in ALW (3.6–6 μg m^{-3}). This loss contributes to approximately 30% of the mid-day loss of the 1,2-IHN isomer, with that fraction increasing to over 50% in the evening (after 18:00 local time), as a result of both the increased ALW concentrations and lower OH.

Our model results are relatively insensitive to additional parameters such as the assumed IHN deposition velocity, horizontal advective loss, or vertical mixing rates (see Appendix B). However, we find that the modeled ratio is quite sensitive to our assumed ALW. The ALW in our model was estimated from aerosol measurements collected in May–July, which, on average, is a more humid time period than August. In addition, the United States has experienced a steady decline in SO_2 emissions

since 2010 (USEPA, 2018) which has been repeatedly linked to the reduction of sulfate in aerosols in the summer (Hand et al., 2012; Paulot et al., 2017). As sulfate affects the hygroscopicity of the particle, lower humidity and sulfate concentrations would result in lower ALW (Carlton and Turpin, 2013) than would be predicted using CalNex-LA ALW measurements. If we have overestimated ALW, than the inferred k^*_{hydro} is too small.

3.4 Atmospheric implications

We have implemented the inferred k^*_{hydro} of 1,2-IHN into the global chemical transport model, GEOS-Chem, that has been recently updated to reflect the most recent laboratory studies of isoprene photochemistry (Bates and Jacob, 2019). Shown in Fig. 3.4 is the change in simulated NO and O_3 when we add 1,2-IHN hydrolysis with a rate similar to that of our 1-D model (in this case, $k^*_{hydro} = 3 \times 10^5$ M atm^{-1} s^{-1}; see Appendix B) to the standard GEOS-Chem model. Consistent with the findings of Paulot et al. (2012), we find that over forested regions, the loss of NO_x via the formation of IHN and its subsequent conversion to HNO_3 through condensed-phase hydrolysis (see Fig. B.8) leads to large reductions in simulated NO levels in the tropics (independent of seasonality; Fig. 3.4A) and during the Northern Hemisphere summer (Fig. 3.4B). This change, in turn, substantially reduces the calculated concentrations of OH (see Fig. B.8) and O_3 (Fig. 3.4C-D). Of note, surface ozone in the southeast US is ~5 ppb lower in the summer with the addition of 1,2-IHN hydrolysis (Fig. 3.4D)—a change that brings the simulations into agreement with ground-based observations. Previously, to properly simulate surface ozone in GEOS-Chem, an ad hoc reduction between 30–60% in NO_x emissions had been suggested (Travis et al., 2016).

Although our laboratory measurements are unable to quantify the aqueous hydrolysis rate of 1,2-IHN, we find that the global impact of this chemistry is largely insensitive to the assumed hydrolysis loss coefficient, provided that k^*_{hydro} is at least 3×10^5 M atm^{-1} s^{-1} (see Fig. B.7). The insensitivity of our simulations to k^*_{hydro} above most of the world's forests is a result of the low calculated OH levels ($[OH]_{avg} < 5 \times 10^5$ molecules cm^{-3}; see Fig. B.10), different from the conditions of the Caltech field site. With such low OH, the gas-phase lifetime of IHN approaches 24 hours and, as a result, hydrolysis outcompetes all other IHN loss processes.

In conclusion, we present a rare observational constraint on the isomer-specific fate of IHN using both laboratory and field measurements obtained using gas

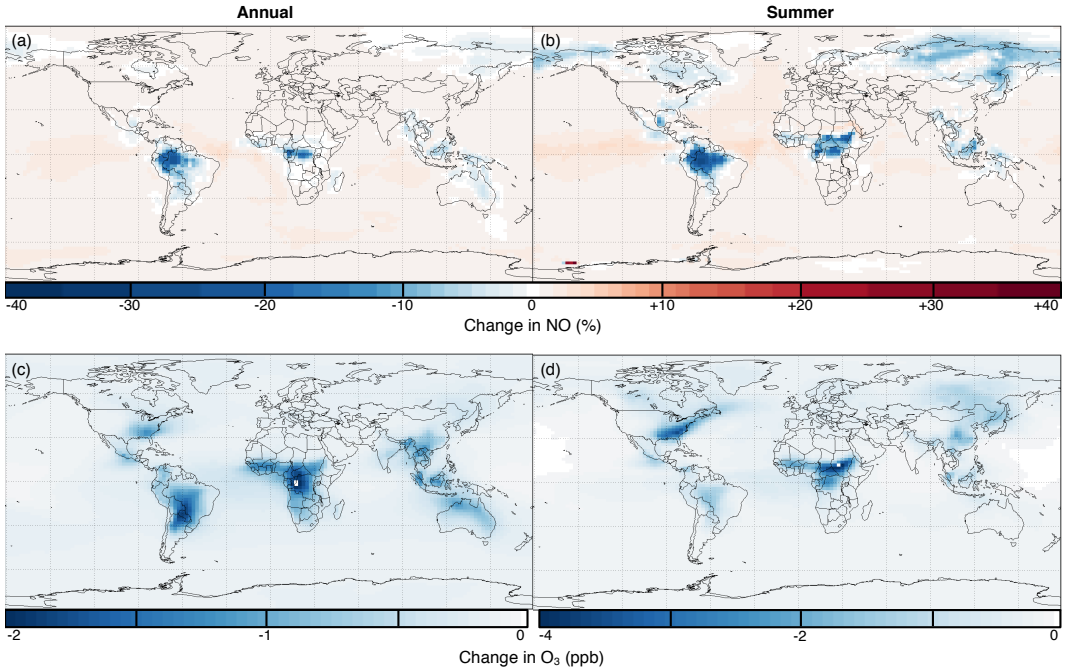

Figure 3.4: The standard GEOS-Chem model was updated to include an 1,2-IHN hydrolysis rate of $k^*_{hydro} = 3 \times 10^5$ M atm^{-1} s^{-1}. The impact of this loss on NO and ozone was then assessed through both annual and summer (1-31 July) simulations conducted in the lowest 1 km of the atmosphere. The addition of this IHN sink resulted in a ~40% decrease in NO in the tropics throughout the year (A), and a lesser, but still substantial decrease in the Northern Hemisphere during the summer (B), with respect to the base model. Likewise, O_3 concentrations also experienced the same spatial and seasonal decrease as NO (C-D). Of note, surface ozone in the southeast US is 5 ppb lower in the summer (D), causing this updated model to better agree with ground-based observations.

chromatography-chemical ionization mass spectrometry. Our data suggest that global atmospheric photochemistry is remarkably sensitive to the hydrolysis of a single isoprene hydroxy nitrate isomer, 1,2-IHN. Using GEOS-Chem, we simulate the effect a hydrolysis rate of at least 3×10^5 M atm^{-1} s^{-1} has on NO, O_3, OH and HNO_3 concentrations in the lower atmosphere. We find that this added loss process represents the majority of the IHN loss over forested regions, resulting in a substantial decrease of simulated NO in the tropics (year-round), and in the Northern Hemisphere during the summer. This drop in NO, in turn, results in lower concentrations of simulated ozone—allowing for better agreement between this model and ground-based observations, especially in the southeast US. Lastly, 1,2-IHN hydrolysis acts as a significant source of HNO_3 that is on par with OH + NO_2.

Acknowledgements

Development of the GC-CIMS was supported by the NSF Major Research Instrumentation Program under Grant AGS-1428482 and the field and laboratory studies it participated in were supported by additional NSF funding (Grant AGS-1240604). We thank the Caltech campus and affiliated staff for accommodating our 2017 field study. Work performed by K.T.V. and H.M.A. was also supported by NSF through the Graduate Research Fellowship.

References

Bates, K. H. and Jacob, D. J. A new model mechanism for atmospheric oxidation of isoprene: global effects on oxidants, nitrogen oxides, organic products, and secondary organic aerosol. *Atmos. Chem. Phys.*, 19(14):9613–9640, 2019. doi: 10.5194/acp-19-9613-2019.

Bean, J. K. and Hildebrandt Ruiz, L. Gas-particle partitioning and hydrolysis of organic nitrates formed from the oxidation of α-pinene in environmental chamber experiments. *Atmos. Chem. Phys.*, 16(4):2175–2184, 2016. doi: 10.5194/acp-16-2175-2016.

Beaver, M. R., Clair, J. M. S., Paulot, F., Spencer, K. M., Crounse, J. D., LaFranchi, B. W., Min, K. E., Pusede, S. E., Wooldridge, P. J., Schade, G. W., Park, C., Cohen, R. C., and Wennberg, P. O. Importance of biogenic precursors to the budget of organic nitrates: observations of multifunctional organic nitrates by CIMS and TD-LIF during BEARPEX 2009. *Atmos. Chem. Phys.*, 12(13):5773–5785, 2012. doi: 10.5194/acp-12-5773-2012.

Boyd, C. M., Sanchez, J., Xu, L., Eugene, A. J., Nah, T., Tuet, W. Y., Guzman, M. I., and Ng, N. L. Secondary organic aerosol formation from the β-pinene+NO_3 system: effect of humidity and peroxy radical fate. *Atmos. Chem. Phys.*, 15(13): 7497–7522, 2015. doi: 10.5194/acp-15-7497-2015.

Browne, E. C. and Cohen, R. C. Effects of biogenic nitrate chemistry on the NOx lifetime in remote continental regions. *Atmos. Chem. Phys.*, 12(24):11917–11932, 2012. doi: 10.5194/acp-12-11917-2012.

Browne, E. C., Min, K.-E., Wooldridge, P. J., Apel, E., Blake, D. R., Brune, W. H., Cantrell, C. A., Cubison, M. J., Diskin, G. S., Jimenez, J. L., Weinheimer, A. J., Wennberg, P. O., Wisthaler, A., and Cohen, R. C. Observations of total $RONO_2$ over the boreal forest: NOx sinks and HNO_3 sources. *Atmos. Chem. Phys.*, 13 (9):4543–4562, 2013. doi: 10.5194/acp-13-4543-2013.

Carlton, A. G. and Turpin, B. J. Particle partitioning potential of organic compounds is highest in the Eastern US and driven by anthropogenic water. *Atmos. Chem. Phys.*, 13(20):10203–10214, 2013. doi: 10.5194/acp-13-10203-2013.

Carlton, A. G., de Gouw, J., Jimenez, J. L., Ambrose, J. L., Attwood, A. R., Brown, S., Baker, K. R., Brock, C., Cohen, R. C., Edgerton, S., Farkas, C. M., Farmer, D., Goldstein, A. H., Gratz, L., Guenther, A., Hunt, S., Jaegló, L., Jaffe, D. A., Mak, J., McClure, C., Nenes, A., Nguyen, T. K., Pierce, J. R., de Sa, S., Selin, N. E., Shah, V., Shaw, S., Shepson, P. B., Song, S., Stutz, J., Surratt, J. D., Turpin, B. J., Warneke, C., Washenfelder, R. A., Wennberg, P. O., and Zhou, X. Synthesis of the Southeast Atmosphere Studies: Investigating fundamental atmospheric chemistry questions. *Bull. Amer. Meteor. Soc.*, 99(3):547–567, 2018. doi: 10.1175/BAMS-D-16-0048.1.

Crounse, J. D., McKinney, K. A., Kwan, A. J., and Wennberg, P. O. Measurement of gas-phase hydroperoxides by chemical ionization mass spectrometry. *Anal. Chem.*, 78(19):6726–6732, 2006. doi: 10.1021/ac0604235.

Darer, A. I., Cole-Filipiak, N. C., O'Connor, A. E., and Elrod, M. J. Formation and stability of atmospherically relevant isoprene-derived organosulfates and organonitrates. *Environ. Sci. Technol.*, 45:1895–1902, 2011. doi: 10.1021/es103797z.

Day, D. A., Liu, S., Russell, L. M., and Ziemann, P. J. Organonitrate group concentrations in submicron particles with high nitrate and organic fractions in coastal southern California. *Atmos. Environ.*, 44(16):1970–1979, 2010. ISSN 1352-2310. doi: 10.1016/j.atmosenv.2010.02.045.

Fisher, J. A., Jacob, D. J., Travis, K. R., Kim, P. S., Marais, E. A., Chan Miller, C., Yu, K., Zhu, L., Yantosca, R. M., Sulprizio, M. P., Mao, J., Wennberg, P. O., Crounse, J. D., Teng, A. P., Nguyen, T. B., St. Clair, J. M., Cohen, R. C., Romer, P., Nault, B. A., Wooldridge, P. J., Jimenez, J. L., Campuzano-Jost, P., Day, D. A., Hu, W., Shepson, P. B., Xiong, F., Blake, D. R., Goldstein, A. H., Misztal, P. K., Hanisco, T. F., Wolfe, G. M., Ryerson, T. B., Wisthaler, A., and Mikoviny, T. Organic nitrate chemistry and its implications for nitrogen budgets in an isoprene- and monoterpene-rich atmosphere: Constraints from aircraft (SEAC^{4}RS) and ground-based (SOAS) observations in the Southeast US. *Atmos. Chem. Phys.*, 16(9):5969–5991, 2016. doi: 10.5194/acp-16-5969-2016.

Fountoukis, C. and Nenes, A. ISORROPIA II: A computationally efficient thermodynamic equilibrium model for K^+-Ca^{2+}-Mg^{2+}-NH_4^+-Na^+-SO_4^{2-}-NO_3^--Cl^--H_2O aerosols. *Atmos. Chem. Phys.*, 7(17):4639–4659, 2007. doi: 10.5194/acp-7-4639-2007.

Giacopelli, P., Ford, K., Espada, C., and Shepson, P. B. Comparison of the measured and simulated isoprene nitrate distributions above a forest canopy. *J. Geophys. Res. Atmos.*, 110(D1), 2005. doi: 10.1029/2004JD005123.

Goliff, W. S., Stockwell, W. R., and Lawson, C. V. The regional atmospheric chemistry mechanism, version 2. *Atmos. Environ.*, 68:174–185, 2013. doi: 10.1016/j.atmosenv.2012.11.038.

Griffith, S. M., Hansen, R. F., Dusanter, S., Michoud, V., Gilman, J. B., Kuster, W. C., Veres, P. R., Graus, M., de Gouw, J. A., Roberts, J., Young, C., Washenfelder, R., Brown, S. S., Thalman, R., Waxman, E., Volkamer, R., Tsai, C., Stutz, J., Flynn, J. H., Grossberg, N., Lefer, B., Alvarez, S. L., Rappenglueck, B., Mielke, L. H., Osthoff, H. D., and Stevens, P. S. Measurements of hydroxyl and hydroperoxy radicals during CalNex-LA: Model comparisons and radical budgets. *J. Geophys. Res. Atmos.*, 121(8):4211–4232, 2016. doi: 10.1002/2015JD024358.

Guenther, A., Zimmerman, P., and Wildermuth, M. Natural volatile organic compound emission rate estimates for U.S. woodland landscapes. *Atmos. Environ.*, 28(6):1197–1210, 1994. doi: 10.1016/1352-2310(94)90297-6.

Guo, H., Liu, J., Froyd, K. D., Roberts, J. M., Veres, P. R., Hayes, P. L., Jimenez, J. L., Nenes, A., and Weber, R. J. Fine particle ph and gas–particle phase partitioning of inorganic species in Pasadena, California, during the 2010 CalNex campaign. *Atmos. Chem. Phys*, 17(9):5703–5719, 2017. doi: 10.5194/acp-17-5703-2017.

Hand, J. L., Schichtel, B. A., Malm, W. C., and Pitchford, M. L. Particulate sulfate ion concentration and SO_2 emission trends in the United States from the early 1990s through 2010. *Atmos. Chem. Phys.*, 12(21):10353–10365, 2012. doi: 10.5194/acp-12-10353-2012.

Horowitz, L. W., Fiore, A. M., Milly, G. P., Cohen, R. C., Perring, A., Wooldridge, P. J., Hess, P. G., Emmons, L. K., and Lamarque, J.-F. Observational constraints on the chemistry of isoprene nitrates over the eastern United States. *J. Geophys. Res. Atmos.*, 112(D12), 2007. doi: 10.1029/2006JD007747.

Hu, K. S., Darer, A. I., and Elrod, M. J. Thermodynamics and kinetics of the hydrolysis of atmospherically relevant organonitrates and organosulfates. *Atmos. Chem. Phys.*, 11(16):8307–8320, 2011. doi: 10.5194/acp-11-8307-2011.

Hyttinen, N., Otkjær, R. V., Iyer, S., Kjaergaard, H. G., Rissanen, M. P., Wennberg, P. O., and Kurtén, T. Computational comparison of different reagent ions in the chemical ionization of oxidized multifunctional compounds. *J. Phys. Chem. A*, 122(1):269–279, 2018. doi: 10.1021/acs.jpca.7b10015.

Jacobs, M. I., Burke, W. J., and Elrod, M. J. Kinetics of the reactions of isoprene-derived hydroxynitrates: Gas phase epoxide formation and solution phase hydrolysis. *Atmos. Chem. Phys.*, 14(17):8933–8946, 2014. doi: 10.5194/acp-14-8933-2014.

Lee, L., Teng, A. P., Wennberg, P. O., Crounse, J. D., and Cohen, R. C. On rates and mechanisms of OH and O_3 reactions with isoprene-derived hydroxy nitrates. *J. Phys. Chem. A*, 118(9):1622–1637, 2014. doi: 10.1021/jp4107603.

Li, J., Mao, J., Fiore, A. M., Cohen, R. C., Crounse, J. D., Teng, A. P., Wennberg, P. O., Lee, B. H., Lopez-Hilfiker, F. D., Thornton, J. A., Peischl, J., Pollack, I. B., Ryerson, T. B., Veres, P., Roberts, J. M., Neuman, J. A., Nowak, J. B., Wolfe,

G. M., Hanisco, T. F., Fried, A., Singh, H. B., Dibb, J., Paulot, F., and Horowitz, L. W. Decadal changes in summertime reactive oxidized nitrogen and surface ozone over the southeast United States. *Atmos. Chem. Phys.*, 18(3):2341–2361, 2018. doi: 10.5194/acp-18-2341-2018.

Liu, S., Shilling, J. E., Song, C., Hiranuma, N., Zaveri, R. A., and Russell, L. M. Hydrolysis of organonitrate functional groups in aerosol particles. *Aerosol Sci. Technol.*, 46(12):1359–1369, 2012. doi: 10.1080/02786826.2012.716175.

Mao, J., Paulot, F., Jacob, D. J., Cohen, R. C., Crounse, J. D., Wennberg, P. O., Keller, C. A., Hudman, R. C., Barkley, M. P., and Horowitz, L. W. Ozone and organic nitrates over the eastern United States: Sensitivity to isoprene chemistry. *J. Geophys. Res. Atmos.*, 118(19):11256–11268, 2013. doi: 10.1002/jgrd.50817.

Mao, J., Carlton, A., Cohen, R. C., Brune, W. H., Brown, S. S., Wolfe, G. M., Jimenez, J. L., Pye, H. O. T., Lee Ng, N., Xu, L., McNeill, V. F., Tsigaridis, K., McDonald, B. C., Warneke, C., Guenther, A., Alvarado, M. J., de Gouw, J., Mickley, L. J., Leibensperger, E. M., Mathur, R., Nolte, C. G., Portmann, R. W., Unger, N., Tosca, M., and Horowitz, L. W. Southeast Atmosphere Studies: Learning from model-observation syntheses. *Atmos. Chem. Phys.*, 18(4):2615–2651, 2018. doi: 10.5194/acp-18-2615-2018.

Müller, J.-F., Peeters, J., and Stavrakou, T. Fast photolysis of carbonyl nitrates from isoprene. *Atmos. Chem. Phys.*, 14(5):2497–2508, 2014. doi: 10.5194/acp-14-2497-2014.

Nguyen, T. B., Crounse, J. D., Teng, A. P., St. Clair, J. M., Paulot, F., Wolfe, G. M., and Wennberg, P. O. Rapid deposition of oxidized biogenic compounds to a temperate forest. *P. Natl. Acad. Sci.*, 112(5):E392–E401, 2015. doi: 10.1073/pnas.1418702112.

Paulot, F., Crounse, J. D., Kjaergaard, H. G., Kroll, J. H., Seinfeld, J. H., and Wennberg, P. O. Isoprene photooxidation: New insights into the production of acids and organic nitrates. *Atmos. Chem. Phys.*, 9(4):1479–1501, 2009. doi: 10.5194/acp-9-1479-2009.

Paulot, F., Henze, D. K., and Wennberg, P. O. Impact of the isoprene photochemical cascade on tropical ozone. *Atmos. Chem. Phys.*, 12(3):1307–1325, 2012. doi: 10.5194/acp-12-1307-2012.

Paulot, F., Fan, S., and Horowitz, L. W. Contrasting seasonal responses of sulfate aerosols to declining SO_2 emissions in the Eastern U.S.: Implications for the efficacy of SO_2 emission controls. *Geophys. Res. Lett.*, 44(1):455–464, 2017. doi: 10.1002/2016GL070695.

Perring, A. E., Pusede, S. E., and Cohen, R. C. An observational perspective on the atmospheric impacts of alkyl and multifunctional nitrates on ozone and secondary organic aerosol. *Chem. Rev.*, 113(8):5848–5870, 2013. doi: 10.1021/cr300520x.

Pye, H. O. T., Chan, A. W. H., Barkley, M. P., and Seinfeld, J. H. Global modeling of organic aerosol: The importance of reactive nitrogen (NO_x and NO_3). *Atmos. Chem. Phys.*, 10(22):11261–11276, 2010. doi: 10.5194/acp-10-11261-2010.

Rindelaub, J. D., McAvey, K. M., and Shepson, P. B. The photochemical production of organic nitrates from α-pinene and loss via acid-dependent particle phase hydrolysis. *Atmos. Environ.*, 100:193–201, 2015. doi: 10.1016/j.atmosenv.2014.11.010.

Rollins, A. W., Browne, E. C., Min, K.-E., Pusede, S. E., Wooldridge, P. J., Gentner, D. R., Goldstein, A. H., Liu, S., Day, D. A., Russell, L. M., and Cohen, R. C. Evidence for NOx control over nighttime SOA formation. *Science*, 337(6099): 1210–1212, 2012. doi: 10.1126/science.1221520.

Romer, P. S., Duffey, K. C., Wooldridge, P. J., Allen, H. M., Ayres, B. R., Brown, S. S., Brune, W. H., Crounse, J. D., de Gouw, J., Draper, D. C., Feiner, P. A., Fry, J. L., Goldstein, A. H., Koss, A., Misztal, P. K., Nguyen, T. B., Olson, K., Teng, A. P., Wennberg, P. O., Wild, R. J., Zhang, L., and Cohen, R. C. The lifetime of nitrogen oxides in an isoprene-dominated forest. *Atmos. Chem. Phys.*, 16(12): 7623–7637, 2016. doi: 10.5194/acp-16-7623-2016.

Ryerson, T. B., Andrews, A. E., Angevine, W. M., Bates, T. S., Brock, C. A., Cairns, B., Cohen, R. C., Cooper, O. R., de Gouw, J. A., Fehsenfeld, F. C., Ferrare, R. A., Fischer, M. L., Flagan, R. C., Goldstein, A. H., Hair, J. W., Hardesty, R. M., Hostetler, C. A., Jimenez, J. L., Langford, A. O., McCauley, E., McKeen, S. A., Molina, L. T., Nenes, A., Oltmans, S. J., Parrish, D. D., Pederson, J. R., Pierce, R. B., Prather, K., Quinn, P. K., Seinfeld, J. H., Senff, C. J., Sorooshian, A., Stutz, J., Surratt, J. D., Trainer, M., Volkamer, R., Williams, E. J., and Wofsy, S. C. The 2010 California research at the nexus of air quality and climate change (CalNex) field study. *J. Geophys. Res. Atmos.*, 118(11):5830–5866, 2013. doi: 10.1002/jgrd.50331.

Shepson, P. B., Mackay, E., and Muthuramu, K. Henry's law constants and removal processes for several atmospheric β-hydroxy alkyl nitrates. *Environ. Sci. Technol.*, 30(12):3618–3623, 1996. doi: 10.1021/es960538y.

Simon, H., Reff, A., Wells, B., Xing, J., and Frank, N. Ozone trends across the United States over a period of decreasing NO_x and VOC emissions. *Environ. Sci. Technol.*, 49(1):186–195, 2015. doi: 10.1021/es504514z.

Squire, O. J., Archibald, A. T., Griffiths, P. T., Jenkin, M. E., Smith, D., and Pyle, J. A. Influence of isoprene chemical mechanism on modeled changes in tropospheric ozone due to climate and land use over the 21st century. *Atmos. Chem. Phys.*, 15(9):5123–5143, 2015. doi: 10.5194/acp-15-5123-2015.

St. Clair, J. M., McCabe, D. C., Crounse, J. D., Steiner, U., and Wennberg, P. O. Chemical ionization tandem mass spectrometer for the in situ measurement of

methyl hydrogen peroxide. *Rev. Sci. Instrum.*, 81(9), 2010. doi: 10.1063/1.3480552.

Teng, A. P., Crounse, J. D., and Wennberg, P. O. Isoprene peroxy radical dynamics. *J. Am. Chem. Soc.*, 139(15):5367–5377, 2017. doi: 10.1021/jacs.6b12838.

Trainer, M., Buhr, M. P., Curran, C. M., Fehsenfeld, F. C., Hsie, E. Y., Liu, S. C., Norton, R. B., Parrish, D. D., Williams, E. J., Gandrud, B. W., Ridley, B. A., Shetter, J. D., Allwine, E. J., and Westberg, H. H. Observations and modeling of the reactive nitrogen photochemistry at a rural site. *J. Geophys. Res. Atmos.*, 96 (D2):3045–3063, 1991. doi: 10.1029/90JD02395.

Travis, K. R., Jacob, D. J., Fisher, J. A., Kim, P. S., Marais, E. A., Zhu, L., Yu, K., Miller, C. C., Yantosca, R. M., Sulprizio, M. P., Thompson, A. M., Wennberg, P. O., Crounse, J. D., St. Clair, J. M., Cohen, R. C., Laughner, J. L., Dibb, J. E., Hall, S. R., Ullmann, K., Wolfe, G. M., Pollack, I. B., Peischl, J., Neuman, J. A., and Zhou, X. Why do models overestimate surface ozone in the southeast united states? *Atmos. Chem. Phys.*, 16(21):13561–13577, 2016. doi: 10.5194/acp-16-13561-2016.

USEPA. Sulfur dioxide trends. https://www.epa.gov/air-trends/sulfur-dioxide-trends, 2018. Accessed 13 Apr 2019.

Vasquez, K. T., Allen, H. M., Crounse, J. D., Praske, E., Xu, L., Noelscher, A. C., and Wennberg, P. O. Low-pressure gas chromatography with chemical ionization mass spectrometry for quantification of multifunctional organic compounds in the atmosphere. *Atmos. Meas. Tech.*, 11:6815–6832, 2018. doi: 10.5194/amt-11-6815-2018.

Wennberg, P. O., Bates, K. H., Crounse, J. D., Dodson, L. G., McVay, R. C., Mertens, L. A., Nguyen, T. B., Praske, E., Schwantes, R. H., Smarte, M. D., St Clair, J. M., Teng, A. P., Zhang, X., and Seinfeld, J. H. Gas-phase reactions of isoprene and its major oxidation products. *Chem. Rev.*, 2018. doi: 10.1021/acs.chemrev.7b00439.

Wolfe, G. M. and Thornton, J. A. The Chemistry of Atmosphere-Forest Exchange (CAFE) model-Part 1: Model description and characterization. *Atmos. Chem. Phys.*, 11(1):77–101, 2011. doi: 10.5194/acp-11-77-2011.

Wolfe, G. M., Hanisco, T. F., Arkinson, H. L., Bui, T. P., Crounse, J. D., Dean-Day, J., Goldstein, A., Guenther, A., Hall, S. R., Huey, G., Jacob, D. J., Karl, T., Kim, P. S., Liu, X., Marvin, M. R., Mikoviny, T., Misztal, P. K., Nguyen, T. B., Peischl, J., Pollack, I., Ryerson, T., St. Clair, J. M., Teng, A., Travis, K. R., Ullmann, K., Wennberg, P. O., and Wisthaler, A. Quantifying sources and sinks of reactive gases in the lower atmosphere using airborne flux observations. *Geophys. Res. Lett.*, 42(19):8231–8240, 2015. doi: 10.1002/2015GL065839.

Wu, S., Mickley, L. J., Jacob, D. J., Logan, J. A., Yantosca, R. M., and Rind, D. Why are there large differences between models in global budgets of tropospheric ozone? *J. Geophys. Res.*, 112:D05302, 2007. doi: 10.1029/2006JD007801.

Xiong, F., McAvey, K. M., Pratt, K. A., Groff, C. J., Hostetler, M. A., Lipton, M. A., Starn, T. K., Seeley, J. V., Bertman, S. B., Teng, A. P., Crounse, J. D., Nguyen, T. B., Wennberg, P. O., Misztal, P. K., Goldstein, A. H., Guenther, A. B., Koss, A. R., Olson, K. F., de Gouw, J. A., Baumann, K., Edgerton, E. S., Feiner, P. A., Zhang, L., Miller, D. O., Brune, W. H., and Shepson, P. B. Observation of isoprene hydroxynitrates in the southeastern United States and implications for the fate of NOx. *Atmos. Chem. Phys.*, 15(19):11257–11272, 2015. doi: 10.5194/acp-15-11257-2015.

Xu, L., Suresh, S., Guo, H., Weber, R. J., and Ng, N. L. Aerosol characterization over the southeastern United States using high-resolution aerosol mass spectrometry: Spatial and seasonal variation of aerosol composition and sources with a focus on organic nitrates. *Atmos. Chem. Phys.*, 15(13):7307–7336, 2015. doi: 10.5194/acp-15-7307-2015.

Zare, A., Romer, P. S., Nguyen, T., Keutsch, F. N., Skog, K., and Cohen, R. C. A comprehensive organic nitrate chemistry: Insights into the lifetime of atmospheric organic nitrates. *Atmos. Chem. Phys.*, 18(20):15419–15436, 2018. doi: 10.5194/acp-18-15419-2018.

Chapter 4

CONCLUSIONS AND FUTURE OUTLOOK

This thesis described methods for the sensitive, non-invasive, isomer-specific detection of oxygenated volatile organic compounds (OVOCs)—atmospheric species which play key roles in the formation of air pollutants such as ozone (O_3) and secondary organic aerosols (SOA). One application of this technology, dubbed the GC-CIMS, was showcased during field and chamber studies performed on the California Institute of Technology campus. Data collected here was used to provide additional insight into the atmospheric fate of the 1,2-isoprene hydroxy nitrate (1,2-IHN), the most abundant IHN isomer.

To recap, by using the GC-CIMS, we were able to obtain observational, *in situ* evidence that the 1,2-IHN experiences a rapid loss not experienced by 4,3-IHN, the second most abundant IHN isomer. Subsequent chamber studies suggested that this loss was likely condensed-phase hydrolysis, a fact that had remained elusive due to analytical challenges that were caused by the isomer's high reactivity and the lack of a pure synthetic standard. Then, through a combination of ^{1}H-NMR and 1D modeling, we determined that this loss pathway was competitive with OH oxidation, at least in Pasadena, CA. It is possible that 1,2-IHN hydrolysis would outcompete OH oxidation in other areas where OH concentrations are lower and/or aerosol liquid water is higher.

Therefore, we conclude that because 1,2-IHN is the dominant IHN isomer—making up between 50 to 80% of the isoprene nitrate concentration globally—this organic nitrate, and by extension, isoprene, should be treated as an important sink of NO_x. Factoring this into global chemical transport models, like GEOS-CHEM, we see that the addition of 1,2-IHN hydrolysis leads to reductions of simulated ozone concentrations, bringing them closer in line with observations. This 1,2-IHN loss process also doubles as a significant source of HNO_3, on par with OH + NO_2, a reaction that is typically cited as the primary way NO_x was removed from the atmosphere (Brown et al., 1999).

This new understanding of the atmospheric chemistry of 1,2-IHN has already been used to elucidate subsequent steps of isoprene's complex oxidation mechanism in both the gas Bates et al. (2021) and particle phases Abellar et al. (2021), as well

as improve our understanding of forest-atmosphere interactions (Wei et al., 2021). It should be noted moving forward, however, that our estimated hydrolysis rate is a lower bound and the actual rate could be much faster. As such, additional research is needed to further constrain this loss and, by extension, improve the accuracy of atmospheric models.

Furthermore, although not included in this thesis, the GC-CIMS has also granted additional insight into other branches of the isoprene oxidation mechanism. Data collected from its deployment during the 2016 Program for Research on Oxidants; Photochemistry, Emissions and Transport–Atmospheric Measurements of Oxidants in Summer (PROPHET-AMOS) campaign captured isomer-level changes in the concentrations of the isoprene hydroxy hydroperoxides (ISOPOOH) (Allen, 2021). ISOPOOH is an important isoprene oxidation product formed in a separate branch from IHN, wherein RO_2 reacts with HO_2 as opposed to NO. The subsequent oxidation of ISOPOOH can lead to the formation of low-volatility products which act as precursors to secondary organic aerosols (SOA) formation.

In the low-NO_x, forested environment at the PROPHET site, preliminary data has shown that the observed isomer ratio of 1,2- to 4,3-ISOPOOH is less than half the value expected based on model simulations. Based on this, we conclude that the model failed to account for some aspect of the ISOPOOH chemistry. However, unlike IHN, the loss processes of ISOPOOH are well-studied, so missing sinks are unlikely to be the culprit. Rather, based on recent chamber studies, we hypothesize that this phenomenon is due to the isomerization of the isoprene peroxy radicals that form 4,3-ISOPOOH (Teng et al., 2017). Incorporating RO_2 isomerization into our box model brings the isomer ratios closer to agreement, but additional work is needed to confirm this finding.

Beyond isoprene chemistry, the GC-CIMS has also supported a number of chamber studies looking at the atmospheric chemistry of other NMHCs (e.g. Praske et al., 2018b; Møller et al., 2019; Xu et al., 2019, 2020). For example, the GC-CIMS was used to explore the reaction kinetics of benzene, which is a known carcinogen that contributes to new-particle formation (Xu et al., 2020). The GC-CIMS has also aided in the investigation of atmospheric autooxidation (Praske et al., 2018b; Møller et al., 2019; Xu et al., 2019), unimolecular chemistry that has only recently been found to be relevant under atmospheric conditions. Although autooxidation has been implicated in the generation of low-volatility molecules (Crounse et al., 2013), experimental data is currently lacking (Praske et al., 2018a).

More recently, the GC-CIMS was deployed on the Caltech campus during the 2021 Re-Evaluating the Chemistry of Air Pollutants in California (RECAP-CA), a campaign that aims to study how the atmospheric chemistry has shifted in the Los Angeles basin in response to decreasing NO_x levels. Here, data collected with the GC-CIMS will be used to study the temporal variability of a range of organic nitrates and peroxides, which can then be used to answer pressing questions regarding ozone and particle formation in the area.

All together, these studies showcase the versatility of this analytical technique, especially when considering that the applications discussed here only represent a subset of its potential. That said, despite its valuable contributions to atmospheric chemistry, limitations currently exist. For instance, many higher volatility OVOCs are unable to be cryotrapped efficiency at our chosen field trapping temperature of -20^{o}C. Although this temperature was chosen as a compromise between analyte retention and avoidance of water retention, further optimization of trapping conditions can improve the chromatography for these species, especially under atmospherically-relevant conditions. In addition, the field version of the GC-CIMS discussed here contains a 1-meter column. Although this has proven sufficient for the isomer-separation of the OVOCs relevant to this thesis, isomers of other atmospheric species can still co-elute, once again hiding crucial structure-activity relationships. Longer GC columns can alleviate this issue, as has been shown through the lab operation of this instrument (Teng et al., 2017; Praske et al., 2018b; Møller et al., 2019; Xu et al., 2019). However, if used during field operation, additional optimization will be required to ensure that the instrument's analysis time is not lengthened to the point where it cannot sufficiently capture diurnal variations of atmospheric species.

In conclusion, the future of the GC-CIMS is full of promise and will almost certainly be used in many more applications than those covered in this thesis. With further improvements, its continued usage will almost certainly increase our understanding of atmospheric chemistry.

References

Abellar, K. A., Cope, J. D., and Nguyen, T. B. Second-order kinetic rate coefficients for the aqueous-phase hydroxyl radical (OH) oxidation of isoprene-derived secondary organic aerosol compounds at 298 K. *Environ. Sci. Technol.*, 55(20): 13728–13736, 2021. doi: 10.1021/acs.est.1c04606.

Allen, H. M. *Constraining the Formation and Fate of Hydroperoxides in the Remote Atmosphere*. PhD thesis, California Insitute of Technology, Pasadena, CA, May 2021.

Bates, K. H., Cope, J. D., and Nguyen, T. B. Gas-phase oxidation rates and products of 1,2-dihydroxy isoprene. *Environ. Sci. Technol.*, 55(20):14294–14304, 2021. doi: 10.1021/acs.est.1c04177.

Brown, S. S., Talukdar, R. K., and Ravishankara, A. Rate constants for the reaction oh+ no2+ m→ hno3+ m under atmospheric conditions. *Chem. Phys. Lett.*, 299 (3-4):277–284, 1999. doi: 10.1016/S0009-2614(98)01283-4.

Crounse, J. D., Nielsen, L. B., Jørgensen, S., Kjaergaard, H. G., and Wennberg, P. O. Autoxidation of organic compounds in the atmosphere. *J. Phys. Chem. Lett.*, 4 (20):3513–3520, 2013. doi: 10.1021/jz4019207.

Møller, K. H., Praske, E., Xu, L., Crounse, J. D., Wennberg, P. O., and Kjaergaard, H. G. Stereoselectivity in atmospheric autoxidation. *J. Phys. Chem. Lett.*, 10(20): 6260–6266, 2019. doi: 10.1021/acs.jpclett.9b01972.

Praske, E., Otkjær, R. V., Crounse, J. D., Hethcox, J. C., Stoltz, B. M., Kjaergaard, H. G., and Wennberg, P. O. Atmospheric autoxidation is increasingly important in urban and suburban north america. *P. Natl. Acad. Sci.*, 115(1):64–69, 2018a. doi: 10.1073/pnas.1715540115.

Praske, E., Otkjær, R. V., Crounse, J. D., Hethcox, J. C., Stoltz, B. M., Kjaergaard, H. G., and Wennberg, P. O. Intramolecular hydrogen shift chemistry of hydroperoxy-substituted peroxy radicals. *J. Phys. Chem. A*, 123(2):590–600, 2018b. doi: 10.1021/acs.jpca.8b09745.

Wei, D., Alwe, H. D., Millet, D. B., Bottorff, B., Lew, M., Stevens, P. S., Shutter, J. D., Cox, J. L., Keutsch, F. N., Shi, Q., Kavassalis, S. C., Murphy, J. G., Vasquez, K. T., Allen, H. M., Praske, E., Crounse, J. D., Wennberg, P. O., Shepson, P. B., Bui, A. A. T., Wallace, H. W., Griffin, R. J., May, N. W., Connor, M., Slade, J. H., Pratt, K. A., Wood, E. C., Rollings, M., Deming, B. L., Anderson, D. C., and Steiner, A. L. FORest Canopy Atmosphere Transfer (FORCAsT) 2.0: Model updates and evaluation with observations at a mixed forest site. *Geosci. Model Dev.*, 14(10):6309–6329, 2021. doi: 10.5194/gmd-14-6309-2021.

Xu, L., Møller, K. H., Crounse, J. D., Otkjær, R. V., Kjaergaard, H. G., and Wennberg, P. O. Unimolecular reactions of peroxy radicals formed in the oxidation of α-pinene and β-pinene by hydroxyl radicals. *J. Phys. Chem. A*, 123(8):1661–1674, 2019. doi: 10.1021/acs.jpca.8b11726.

Xu, L., Møller, K. H., Crounse, J. D., Kjaergaard, H. G., and Wennberg, P. O. New insights into the radical chemistry and product distribution in the oh-initiated oxidation of benzene. *Environ. Sci. Technol.*, 54(21):13467–13477, 2020. doi: 10.1021/acs.est.0c04780.

Appendix A

SUPPLEMENTAL INFORMATION FOR LOW-PRESSURE GAS CHROMATOGRAPHY WITH CHEMICAL IONIZATION MASS SPECTROMETRY FOR QUANTIFICATION OF MULTIFUNCTIONAL ORGANIC COMPOUNDS IN THE ATMOSPHERE

A.1 Instrument calibration

Instrument calibrations were performed using four authentic standards for hydrogen cyanide (HCN), sulfur dioxide (SO_2), hydroxyacetone (HAc) and glycolaldehyde (GLYC) with HRToF-CIMS. For HCN and SO_2, calibrations were performed using a standard gas mixture (300 ppmv in N_2 and 50 ppmv in N_2, respectively) which were individually diluted with N_2 using mass flow controllers prior to being sampled by the HRToF-CIMS. Cylinder concentrations of these two gases were verified using Fourier-transform infrared spectroscopy (FTIR) using cross section data archived in the Pacific Northwest National Lab (PNNL) IR database (Sharpe et al., 2004). Gas-phase HAc mixture was created by flowing dry N_2 over the commercially available compound (Aldrich, 90%) into a 0.1 m^3 bag made of fluorinated ethylene propylene (Teflon-FEP) to obtain several ppmv HAc. This mixture was then further diluted with N_2 after being measured by the FTIR before entering the instrument. Gas-phase GLYC was produced by flowing dry N_2 through a three-ported vial which contained the commercially available glycolaldehyde dimer (Aldrich). During this process, the three way vial was gently heated and cotton was inserted downstream of the vial to collect particles and low vapor pressure impurities before the gas was transferred to the 0.1 m^3 bag. The remainder of the procedure for GLYC mirrors that of HAc.

Though we were able to calibrate these four gases, many compounds of interest are not commercially available and difficult to synthesize and purify. Therefore, the above experiments were performed simultaneously on the cToF-CIMS in order to directly compare the sensitivities of these two instruments. On average, the cToF-CIMS was 1.37±0.22 times more sensitive than HRToF-CIMS under the same operating conditions of the field deployments. For the analysis described within the main text, we use this ratio between the two instrument sensitivities to convert previously determined cToF-CIMS sensitivities from calibrations or estimated from the

ion-molecule collision rate which can be calculated using the dipole and polarizability of the analyte species (Paulot et al., 2009; Garden et al., 2009; Crounse et al., 2011).

A.2 Instrument characterization

A number of chamber experiments were performed to properly characterize the GC-HRToF-CIMS both prior to and following field deployment. A list of experiments discussed in this study can be found in Table A.1.

Reagents

1-propene (propene) (> 99%), 1-butene (> 99%), *cis*-2-butene (> 99%), *trans*-2-butene (> 99%) 2-methyl-propene (> 99%), isoprene (> 98%) and hydrogen peroxide (H_2O_2; 30% by weight in water) were purchased from Sigma Aldrich and used without further purification in the amounts listed in Table A.1. A nitric oxide standard gas tank (NO; 1994 ppmv in high purity N_2) used for the majority of experiments was prepared by Matheson. Methyl nitrite (CH_3ONO) was synthesized, purified and stored in a glass trap submerged in liquid nitrogen using methods described in Taylor et al. (1980). In most cases, CH_3ONO served as the HO_x precursor.

Chamber experiments

Instrument characterization experiments were conducted in either a 0.1 m^3 or 0.8 m^3 Teflon bag with a 6.35 mm PFA port used for the introduction and sampling of gases. During each experiment, the bag was filled with appropriate concentrations of reactants and placed inside a enclosure with UV reflective surfaces and eight UV lights ($\lambda_{peak} = 350$ nm). Addition of the alkene, CH_3ONO and NO was accomplished by filling a 500 cm^3 glass bulb with the compound to the desired pressure before filling with N_2 to reach approximately 993 hPa. If needed, the reagent gas was serially diluted up to two times by pumping down the bulb to the desired pressure and backfilling again with N_2. The contents of the bulb were then transferred to the chamber with the remaining bag volume filled with dry zero air. For experiment 4, H_2O_2 served as the HO_x source. Addition of H_2O_2 into the chamber was performed by flowing 20 L min^{-1} N_2 over 8 μL of H_2O_2 contained in a shallow glass vial for approximately 10 - 15 minutes to create a bag concentration of ~2 ppmv H_2O_2. In experiment 6, high RH conditions (~50%) were created by filling a portion of

Table A.1: Instrument characterization experiment list

Expt	HO_x Source, ppbv	NO, ppbv	VOC, ppbv	Objective
1	CH_3ONO, 50	100	Isoprene, 50	IonSrc Enhancement Ratio
2	CH_3ONO, 100	500	Isoprene, 100	IHN Transmission
				IonSrc Enhancement Ratio
3	CH_3ONO, 100	500	Isoprene, 100	IHN Peak Assignment
4	H_2O_2, 2000	0	Isoprene, 100	ISOPOOH + IEPOX Peak Assignment
				ISOPOOH + IEPOX Transmission
5	CH_3ONO, 100	0	Isoprene, 100	HPALD Peak Assignment
6	CH_3ONO, 100	500	Isoprene, 100	Column Humidity Effect
7	CH_3ONO, 100	500	*trans*-2-Butene, 100	Butene HN Peak Assignment
8	CH_3ONO, 100	500	2-methyl-Propene, 100	Butene HN Peak Assignment
9	CH_3ONO, 100	500	1-Butene, 100	Butene HN Peak Assignment
10	CH_3ONO, 100	500	*cis*-2-Butene, 100	Butene HN Peak Assignment
11	CH_3ONO, 100	500	Propene, 100	Propene HN Peak Assignment
12	CH_3ONO, 100	500	Propene, 100	Trap Linearity Test
			Isoprene, 100	

the bag volume with dry zero air that has passed through a water bubbler prior to entering the chamber.

Once all reagents were in the chamber bag, photochemistry was initiated upon illumination of 1-8 UV lights. Alkene oxidation occurred at approximately 298 K, with the exception of experiment 5 which was performed at an elevated temperature (315 K) to allow for increased rates of unimolecular isomerization. Experiment 5 also required longer peroxy radical lifetimes to produce a sufficient GC signal of these isomerization products. This was performed by using a single UV light in which all direct radiation was blocked allowing only the photons scattered off the walls to contribute to the chemistry.

For the majority of experiments, photochemistry was stopped when approximately 10% of the alkene had reacted, to minimize secondary chemistry of products. Chamber air was then sampled by the GC-HRToF-CIMS at approximately 2-3 L min^{-1} through ~2.4 m of 5.84 mm ID tubing to reduce residence time in and speed equilibration of the sampling line. Chamber analysis typically alternated between the direct CIMS and GC-CIMS sampling to assess any changes in concentration or transmission that may occur throughout the experiment. In most cases, GC effluent was directed into the ion source to allow for enhanced signal to noise (IS mode, see main text). Divergence from this procedure occurred during experiments 1 and 2 when determining the ion source enhancement ratio. During this time, each GC cycle alternated between IS mode and FT mode and the ratio of these two types of GC signals which were used to determine the signal enhancement. A similar procedure was followed when assessing the GC transmission of targeted analytes. In addition, output from the GC during trapping was also occasionally directed into the mass spectrometer to monitor potential breakthrough.

A.3 Previous design of GC assembly

Instrument upgrades occurred between the PROPHET and Caltech field studies to improve the chromatography and significantly reduce the need for GC downtime due to cooling system maintenance. These upgrades included a redesign of the GC assembly, which was necessary to fix some key issues experienced at PROPHET, such as large temperature gradients across the column and poor temperature control as a whole. The previous version of the field deployable GC assembly can be seen in Fig. A.1. Rather than two aluminum plates, this assembly consisted of a thin copper band. The column rested along the inner diameter of this band and was held

within a 1.59 mm O.D. copper tube. The GC was cooled as liquid CO_2 expanded and flowed along 3.18 mm tubing that was soldered onto the inside of the band (to increase thermal contact). The CO_2 liquid entered at one location in the ring positioned near the two ends of the column and its flow was split at a stainless steel tee to allow both sides of the ring to cool evenly. CO_2 flow and temperature were regulated as described in the main text, however GC temperature was measured at only one location on the ring, near the CO_2 inlet (Fig. A.1, red star).

Unfortunately, by having the CO_2 flow enter through only one location in the ring, we found that the temperature gradient of opposite sides of the ring could exceed several degrees. In addition, because temperature was only monitored in one location near the coldest point of the column, it is difficult to assess the quality of the GC trapping conditions. In contrast, the redesigned GC allows CO_2 to enter from the center of the plates and move outward to the diameter of the column ring. This ensures that the entire GC column is cooled at approximately the same rate. Furthermore, the addition of two more RTDs along the column also allow us to monitor the temperature gradient in real time and provides finer temperature control overall.

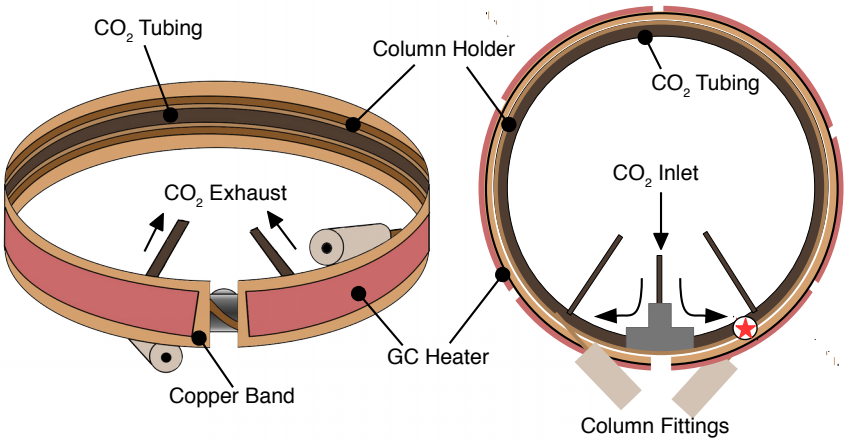

Figure A.1: Original design of the GC cryotrapping and heating assembly used during the PROPHET campaign. Here, the GC assembly consists of a thin copper band. The GC column is held within a 1.59 mm O.D. copper tube which makes thermal contact along the inner diameter of the outer band. To cool the column, the CO_2 enters through a short pieces of 3.18 mm O.D. copper tubing and its flow is split at a stainless steel tee (as shown in the right diagram) so both sides of the ring can cool evenly. Heaters are adhered to the outside of the copper band (red) and GC temperature was monitored at one location, marked by a red star.

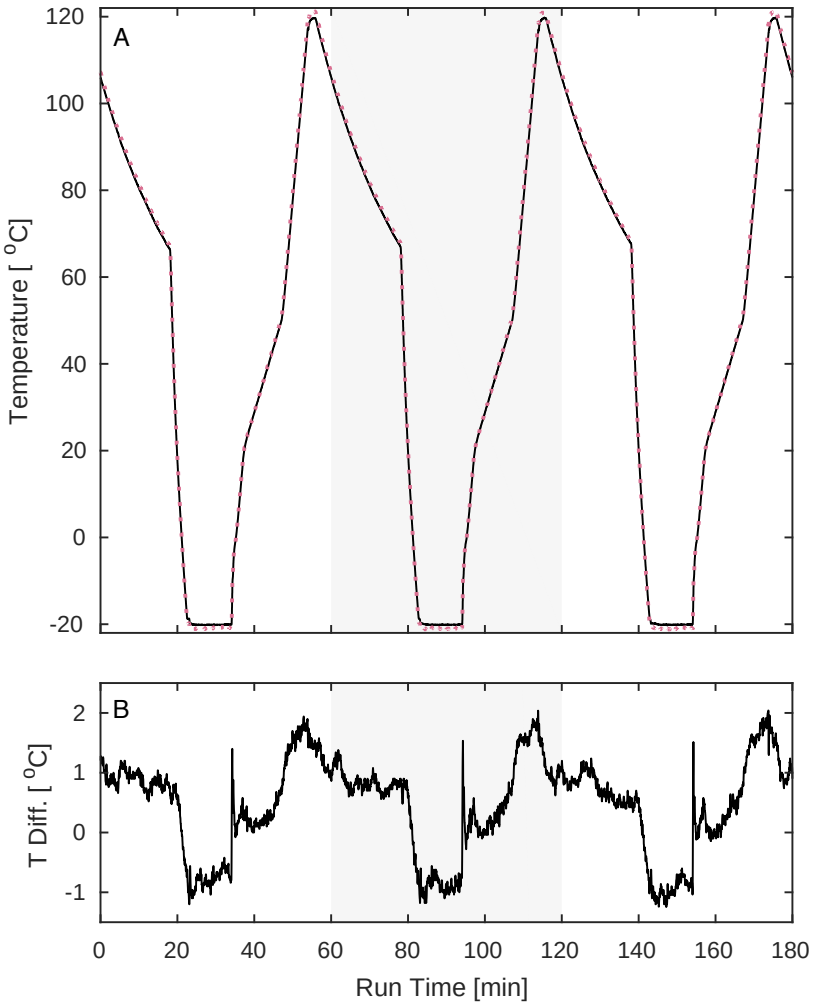

Figure A.2: Thermal cycle of GC-CIMS during operation, showing (A) temperature profiles for three consecutive GC runs demonstrating the reproducibility of GC temperature despite frequent thermal cycling. In addition, (B) temperature difference between locations (1) and (2) on the GC (see Fig. 2, main text) show a consistently small temperature gradient (< 2^{o}C) across the column during the temperature program. Ambient temperatures during these GC cycles ranged between 27.8 - 33.2^{o}C.

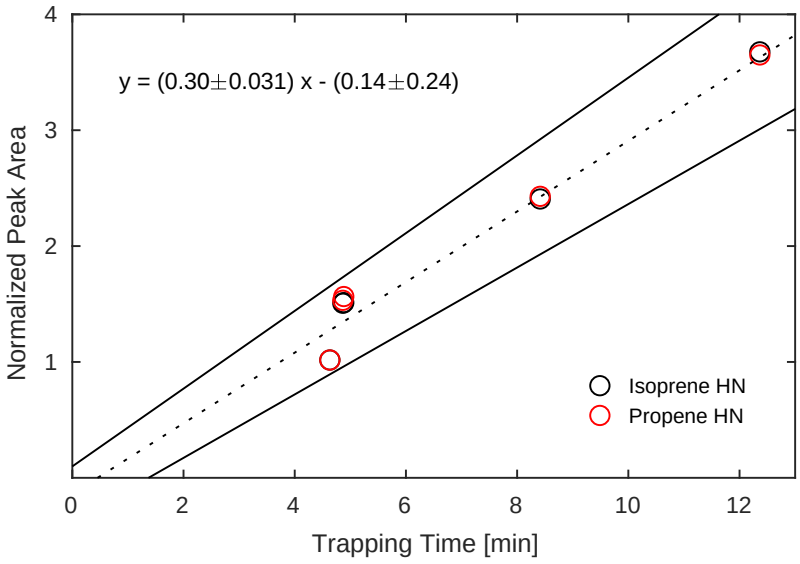

Figure A.3: Chromatogram peak areas as a function of trapping time (and, as a result, trapping volume). Analytes were cryofocused on the GC column held at -20^{o}C. Circles represent the sum of the peak areas of the two dominant IHN isomers (black) and the two isomers of propene HN (red) normalized to samples trapped at 4 minutes.

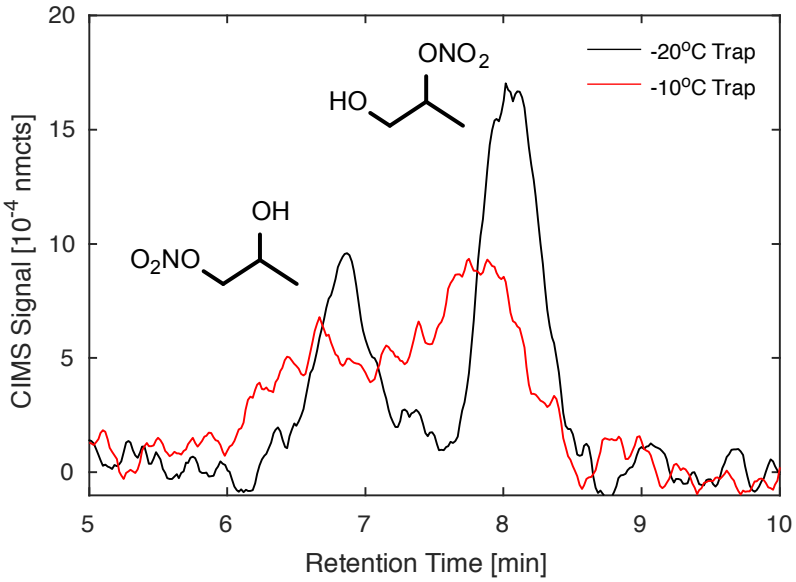

Figure A.4: Comparison of consecutive chromatograms obtained during the Caltech field study of propene HN trapped at -20^{o}C (black) and -10^{o}C (red), demonstrating the effect trapping temperature can have on the chromatography of higher volatile species.

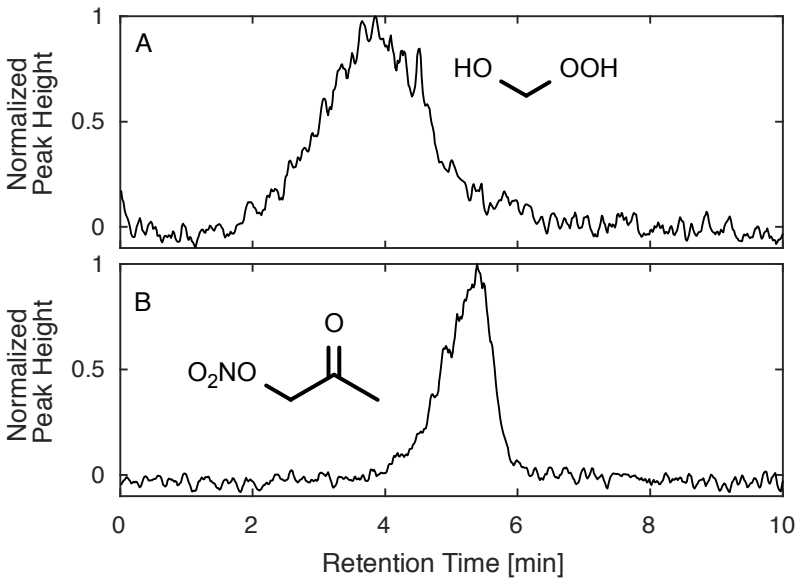

Figure A.5: Chromatograms obtained during the Caltech field study field data for (A) hydroxymethyl hydroperoxide (HMHP) and (B) propanone nitrate (PROPNN) demonstrating irregular peak shapes that can result for higher volatility species during typical trapping conditions used in this study. Further optimization of GC cryotrapping is needed in order to better quantify these compounds through GC analysis. GC signal shown here has been normalize to the largest peak in the displayed window.

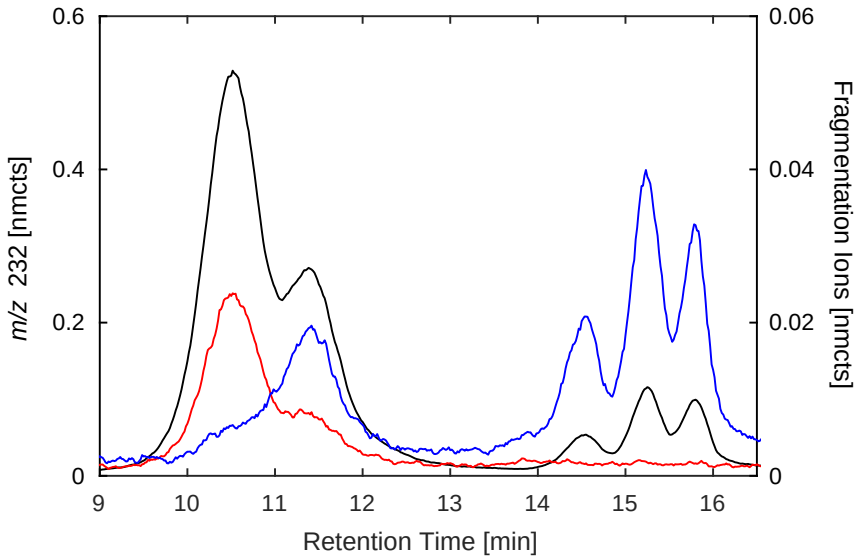

Figure A.6: Examples of fragmentation ions of IHN resulting from direct electron attachment to IHN. The primary product ion from IHN clustering with CF_3O^- (*m/z* 232, black) is compared with fragmentation ions resulting from electron attachment (*m/z* 99, blue and *m/z* 146, red) These fragment ions can provide additional structural information. For example, *m/z* 99 has high yields from primary and secondary IHN structures while *m/z* 146 has high yields from β-hydroxy nitrates.

References

Crounse, J. D., Paulot, F., Kjaergaard, H. G., and Wennberg, P. O. Peroxy radical isomerization in the oxidation of isoprene. *Phys. Chem. Chem. Phys.*, 13:13607–13613, 2011. doi: 10.1039/C1CP21330J.

Garden, A. L., Paulot, F., Crounse, J. D., Maxwell-Cameron, I. J., Wennberg, P. O., and Kjaergaard, H. G. Calculation of conformationally weighted dipole moments useful in ion-molecule collision rate estimates. *Chem. Phys. Lett.*, 474(1):45–50, 2009. doi: 10.1016/j.cplett.2009.04.038.

Paulot, F., Crounse, J. D., Kjaergaard, H. G., Kroll, J. H., Seinfeld, J. H., and Wennberg, P. O. Isoprene photooxidation: New insights into the production of acids and organic nitrates. *Atmos. Chem. Phys.*, 9(4):1479–1501, 2009. doi: 10.5194/acp-9-1479-2009.

Sharpe, S. W., Johnson, T. J., Sams, R. L., Chu, P. M., Rhoderick, G. C., and Johnson, P. A. Gas-phase databases for quantitative infrared spectroscopy. *Appl. Spectrosc.*, 58(12):1452–1461, 2004. doi: 10.1366/0003702042641281. PMID: 15606959.

Taylor, W. D., Allston, T. D., Moscato, M. J., Fazekas, G. B., Kozlowski, R., and Takacs, G. A. Atmospheric photodissociation lifetimes for nitromethane, methyl nitrite, and methyl nitrate. *Int. J. Chem. Kinet.*, 12(4):231–240, 1980. doi: 10.1002/kin.550120404.

Appendix B

SUPPLEMENTAL INFORMATION FOR RAPID HYDROLYSIS OF TERTIARY ISOPRENE NITRATE EFFICIENTLY REMOVES NOX FROM THE ATMOSPHERE

B.1 Caltech field study

Data was obtained between August 1–17, 2017. During this time, the GC-CIMS instrument was located on the top of the 44 m central library (34.1368 °N, 118.126 °W) on the Caltech campus in Pasadena, CA. Pasadena is a part of the Los Angeles Metropolitan area and the South Coast Air Basin (SoCAB). As such, it is located near a multitude of mobile and industrial sources of anthropogenic pollution. However, the field site is also in close proximity to local vegetation which is made up of known isoprene emitters, such as oak and eucalyptus trees (Guenther et al., 1994). Thus, biogenic emissions also influence the area (Washenfelder et al., 2011; Pollack et al., 2013).

The field site experienced daytime (10:00 - 20:00 PDT) relative humidities between 42 - 64% and warm temperatures (a mean low of 20°C and a mean high of 31°C). The instrument was placed on the southwest corner of the roof of the central library and inlet protruded from the south face of the building, sampling into the majority of the daytime winds. Back trajectories (Fig. B.1) show that, on average, air masses passed through downtown Los Angeles approximately one hour before reaching the field site in the early afternoon.

B.2 Data processing and uncertainty

Data processing of the GC data presented in this work has been discussed by Vasquez et al. (2018). As the 1,2-IHN and 4,3-IHN isomers are not completely separated with our GC configuration, we used a web-available MATLAB peakfit function (O'Haver, 2017) and modified it to support an exponentially modified gaussian peak shape in which individual peaks had fixed widths and distinct tailing constants, to deconvolve the chromatogram. Peak parameters were chosen by minimizing the root mean square (rms) difference between the data and the peak fitting model. Sensitivity of the fitted peak area to the fitting parameters was estimated using a bootstrapping method (**?**). We varied both the chosen peak widths and tailing constants by ±40% over 1000 trials. Trials that degraded the fit beyond 1σ of the rms error were

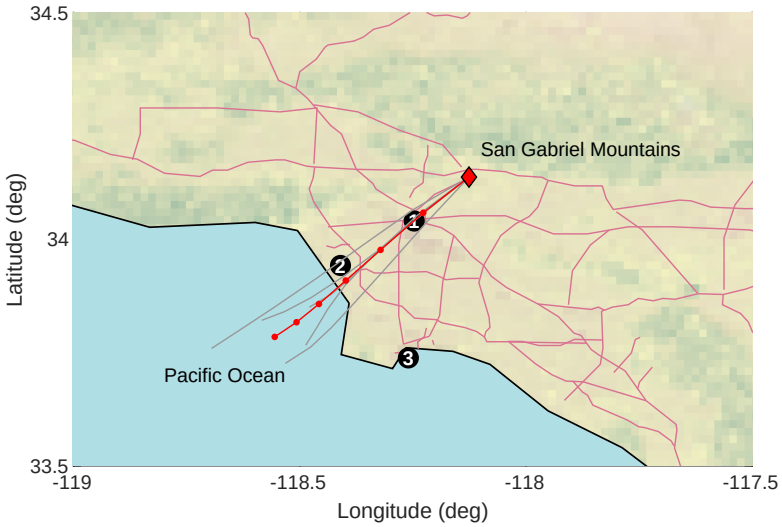

Figure B.1: Map of southern California indicating the location of the Caltech field site (red diamond), major highways (pink) and the following three locations: (1) downtown Los Angeles, (2) the Los Angeles International Airport and (3) the Port of Los Angeles. The average HYSPLIT back trajectory (Stein et al., 2015) for 15:00 PDT (red line) is shown for five randomly selected clear, sunny days (gray) during the study. Each red circle on the average back trajectory represents 1 hour elapsed time.

disregarded. The calculated peak areas were then scaled by their relative CIMS sensitivities and GC transmission factors, before being normalized by the volume of air collected on the column in order to determine the corresponding ambient concentrations. The CIMS sensitivities of 1,2-IHN and 4,3-IHN are assumed to be similar (Teng et al., 2017). Both isomers have been shown to have GC transmission efficiencies near 100% (Lee et al., 2014; Teng et al., 2017; Vasquez et al., 2018).

B.3 Hydrolysis kinetics experiments

B.3.1 IHN hydrolysis in a humid chamber

Chamber experiments were conducted to probe the kinetics of condensed-phase hydrolysis of 1,2-IHN. For these experiments, isoprene, NO and methyl nitrite (CH_3ONO, OH source) were added to a 24 m^3 Teflon bag. UV lights were illuminated for a few minutes to oxidize approximately 10% of the isoprene in the chamber, limiting the production of second-generation products. Oxidation products were then observed in the dark using the GC-CIMS (see Materials and Methods in main text).

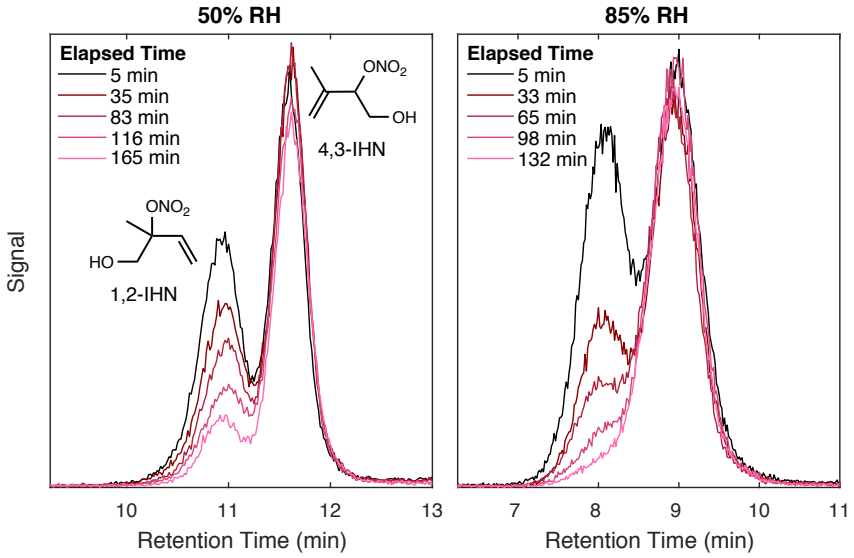

Figure B.2: High NOx isoprene oxidation experiments were performed at 50% (left) and 85% (right) RH. The lifetime of the 1,2-IHN isomers was found to be strongly dependent on humidity. Under completely dry conditions in a clean Teflon bag, the area of the 1,2-IHN isomer peak is 1.5 times that of 4,3-IHN. We note that different temperature programs were used for these two data sets. As a result, the resolution and retention time of these isomers are not identical.

Experiments were performed at 50% and 85% relative humidity at 25°C (Fig. B.2). During these experiments, a rapid decay of the 1,2-IHN isomer was observed and its lifetime was found to be strongly dependent on humidity levels, resulting in a lifetime of 45 minutes at 50% RH and 15 minutes at 85% RH. In contrast, there was no observed decay of the 4,3-IHN isomer at either humidity during the course of the experiments, which is consistent with its longer lifetime against hydrolysis (Jacobs et al., 2014). Corresponding signal increases were observed at *m/z* 187 (CF_3O^- cluster with neutral of mass of 102 amu), consistent with formation of isoprene diol, a product of IHN hydrolysis. In addition, we observe an initial small production of *E*-1,4-IHN isomer during the dark portion of the experiments, subsequently followed by first-order decay. We hypothesize this production arises from the condensed-phase isomerization of 1,2-IHN, similar to what has been previously observed during the GC-analysis of 1,2-IHN (Teng et al., 2017).

Hydrolysis was likely occurring on the chamber walls. Similar experiments with high levels (up to 500 μg m^{-3}) of ammonium sulfate particulate mass did not alter the decay rate in a measurable manner compared to experiments without seed. Experiments conducted under dry conditions (<5% RH) had significantly lower

loss rates for 1,2-IHN. Experiments conducted in a smaller chamber (1 m^3) using a clean Teflon bag showed that the 1,2-IHN concentrations remained stable at elevated humidities (>80%) over a 12 hour period, despite a higher gas-wall interaction rate. We suggest that accumulation of deposited material on the walls of the large chamber (such as H_2SO_4 and other salts derived from deposited seed particles, and possibly low-volatility organic material) can take up water under high humidity, creating a condensed-phase reservoir within which the hydrolysis can occur.

B.3.2 Synthesis of 1,2-IHN

1,2-IHN synthesis was performed by combining anhydrous nitric acid with 2-methyl-2-vinyloxirane (Sigma-Aldrich) in dry dichloromethane. Special care was taken to minimize the amount of H_2O present in the reaction mixture by purging the headspace of the reaction vessel with dry nitrogen. Typical synthesis: 330 mg (4.0 mmol) 2-methyl-2-vinyloxirane was dissolved 8 ml anhydrous methylene chloride (Sigma-Aldrich). This was placed in a 100 ml round bottom flask with a teflon-coated magnetic stir bar, briefly purged with dry N_2, and cooled to $-10°C$ using an isopropanol bath that was cooled with liquid nitrogen (LN_2). With rapid stirring, a mixture of 250 mg (4.0 mmol) anhydrous HNO_3 in 7 ml methylene chloride was slowly added (1-2 drops per second) with N_2 purge. After HNO_3 addition, the cold bath was removed, and the mixture was allowed to warm to room temperature with stirring. Anhydrous HNO_3 was produced just before each synthesis using the reaction of $NaNO_3$ with H_2SO_4, as described by McCabe et al. (2003) Products were analyzed by evaporating a small amount of the crude reaction mixture into a 100 L Teflon pillow bag and analyzing the gas composition with the GC-CIMS. Initially, 1,2-IHN was the most abundant IHN isomer (1,2-IHN >70% of total IHN). Using gas-phase quantification (GC-CIMS), total IHN yield was small (typically a few percent (mol/mol) of the starting epoxide). Separation of 1,2-IHN from other products in the reaction mixture was attempted using flash chromatography with silica gel, however, no 1,2-IHN was collected from the column. It is likely that residual H_2O or hydroxy groups attached directly to the silica gel is sufficient to hydrolyze the 1,2-IHN on the column.

^{1}H NMR spectra of the crude reaction mixture (after removal of the methylene chloride by vacuum distillation at $-15°C$) is shown in Fig. B.3. Signals arising from 1,2-IHN are identified by comparing the initial NMR spectra to one taken after leaving the reaction mixture at room temperature for 4 hours and observing which signals decayed (Fig. B.4). 1,2-IHN is highly reactive. We observe that 1,2-IHN

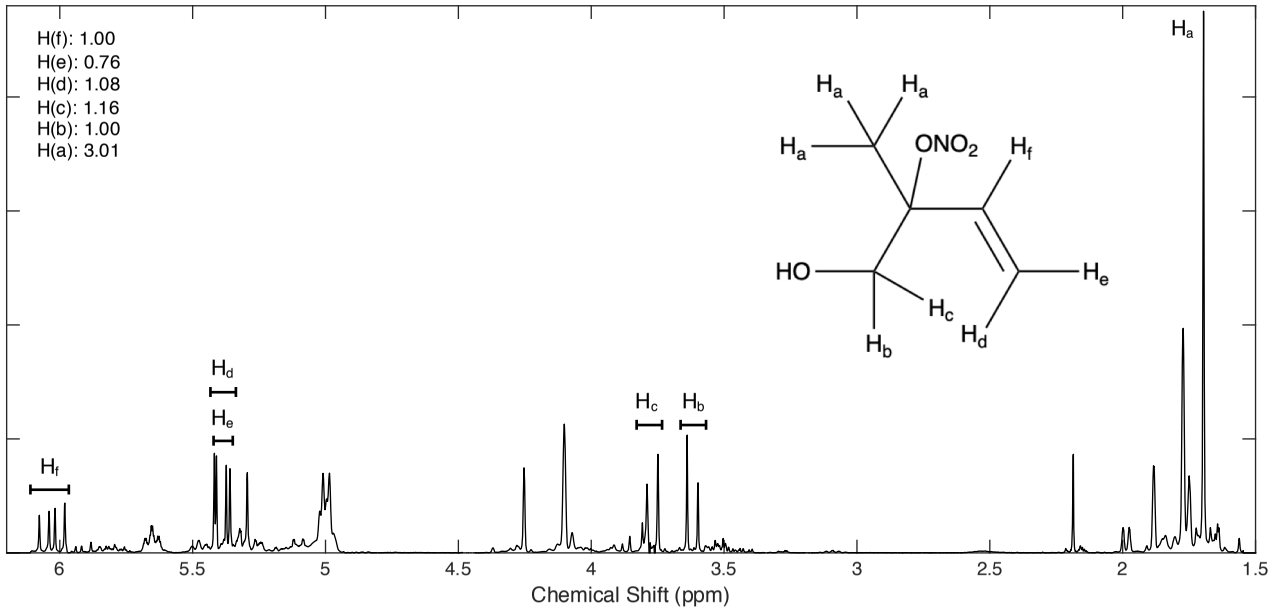

Figure B.3: ^{1}H NMR spectra (300 MHz) of 1,2-IHN in deuterated chloroform (Sigma Aldrich, 99.8% D). δ 6.03 (dd, J = 17.7, 11.0 Hz, 1H-H_f), 5.394 (d, J = 11.0, Hz, 1H-H_e), 5.391 (d, J = 17.6, Hz, 1H-H_d), 3.77 (d, J = 12.2, Hz, 1H-H_c), 3.62 (d, J = 12.3, Hz, 1H-H_b), 1.70 (s, 3H-H_a). It appears that the geminal coupling between H_d and H_e is quite small and not resolved with this spectrometer.

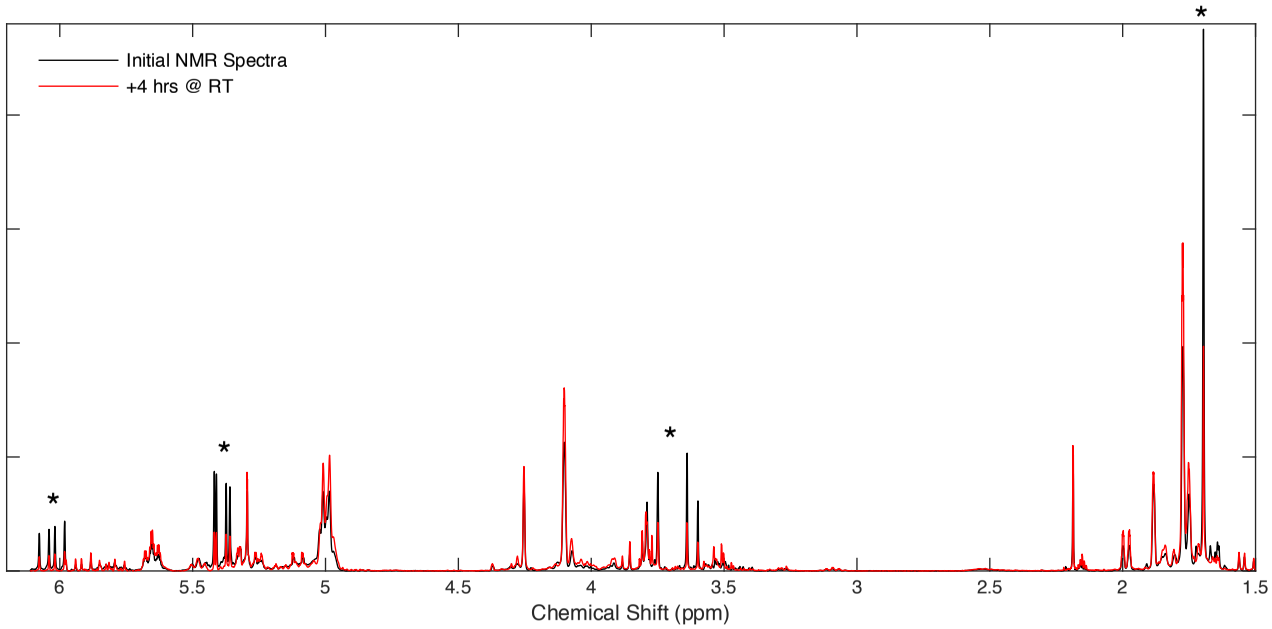

Figure B.4: ^{1}H NMR spectra of crude 1,2-IHN synthetic mixture taken 4 hours apart with sample resting at room temperature between analyses. Signals strongly decaying with time are believed to arise from 1,2-IHN hydrogens (*).

(crude reaction mixture) decays in dry methylene chloride at −15° C with a lifetime of 1 day, likely through reactions with itself, or other species present in the reaction mixture.

B.3.3 Synthesis of 4,3-IHN

Synthesis of 4,3-IHN was conducted in a manner similar to the IHN synthesis described by Lee et al. (2014) In place of 2-methyl-2-vinyloxirane, (1-methylethenyl)oxirane was used. Because this epoxide is not commercially available it was synthesized according to the method described by Harwood et al. (1990), though scale was reduced by a factor of 4. After synthesis of the hydroxy nitrate, the crude reaction mixture was analyzed using GC-CIMS as described above for 1,2-IHN. The distribution of the IHN isomers as analyzed in the gas-phase was: 89% 4,3-, 1% *Z*-4,1-, and 10% *E*-4,1-IHN. The overall IHN molar yield was approximately 13% of the starting epoxide. After removal of methylene chloride at −15°C using vacuum, the crude mixture was purified using flash chromatography. A column composed of six inches of 400 mesh silica gel within a 2.54 cm O.D. pyrex tube was prepared using a solvent mixture of 1:1 ethyl acetate:hexanes. After flowing about 1 column volume of solvent to condition the column, the concentrated crude reaction mixture was charged to the top of the column. The column was run under gravity for about 4 hours, collecting 5-15 ml aliquots, monitoring the output composition using TLC, and CIMS. A C_5-diol was found to elute very rapidly (first 2-3 aliquots). The IHN isomers eluted much later, however, separation of the isomers was quite good when collecting 5 ml aliquots. Elution order was observed to be 4,3-, *Z*-4,1-, *E*-4,1-IHN, as verified by NMR and GC-CIMS. Aliquots containing the same isomers were combined, solvent was removed, and products were diluted with methylene chloride for storage.

B.3.4 IHN hydrolysis in D_2O

IHN hydrolysis kinetics in D_2O were studied using ^{1}H NMR methods similar to experiments described by Eddingsaas et al. (2010). NMR spectra were acquired using a Varian 600 MHz spectrometer with sample probe controlled to 25° C. Additional reference spectra were collected in $CDCl_3$ using a Varian 300 MHz instrument. For the kinetics experiments, an NMR tube was charged with D_2O and used to tune the spectrometer, collecting a single sample. The tube was then removed from the NMR and a small aliquot of the 1,2-IHN concentrated synthetic mixture was combined with the D_2O in the NMR tube. The tube was inverted several

times to promote mixing, and quickly reinserted into the NMR probe. Sequential spectra were collected over time with an acquisition period of 22.6 s. A period of approximately 45 s elapsed between addition of the synthetic mixture to the D_2O and the end of acquisition for the first spectrum. While signals from 1,2-IHN, *E* and *Z*-1,4-IHN are readily apparent in reference spectra in $CDCl_3$, no signals from 1,2-IHN are observed for spectra in D_2O.

No 1,2-IHN signals were observed in the NMR spectra of the D_2O sample. Thus, we can only place lower limits on the hydrolysis rate of 1,2-IHN in D_2O at 298 K. Using the signal to noise of the NMR spectra in D_2O experiment, signals from the *E* and *Z*-1,4-IHN in the D_2O experiment, the ratio of signals from 1,2-IHN to *E*- or *Z*-1,4-IHN, and assuming the initial distribution of isomers is the same between the reference and the D_2O experiments, we constrain the hydrolysis lifetime of 1,2-IHN in D_2O to be less than 10 s.

The hydrolysis rate coefficients of *E* and *Z*-1,4-IHN in D_2O at 298 K were measured to be $(10.1 \pm 0.4) \times 10\ s^{-3}$ and $(5.3 \pm 0.2) \times 10^{-3}\ s^{-1}$, respectively (Fig. B.5). The bulk hydrolysis rate of *E* and *Z*-1,4-IHN has been previously reported by Jacobs et al. (2014) as $(6.76 \pm 0.09) \times 10^{-3}\ s^{-1}$. At the time, Jacobs et al. (2014) could not resolve these two isomers. Subsequently, in $CDCl_3$ they determined that the mixture had a ratio of 2.6:1 (Elrod, 2020). Using this initial ratio and the isomer specific rate constants to calculate the total 1,4-IHN amount over the time scale of the Jacobs et al. (2014) experiments, these two studies are in broad agreement.

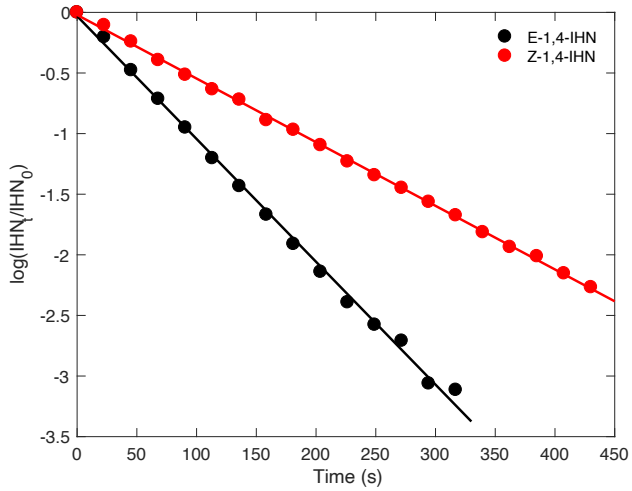

Figure B.5: First-order decay of NMR signal for *E*-1,4-IHN (black) and *Z*-1,4-IHN (red) in D_2O at 298 K.

B.3.5 IHN Henry's law constants

The concentration of the purified 4,3-IHN solution was determined by evaporating a known volume of solution into a known volume of air, and analyzing this using GC-CIMS. A known volume of the 4,3-IHN solution was combined with 6 mL H_2O in a multi-neck round bottom flask (RBF). The flask was cooled to 0°C in an ice bath with stir bars in both the RBF and the ice bath, slowly stirring. A small flow of N_2 was passed through the headspace of the RBF using a flow controller. After the RBF, a large flow of N_2 diluted the effluent from the RBF and carried the analytes to the CIMS where the 4,3-IHN was quantified. Using the ratio of the gas flows, the concentration above the solution was calculated. This, along with the assumption of headspace saturation allowed for calculation of the Henry's Law constant. The saturation assumption was checked by reducing the flow though the RBF by a factor of 2. Similar methods were used to quantify the Henry's law constant of 1,2-IHN and 4,3-IHN in octanol. The results from these experiments are listed in Table B.1. It was not possible to determine the Henry's law constant for 1,2-IHN in water using this method.

Table B.1: Experimentally determined Henry's law constants (K_H) for 1,2-IHN and 4,3-IHN in water and octanol at 0°C

	K_H (10^4 M atm^{-1})	
Isomer	Water	Octanol
1,2-IHN	—	1.4 ± 0.2
4,3-IHN	3.1 ± 0.8	0.9 ± 0.3

B.4 IHN photolysis

To estimate the photolysis rate, a 1 m^3 Teflon bag containing synthesized 1,2-IHN was placed in direct sunlight for five hours in Pasadena, CA on March 26, 2015 between 10:00 –15:00 local time. 50 μL of the 1,2-IHN reaction mixture was combined with 650 μL acetone and a droplet of this solution was placed in a three-way vial. Dry air was then blown over this droplet, and the evaporated reaction mixture was collected in a FEP Teflon pillow bag. Contents of the bag were measured with the GC-CIMS both before and after exposure to sunlight. Chromatograms show that 1,2-IHN, and *E* and *Z*-1,4-IHN were present in significant quantities and 4,3-IHN was present in trace amounts. 1,2-butanediol was added to the bag to estimate OH oxidation during the experiment. It is assumed that 1,2-butanediol did not photolyze significantly over the time scale of this experiment.

Over the course of five hours of exposure to sunlight, and correcting for OH oxidation (using butanediol signal), 1,2-IHN decreased by about 10%. This places an upper limit to the photolysis rate of $(1.0 \pm 1.0) \times 10^{-5}$ s^{-1} for this experiment. Adjusting this number for the difference in photon flux between March 26 and August 1, we calculate an upper limit to the 1,2-IHN photolysis rate of 1.2×10^{-5} s^{-1} or approximately 22 daylight hours.

B.5 1D model description

The one-dimensional (1D) atmospheric model used in this work simulates the emission, deposition, vertical transport, and photochemical oxidation of 250 chemical species in an atmospheric column tuned to replicate conditions observed during the 2010 CalNex campaign (May–June, 2010). The model consists of 40 vertical layers ranging from the ground (0.05 m) to 800 m. The first 39 layers exist within the range of the daytime boundary layer, with the 40th layer representing the free troposphere. Depending on the time of day, the uppermost layers (33–40) represent either the boundary layer or the nocturnal residual layer. Layer heights within the boundary layer are calculated similarly to previous 1D models and increase exponentially with altitude (Wolfe and Thornton, 2011; Bryan et al., 2012), while the free troposphere layer has a prescribed height of 100 m. Simulations are run for 24 hours with a time step of one minute. Diurnal meteorological variables and emission rates are provided as model inputs, as explained in more detail subsequently.

Vertical transport is simulated in the model using K-theory, a first-order flux-gradient approach common to 1D atmospheric models (Wolfe and Thornton, 2011; Bryan et al., 2012; Ashworth et al., 2015). Layer-specific K-values, or eddy diffusivities, are calculated using the following equation (Bryan et al., 2012):

$$K_i = l_i^2 \left| \frac{dv}{dz_i} \right| f \tag{B.1}$$

where l_i is the vertical length scale for eddies in each layer, $\frac{dv}{dz_i}$ is the local vertical gradient of horizontal wind velocity, and f represents a stability parameter. From 10:00–17:00, the boundary layer is assumed to be fully developed and K-values are calculated from the ground to 700 m using vertical wind profiles calculated from ground level measurements. At night (20:00–06:00), mixing is effectively restricted to the bottom 250 m, meant to represent the nocturnal boundary layer in the Los Angeles area. During development and decline of the boundary layer (06:00–10:00 and 17:00–20:00), K-values are interpolated between those used at night and midday.

Midday mixing between the top of the boundary layer and the free troposphere is assigned a K-value of 5 m^2 s^{-1}. Simulated IHN isomer ratios are insensitive to the free tropospheric layer height and the mixing rate between the boundary layer and the free troposphere.

The model combines the RACM2 chemical mechanism (Goliff et al., 2013), which simulates oxidation of lumped VOC classes for use in regional models, with the condensed isoprene oxidation mechanism from Wennberg et al. (2018), resulting in a system with 250 chemical species and 583 chemical reactions. Photolysis rates provided by the individual mechanisms are scaled to achieve agreement between modeled and measured values of the hydroxyl radical during CalNext 2010 (Griffith et al., 2016) and the photolysis rate of NO_2 (jNO_2). Emissions of non-biogenic lumped VOCs used in the RACM2 mechanism were obtained from the California Air Resources Board (CARB) database. Emissions data were available for the week of July 22–28, 2012. While these data do not correspond with the exact timeframe of the CalNex campaign, the use of data from the same month (July, in both cases) and the inclusion of an advective term described below produce reasonable simulation of the lumped VOC concentrations and there is good agreement between measured and modeled oxidant concentrations. Given uncertainty in local isoprene emissions due to vegetation heterogeneity in and around the Pasadena area, we performed sensitivity tests to determine a reasonable peak emission rate that, when diurnally scaled by the solar zenith angle, produced agreement between measured and modeled isoprene concentrations. This process suggests a peak effective rate of ~0.3 mg m^2 hr^{-1}. This value agrees well with model estimates for the region using the MEGAN model (Guenther et al., 2012; Misztal et al., 2016).

Two types of advective processes are simulated within the model. Given the difficulty in quantifying the influence of advection on local concentrations, we include an advective mixing term similarly to Wolfe and Thornton (Wolfe and Thornton, 2011) that pushes the model towards agreement with measured diurnal concentrations. The magnitude of this first order advective term is proportional to the difference between the modeled and measured concentration at each step. This advective term is only incorporated for parent VOCs, NO, NO_2, and O_3 in the bottom 20 layers of the model, which encompasses the region from the ground to ~20 m. Importantly, this term is not included in the differential equations governing IHN isomer production and loss. The model also includes an advective loss term to prevent unrealistic accumulation of oxidation products within the column. The magnitude of this loss

rate is based on layer-dependent horizontal wind velocities and an assumed width of the Los Angeles basin (k_{wind} = v_i/125 km) (Pratt et al., 2012).

Deposition velocities of IHN isomers are assumed to follow a diurnal pattern proportional to the cosine of the solar zenith angle with peak (midday) value of 2 cm s^{-1}, following measurements by Nguyen et al. (2015). Deposition velocities of other species are calculated using the formula of Gao et al. (1993) for deposition to the ground, with Henry's law constants and reactivity values taken from Ashworth et al. (2015). The model assumes deposition occurs within the lowest 5 m of the domain, and first-order deposition rates are calculated by dividing the deposition velocity by this 5 m sub-domain height (Pratt et al., 2012).

Diurnal mass loadings of aerosol liquid water (ALW) used to model IHN partitioning were calculated using ISORROPIA II (Fountoukis and Nenes, 2007). Ground-level measurements of temperature, relative humidity, and mass loadings of inorganic aerosol components (SO_4, NH_4, and NO_3) collected during CalNex 2010 were used as model inputs. The CalNex data set for the LA ground site is publicly available at esrl.noaa.gov/csl/groups/csl7/measurements/2010calnex/Ground/DataDownload. Organic aerosol was not assumed to contribute to water uptake. Other salts not accurately quantified (e.g., Cl, Na, etc.) were not included in the ALW calculation given their small contribution to aerosol mass loadings in the Los Angeles region (Hayes et al., 2013). Aerosol mass loadings were assumed constant with altitude. The assumption of vertically invariant aerosol mass loadings is likely inaccurate in the early morning, as vehicular emissions within a shallow boundary layer produce substantial inorganic nitrate aerosol (Hayes et al., 2013), increasing ALW in the boundary layer but not the residual layer. However, without additional constraints or more complex modeling it is difficult to quantify the influence of this assumption. Nevertheless, assuming a constant aerosol vertical profile should lead to an overestimate of the integrated amount of ALW within the column, rather than an underestimate, therefore producing a conservative (i.e., low) estimate of the IHN $K_H \times k_{(aq)}$ product (k^*_{hydro}). It is also important to note that particle pH has been shown to accelerate the hydrolysis rate of other organic nitrates (Jacobs et al., 2014; Rindelaub et al., 2015; Boyd et al., 2015). However, because particle pH in Pasadena is thought to be low compared to other parts of the country (Guo et al., 2017; Chen et al., 2019), again, the hydrolysis loss coefficient, k^*_{hydro}, determined in this study is likely to represent a lower bound.

Both Henry's law coefficients (K_H) as well as the aqueous hydrolysis rate ($k_{(aq)}$) are functions of temperature. Unfortunately, these dependences are not well-known for the IHN isomers, therefore we provided the following estimates for these parameters:

$$K_H(T) = \frac{K_H(273)}{e^{9622/273}} e^{9622/T} \tag{B.2}$$

$$k_{(aq)}(T) = k_0(298K) \times e^{-6000/T}. \tag{B.3}$$

The temperature dependence for K_H is based on findings from Shepson et al. (1996). For 4,3-IHN, $K_H(273)$ is the experimentally determined value listed on Table B.1. For 1,2-IHN, we use 3×10^5 M atm^{-1} which is based on 4-nitroxy-3-methyl-2-butanol, which is typically used as the chemical analog 1,2-IHN. We note that the order of magnitude difference between the two Henry's law constants is not unreasonable, as this was also observed with the equivalent isomers of the isoprene hydroxy hydroperoxides (ISOPOOH) (Rivera Rios, 2018). For $k_{(aq)}$, the temperature dependence simply assumes a doubling in the hydrolysis rate for every 10 degrees increase in temperature. For 4,3-IHN, k_0 is set to 5.55×10^3, giving a rate of 1×10^{-5} s^{-1} at 298 K, matching the rate determined by Jacobs et al. (2014). For 1,2-IHN, k_0 is changed to obtain different values of the k^*_{hydro} product. It should be noted that while these temperature dependences are large, they have opposite signs, and thus the product of these two parameters, represented by k^*_{hydro}, largely cancel each other out, increasing only by a factor of 1.25 from the ground to the top of the boundary for midday simulations (Fig. B.6).

B.6 GEOS-Chem

B.6.1 Description of GEOS-Chem Simulations

Simulations of 1,2-IHN hydrolysis and its effects were conducted using version 11-02c of the GEOS-Chem global chemical transport model (Bey et al., 2001), run at $2^\circ \times 2.5^\circ$ horizontal resolution with 72 vertical layers extending through the stratosphere. GEOS-Chem incorporates assimilated meteorological observations from the NASA Goddard Earth Observing System - Forward Processing (GEOS-FP) data product from the NASA Global Modeling and Assimilation Office (GMAO). We used the standard HEMCO emissions (Keller et al., 2014), including isoprene emissions from the MEGAN v2.1 inventory scaled uniformly to 535 Tg a^{-1} (Guenther et al., 2012), along with observationally fixed tropospheric methane. We conducted both month-long (July 1–31 2014) and annual (August 1, 2014–July 31, 2015) simulations, following one year of initialization from July 1, 2013. Hourly mixing ratios

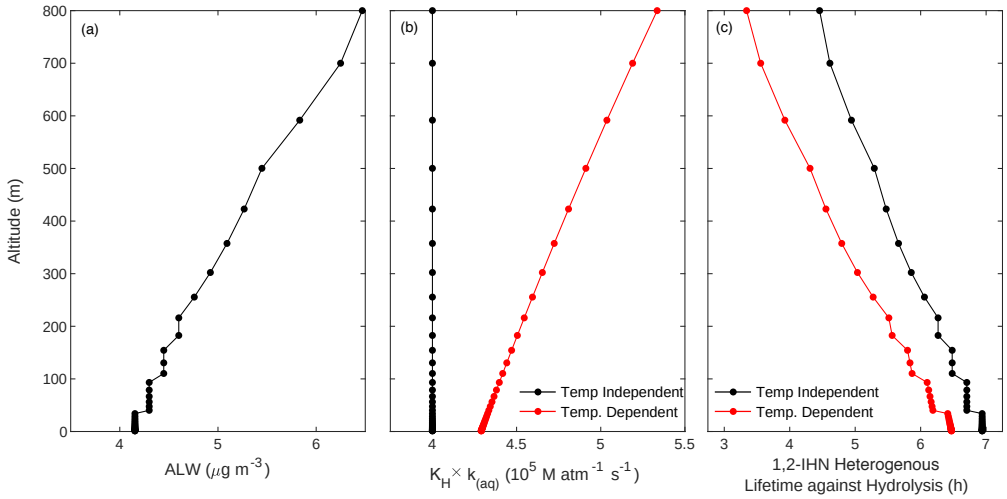

Figure B.6: Midday (noon local time) Los Angeles boundary layer profile of (A) the calculated aerosol liquid water (ALW) used to model IHN partitioning, (B) the product of the estimated 1,2-IHN Henry's law constant (K_H) and aqueous hydrolysis rate ($k_{(aq)}$) using both temperature independent (black) and dependent (red) values, and (C) the 1,2-IHN heterogenous lifetime against hydrolysis calculated from our model using temperature independent (black) and dependent (red) values of K_H and $k_{(aq)}$.

of species of interest were output in surface-level grid boxes containing specified locations (see below) from the month-long simulations, while annual mean mixing ratios and total species production and loss statistics were output from year-long simulations.

GEOS-Chem incorporates an editable chemical mechanism with gas-phase and heterogeneous chemistry. For all simulations performed herein, we replaced the default isoprene oxidation scheme with the Mini-CIM mechanism described in Bates and Jacob (2019), which separates the 1,2- and 4,3-IHN isomers and incorporates a number of additional updates to isoprene chemistry based on the reduced mechanism compiled by Wennberg et al. (2018). The aerosol uptake and hydrolysis of isoprene nitrates in GEOS-Chem is parameterized with an irreversible reactive uptake coefficient (γ). In their analysis of organic nitrate chemistry in the Southeast United States, Fisher et al. (2016) used a constant γ of 0.005 for all isoprene nitrates. Marais et al. (2016) introduced a mechanistic formulation for γ which incorporates an effective Henry's law constant (K_H, M atm^{-1}, accounting for rapid dissociation or hydration equilibria in the aqueous phase) and a pseudo-first-order aqueous-phase reaction rate constant ($k_{(aq)}$, s^{-1}). Marais et al. (2016) used $K_H = 3.3 \times 10^5$ M atm^{-1} for all isoprene-derived nitrates, $k_{(aq)} = 1.6 \times 10^{-5}$ s^{-1} for lumped β-hydroxynitrates, and $k_{(aq)} = 6.8 \times 10^{-3}$ s^{-1} for δ-hydroxynitrates and dihydroxy-dinitrates. Here, we

updated the K_H of 4,3-IHN to match the value listed in Table B.1, but leave the 1,2-IHN K_H as 3×10^5 M atm^{-1}, for reasons discussed in the main text. We further updated the $k_{(aq)}$ of 4,3-IHN to be $1.0{\times}10^{-5}$ s^{-1}, and performed individual simulations with 1,2-IHN $k_{(aq)}$ values of 0, 0.1, 1, 10, and 100 s^{-1}. In our analysis, we compared the resulting mixing ratios as well as total production and loss of species of interest between these simulations employing different 1,2-IHN $k_{(aq)}$ values and against simulations using the baseline K_H and $k_{(aq)}$ values from Marais et al. (2016) and Fisher et al. (2016).

We also include the hydrolysis of monoterpene nitrates (MTN), as implemented in the current default GEOS-CHem set up. As currently described in Fisher et al. (2016), this chemistry is largely based on the scheme developed by Browne et al. (2014) for use in WRF-Chem, which was built on the RACM2 scheme developed by Goliff et al. (2013). In our simulations, we do not include fast tertiary nitrate hydrolysis of the other compounds besides IHN. Thus, these simulations may underestimate the contribution of hydrolysis towards shortening the NO_x lifetime. As one example, OH oxidation of 1,2-isoprene hydroperoxy nitrate (IPN) is thought to yield several second-generation tertiary nitrates (Wennberg et al., 2018), which will also likely undergo rapid hydrolysis.

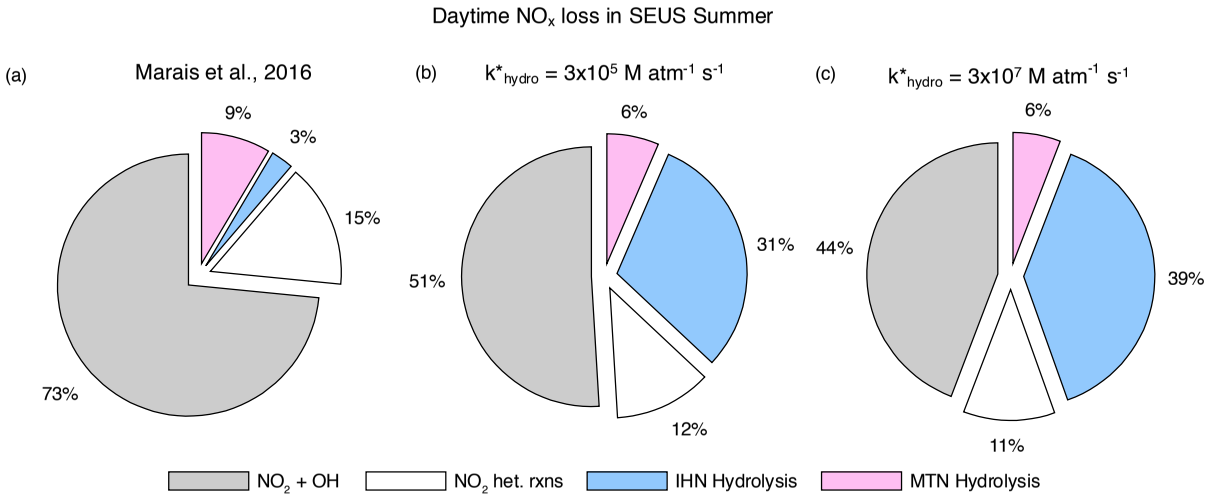

Figure B.7: Pie charts showing the global impact IHN hydrolysis has on the different daytime NO_x pathways in the lower 1 km of the atmosphere over the southeast USA in the summer when (A) using parameters from Marais et al. (2016), (B) setting $k_{(aq)}$ to 1 s^{-1}, and (C) setting $k_{(aq)}$ to 100 s^{-1}. The global impact of this chemistry remains largely unchanged when $k_{(aq)}$ is set above 1 s^{-1}.

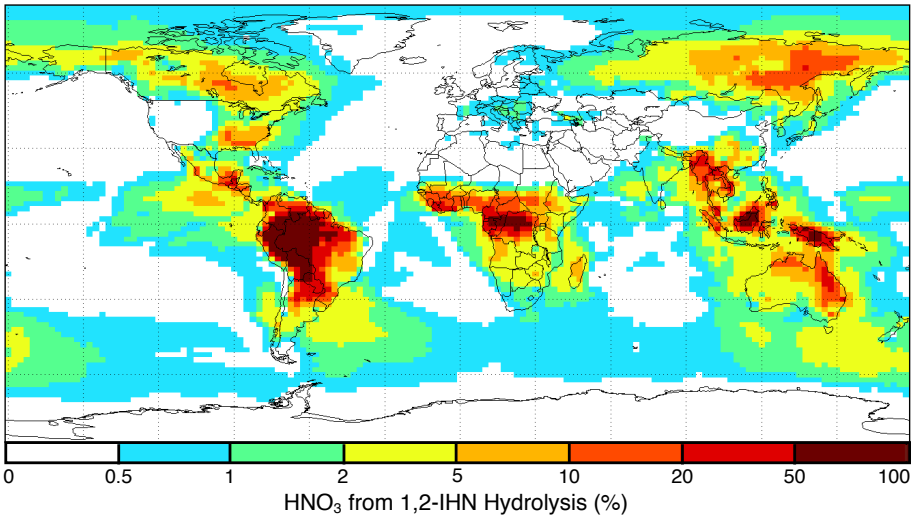

Figure B.8: Annually averaged fraction of HNO_3 attributed to 1,2-IHN hydrolysis in the lowest 1 km of the atmosphere, as calculated with GEOS-Chem when a 1,2-IHN hydrolysis rate of $k^*_{hydro} = 3 \times 10^5$ M atm^{-1} s^{-1} has been included.

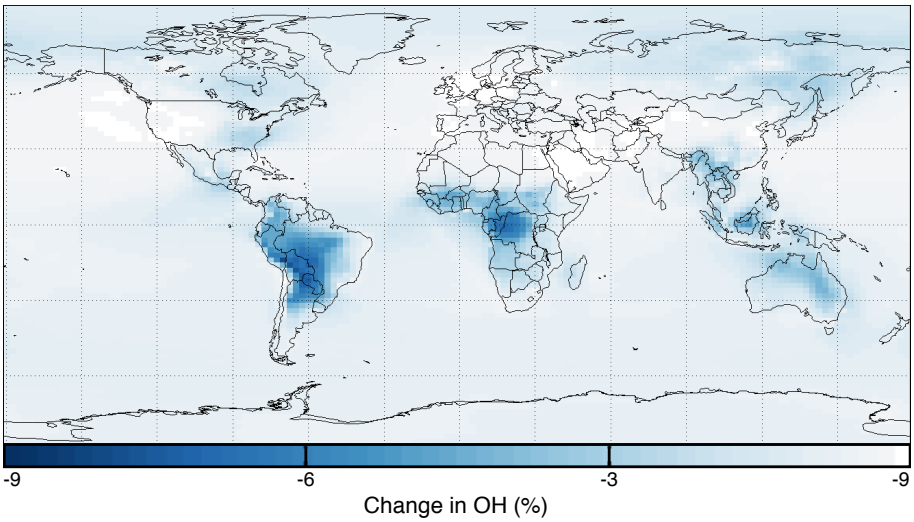

Figure B.9: Annually averaged change in OH in the lowest 1 km of the atmosphere when comparing the standard GEOS-Chem model with one that includes a 1,2-IHN hydrolysis rate of $k^*_{hydro} = 3 \times 10^5$ M atm^{-1} s^{-1}.

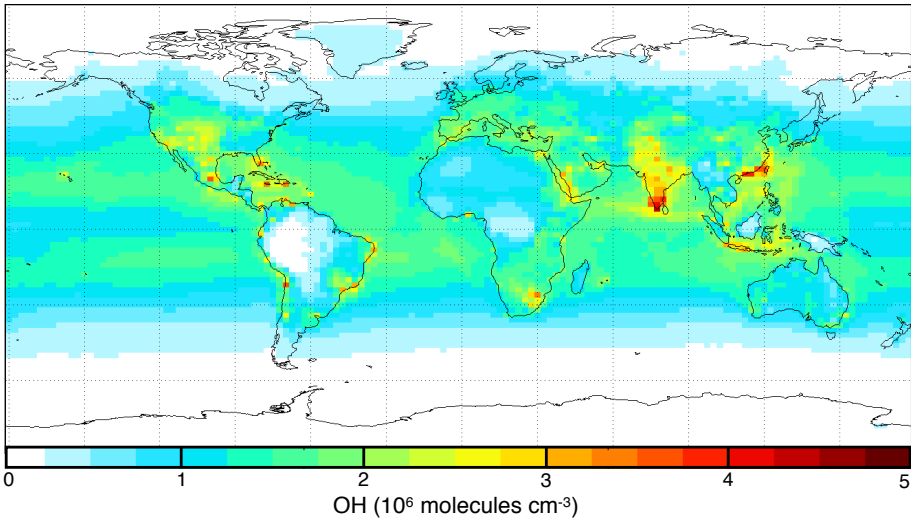

Figure B.10: Annually averaged OH concentrations in the lowest 1 km of the atmosphere, as calculated with GEOS-Chem when a 1,2-IHN hydrolysis rate of $k^{*}_{hydro} = 3 \times 10^{5}$ M atm^{-1} s^{-1} has been included.

References

Ashworth, K., Chung, S. H., Griffin, R. J., Chen, J., Forkel, R., Bryan, A. M., and Steiner, A. L. FORest Canopy Atmosphere transfer (FORCAsT) 1.0: a 1-D model of biosphere-atmosphere chemical exchange. *Geosci. Model Dev.*, 8(11): 3765–3784, 2015. doi: 10.5194/gmd-8-3765-2015.

Bates, K. H. and Jacob, D. J. A new model mechanism for atmospheric oxidation of isoprene: global effects on oxidants, nitrogen oxides, organic products, and secondary organic aerosol. *Atmos. Chem. Phys.*, 19(14):9613–9640, 2019. doi: 10.5194/acp-19-9613-2019.

Bey, I., Jacob, D. J., Yantosca, R. M., Logan, J. A., Field, B. D., Fiore, A. M., Li, Q., Liu, H. Y., Mickley, L. J., and Schultz, M. G. Global modeling of tropospheric chemistry with assimilated meteorology: Model description and evaluation. *J. Geophys. Res. Atmos.*, 106(D19):23073–23095, 2001. doi: 10.1029/2001JD000807.

Boyd, C. M., Sanchez, J., Xu, L., Eugene, A. J., Nah, T., Tuet, W. Y., Guzman, M. I., and Ng, N. L. Secondary organic aerosol formation from the β-pinene+NO_3 system: effect of humidity and peroxy radical fate. *Atmos. Chem. Phys.*, 15(13): 7497–7522, 2015. doi: 10.5194/acp-15-7497-2015.

Browne, E. C., Wooldridge, P. J., Min, K.-E., and Cohen, R. C. On the role of monoterpene chemistry in the remote continental boundary layer. *Atmos. Chem. Phys.*, 14(3):1225–1238, 2014. doi: 10.5194/acp-14-1225-2014.

Bryan, A. M., Bertman, S. B., Carroll, M. A., Dusanter, S., Edwards, G. D., Forkel, R., Griffith, S., Guenther, A. B., Hansen, R. F., Helmig, D., Jobson, B. T., Keutsch, F. N., Lefer, B. L., Pressley, S. N., Shepson, P. B., Stevens, P. S., and Steiner, A. L. In-canopy gas-phase chemistry during CABINEX 2009: Sensitivity of a 1-d canopy model to vertical mixing and isoprene chemistry. *Atmos. Chem. Phys.*, 12(18):8829–8849, 2012. doi: 10.5194/acp-12-8829-2012.

Chen, Y., Shen, H., and Russell, A. G. Current and future responses of aerosol pH and composition in the U.S. to declining SO_2 emissions and increasing NH_3 emissions. *Environ. Sci. Tech.*, 53(16):9646–9655, 2019. doi: 10.1021/acs.est.9b02005.

Eddingsaas, N. C., VanderVelde, D. G., and Wennberg, P. O. Kinetics and products of the acid-catalyzed ring-opening of atmospherically relevant butyl epoxy alcohols. *J. Phys. Chem. A*, 114(31):8106–8113, 2010. doi: 10.1021/jp103907c.

Elrod, M. personal communication, 2020.

Fisher, J. A., Jacob, D. J., Travis, K. R., Kim, P. S., Marais, E. A., Chan Miller, C., Yu, K., Zhu, L., Yantosca, R. M., Sulprizio, M. P., Mao, J., Wennberg, P. O., Crounse, J. D., Teng, A. P., Nguyen, T. B., St. Clair, J. M., Cohen, R. C., Romer, P., Nault, B. A., Wooldridge, P. J., Jimenez, J. L., Campuzano-Jost, P.,

Day, D. A., Hu, W., Shepson, P. B., Xiong, F., Blake, D. R., Goldstein, A. H., Misztal, P. K., Hanisco, T. F., Wolfe, G. M., Ryerson, T. B., Wisthaler, A., and Mikoviny, T. Organic nitrate chemistry and its implications for nitrogen budgets in an isoprene- and monoterpene-rich atmosphere: Constraints from aircraft (SEAC^{4}RS) and ground-based (SOAS) observations in the Southeast US. *Atmos. Chem. Phys.*, 16(9):5969–5991, 2016. doi: 10.5194/acp-16-5969-2016.

Fountoukis, C. and Nenes, A. ISORROPIA II: A computationally efficient thermodynamic equilibrium model for K^+-Ca^{2+}-Mg^{2+}-NH_4^+-Na^+-SO_4^{2-}-NO_3^--Cl^--H_2O aerosols. *Atmos. Chem. Phys.*, 7(17):4639–4659, 2007. doi: 10.5194/acp-7-4639-2007.

Gao, W., Wesely, M. L., and Doskey, P. V. Numerical modeling of the turbulent diffusion and chemistry of NOx , O_3, isoprene, and other reactive trace gases in and above a forest canopy. *J. Geophys. Res. Atmos.*, 98(D10):18339–18353, 1993. doi: 10.1029/93JD01862.

Goliff, W. S., Stockwell, W. R., and Lawson, C. V. The regional atmospheric chemistry mechanism, version 2. *Atmos. Environ.*, 68:174–185, 2013. doi: 10.1016/j.atmosenv.2012.11.038.

Griffith, S. M., Hansen, R. F., Dusanter, S., Michoud, V., Gilman, J. B., Kuster, W. C., Veres, P. R., Graus, M., de Gouw, J. A., Roberts, J., Young, C., Washenfelder, R., Brown, S. S., Thalman, R., Waxman, E., Volkamer, R., Tsai, C., Stutz, J., Flynn, J. H., Grossberg, N., Lefer, B., Alvarez, S. L., Rappenglueck, B., Mielke, L. H., Osthoff, H. D., and Stevens, P. S. Measurements of hydroxyl and hydroperoxy radicals during CalNex-LA: Model comparisons and radical budgets. *J. Geophys. Res. Atmos.*, 121(8):4211–4232, 2016. doi: 10.1002/2015JD024358.

Guenther, A., Zimmerman, P., and Wildermuth, M. Natural volatile organic compound emission rate estimates for U.S. woodland landscapes. *Atmos. Environ.*, 28(6):1197–1210, 1994. doi: 10.1016/1352-2310(94)90297-6.

Guenther, A. B., Jiang, X., Heald, C. L., Sakulyanontvittaya, T., Duhl, T., Emmons, L. K., and Wang, X. The Model of Emissions of Gases and Aerosols from Nature version 2.1 (MEGAN2.1): An extended and updated framework for modeling biogenic emissions. *Geosci. Model Dev.*, 5(6):1471–1492, 2012. doi: 10.5194/gmd-5-1471-2012.

Guo, H., Liu, J., Froyd, K. D., Roberts, J. M., Veres, P. R., Hayes, P. L., Jimenez, J. L., Nenes, A., and Weber, R. J. Fine particle ph and gas–particle phase partitioning of inorganic species in Pasadena, California, during the 2010 CalNex campaign. *Atmos. Chem. Phys*, 17(9):5703–5719, 2017. doi: 10.5194/acp-17-5703-2017.

Harwood, L. M., Casey, G., and Sherlock, J. A simple laboratory procedure for preparation of (1-methylethenyl)oxirane (3,4-epoxyisoprene). *Synth. Chem.*, 20 (9):1287–1292, 1990. doi: 10.1080/00397919008052839.

Hayes, P. L., Ortega, A. M., Cubison, M. J., Froyd, K. D., Zhao, Y., Cliff, S. S., Hu, W. W., Toohey, D. W., Flynn, J. H., Lefer, B. L., Grossberg, N., Alvarez, S., Rappenglueck, B., Taylor, J. W., Allan, J. D., Holloway, J. S., Gilman, J. B., Kuster, W. C., de Gouw, J. A., Massoli, P., Zhang, X., Liu, J., Weber, R. J., Corrigan, A. L., Russell, L. M., Isaacman, G., Worton, D. R., Kreisberg, N. M., Goldstein, A. H., Thalman, R., Waxman, E. M., Volkamer, R., Lin, Y. H., Surratt, J. D., Kleindienst, T. E., Offenberg, J. H., Dusanter, S., Griffith, S., Stevens, P. S., Brioude, J., Angevine, W. M., and Jimenez, J. L. Organic aerosol composition and sources in Pasadena, California, during the 2010 CalNex campaign. *J. Geophys. Res. Atmos.*, 118(16):9233–9257, 2013. doi: 10.1002/jgrd.50530.

Jacobs, M. I., Burke, W. J., and Elrod, M. J. Kinetics of the reactions of isoprene-derived hydroxynitrates: Gas phase epoxide formation and solution phase hydrolysis. *Atmos. Chem. Phys.*, 14(17):8933–8946, 2014. doi: 10.5194/acp-14-8933-2014.

Keller, C. A., Long, M. S., Yantosca, R. M., Da Silva, A., Pawson, S., and Jacob, D. J. HEMCO v1. 0: A versatile, ESMF-compliant component for calculating emissions in atmospheric models. *Geosci. Model Dev.*, 7(4):1409–1417, 2014. doi: 10.5194/gmd-7-1409-2014.

Lee, L., Teng, A. P., Wennberg, P. O., Crounse, J. D., and Cohen, R. C. On rates and mechanisms of OH and O_3 reactions with isoprene-derived hydroxy nitrates. *J. Phys. Chem. A*, 118(9):1622–1637, 2014. doi: 10.1021/jp4107603.

Marais, E. A., Jacob, D. J., Jimenez, J. L., Campuzano-Jost, P., Day, D. A., Hu, W., Krechmer, J., Zhu, L., Kim, P. S., Miller, C. C., Fisher, J. A., Travis, K., Yu, K., Hanisco, T. F., Wolfe, G. M., Arkinson, H. L., Pye, H. O. T., Froyd, K. D., Liao, J., and McNeill, V. F. Aqueous-phase mechanism for secondary organic aerosol formation from isoprene: Application to the southeast united states and co-benefit of so_2 emission controls. *Atmos. Chem. Phys.*, 16(3):1603–1618, 2016. doi: 10.5194/acp-16-1603-2016.

McCabe, D. C., Brown, S. S., Gilles, M. K., Talukdar, R. K., Smith, I. W., and Ravishankara, A. R. Kinetics of the removal of OH(v=1) and OD(v=1) by HNO_3 and DNO_3 from 253 to 383 K. *J. Phys. Chem. A*, 107(39):7762–7769, 2003. doi: 10.1021/jp0346413.

Misztal, P. K., Avise, J. C., Karl, T., Scott, K., Jonsson, H. H., Guenther, A. B., and Goldstein, A. H. Evaluation of regional isoprene emission factors and modeled fluxes in california. *Atmos Chem Phys*, 16(15):9611–9628, 2016. doi: 10.5194/acp-16-9611-2016.

Nguyen, T. B., Crounse, J. D., Teng, A. P., St. Clair, J. M., Paulot, F., Wolfe, G. M., and Wennberg, P. O. Rapid deposition of oxidized biogenic compounds to a temperate forest. *P. Natl. Acad. Sci.*, 112(5):E392–E401, 2015. doi: 10.1073/pnas.1418702112.

O'Haver, T. Peak fitters, Aug 2017. URL https://terpconnect.umd.edu/~toh/spectrum/InteractivePeakFitter.htm.

Pratt, K. A., Mielke, L. H., Shepson, P. B., Bryan, A. M., Steiner, A. L., Ortega, J., Daly, R., Helmig, D., Vogel, C. S., Griffith, S., Dusanter, S., Stevens, P. S., and Alaghmand, M. Contributions of individual reactive biogenic volatile organic compounds to organic nitrates above a mixed forest. *Atmos. Chem. Phys.*, 12(21): 10125–10143, 2012. doi: 10.5194/acp-12-10125-2012.

Rindelaub, J. D., McAvey, K. M., and Shepson, P. B. The photochemical production of organic nitrates from α-pinene and loss via acid-dependent particle phase hydrolysis. *Atmos. Environ.*, 100:193–201, 2015. doi: 10.1016/j.atmosenv.2014.11.010.

Rivera Rios, J. C. *Atmospheric Chemistry of Isoprene Hydroxyhydroperoxides*. PhD thesis, Harvard University, 2018.

Shepson, P. B., Mackay, E., and Muthuramu, K. Henry's law constants and removal processes for several atmospheric β-hydroxy alkyl nitrates. *Environ. Sci. Technol.*, 30(12):3618–3623, 1996. doi: 10.1021/es960538y.

Teng, A. P., Crounse, J. D., and Wennberg, P. O. Isoprene peroxy radical dynamics. *J. Am. Chem. Soc.*, 139(15):5367–5377, 2017. doi: 10.1021/jacs.6b12838.

Vasquez, K. T., Allen, H. M., Crounse, J. D., Praske, E., Xu, L., Noelscher, A. C., and Wennberg, P. O. Low-pressure gas chromatography with chemical ionization mass spectrometry for quantification of multifunctional organic compounds in the atmosphere. *Atmos. Meas. Tech.*, 11:6815–6832, 2018. doi: 10.5194/amt-11-6815-2018.

Washenfelder, R. A., Young, C. J., Brown, S. S., Angevine, W. M., Atlas, E. L., Blake, D. R., Bon, D. M., Cubison, M. J., Gouw, J. A. d., Dusanter, S., Flynn, J., Gilman, J. B., Graus, M., Griffith, S., Grossberg, N., Hayes, P. L., Jimenez, J. L., Kuster, W. C., Lefer, B. L., Pollack, I. B., Ryerson, T. B., Stark, H., Stevens, P. S., and Trainer, M. K. The glyoxal budget and its contribution to organic aerosol for Los Angeles, California, during CalNex 2010. *J. Geophys. Res. Atmos.*, 116 (D21), 11 2011. doi: 10.1029/2011JD016314.

Wennberg, P. O., Bates, K. H., Crounse, J. D., Dodson, L. G., McVay, R. C., Mertens, L. A., Nguyen, T. B., Praske, E., Schwantes, R. H., Smarte, M. D., St Clair, J. M., Teng, A. P., Zhang, X., and Seinfeld, J. H. Gas-phase reactions of isoprene and its major oxidation products. *Chem. Rev.*, 2018. doi: 10.1021/acs.chemrev.7b00439.

Wolfe, G. M. and Thornton, J. A. The Chemistry of Atmosphere-Forest Exchange (CAFE) model-Part 1: Model description and characterization. *Atmos. Chem. Phys.*, 11(1):77–101, 2011. doi: 10.5194/acp-11-77-2011.

Appendix C

TECHNICAL DOCUMENTATION FOR THE GAS CHROMATOGRAPHY-TIME-OF-FLIGHT-CHEMICAL IONIZATION MASS SPECTROMETER

C.1 Summary

The GC-HRToF-CIMS was designed and assembled at Caltech between 2015 and 2016. It has been deployed to two field studies (the PROPHET campaign in 2016 and a small field study at Caltech in 2017). Modifications to the 1 meter GC column setup occurred in 2017 prior to the Caltech study. This and the two instrument deployments are described in Vasquez et al. (2018). Construction of a second GC module capable of supporting longer columns (5+ m) has also occurred.

The instrument consists of the high-resolution time-of-flight chemical ionization mass spectrometer (HRToF-CIMS), a custom-built low-pressure gas chromatography (GC) system, a hot calibration systems, an NTP-GPS satellite receiver, and flow and power systems. Instrument components are monitored or controlled with a Diamond Systems Hercules single board computer (SBC), one of two Athena SBCs or a Windows PC machine. All computers are located on the same local network. The Hercules SBC contains the software source code which allows the user to remotely control or automate the instrument, while the Windows PC contains the data acquisition software for the CIMS.

During operation, all equipment is held in a aluminum rack that measures 1.1 m x 1.7 m x 0.9 m (W x H x D). When deployed in the field, the instrument rack is covered with lightweight paneling for weatherproofing and insulation, and uses two HVAC units to regulate the internal temperature. This complete field setup weighs approximately 275 kg. In addition, during field operation, the instrument setup requires two scroll pumps, a regenerative blower pump, a weather station and, if conditions are appropriate, 3-D sonic anemometers. This equipment is located separately from the main instrument rack and are housed in their own weatherproofed enclosures, if necessary.

Many of the individual components that make up the GC-HRToF-CIMS are commercial and have their own manuals. Wiring diagrams and component data sheets are available on the Wennberg Lab wiki (login required) and will not be duplicated

here. Instead, this appendix will serve to fill any information gaps regarding instrument operation, maintenance and basic troubleshooting. It will also serve as technical documentation for non-commercial components such as the GC and the data acquisition software.

References

Vasquez, K. T., Allen, H. M., Crounse, J. D., Praske, E., Xu, L., Noelscher, A. C., and Wennberg, P. O. Low-pressure gas chromatography with chemical ionization mass spectrometry for quantification of multifunctional organic compounds in the atmosphere. *Atmos. Meas. Tech.*, 11:6815–6832, 2018. doi: 10.5194/amt-11-6815-2018.

C.2 Instrument components

C.2.1 Mass spectrometer

TOFWERK AG

Uttigenstrasse 22

CH-3600 Thun, Switzerland

www.tofwerk.com

Tel: +41 33-511-1151

Description:

The HRToF-CIMS is a commercially built device (Tofwerk) that has been modified in-house. The development of this mass spectrometer builds upon methods established on another custom-built CIMS (CIT-CIMS) present in the Wennberg lab.

References

Crounse, J. D., McKinney, K. A., Kwan, A. J., and Wennberg, P. O. Measurement of gas-phase hydroperoxides by chemical ionization mass spectrometry. *Anal. Chem.*, 78(19):6726–6732, 2006. doi: 10.1021/ac0604235.

DeCarlo, P. F., Kimmel, J. R., Trimborn, A., Northway, M. J., Jayne, J. T., Aiken, A. C., Gonin, M., Fuhrer, K., Horvath, T., Docherty, K. S., Worsnop, D. R., and Jimenez, J. L. Field-deployable, high-resolution, time-of-flight aerosol mass spectrometer. *Anal. Chem.*, 78(24):8281–8289, 2006. doi: 10.1021/ac061249n.

C.2.1.1 Reagent gas

The CIMS reagent is a CF_3OOCF_3 gas synthesized in-house. During operation, CF_3OOCF_3 is held in a pressurized stainless steel vessel located in the ToF gas handling box (hereafter, gas box). To form the reagent ion, the reagent gas is diluted with nitrogen and then ionized using Po-210 ionization source (NRD, LLC Po-2021, initial activity: 10 mCi). This produces CF_3O^- which interacts with the analytes by forming ion clusters (*m/z* = target mass + 85) or fluoride-transfer ions (*m/z* = target mass + 19). CF_3O^- allows the HRToF-CIMS to be sensitive towards the detection of many oxygenated multifunctional compounds with an LOD of approximately 10 pptv during direct sampling for a 1 s integration period.

References

Crounse, J. D., McKinney, K. A., Kwan, A. J., and Wennberg, P. O. Measurement of gas-phase hydroperoxides by chemical ionization mass spectrometry. *Anal. Chem.*, 78(19):6726–6732, 2006. doi: 10.1021/ac0604235.

Huey, L. G., Villalta, P. W., Dunlea, E. J., Hanson, D. R., and Howard, C. J. Reactions of CF_3O^- with atmospheric trace gases. *J. Phys. Chem.*, 100(1):190–194, 1996. doi: 10.1021/jp951928u.

Hyttinen, N., Otkjær, R. V., Iyer, S., Kjaergaard, H. G., Rissanen, M. P., Wennberg, P. O., and Kurtén, T. Computational comparison of different reagent ions in the chemical ionization of oxidized multifunctional compounds. *J. Phys. Chem. A*, 122(1):269–279, 2018. doi: 10.1021/acs.jpca.7b10015.

C.2.1.2 ToF power supply (TPS)

The high voltages for the mass spectrometer are controlled by the ToF power supply (TPS), supplied by Tofwerk. The TPS communicates to a Windows PC (located on the instrument rack) through a serial connection and is connected to the local instrument network via an Ethernet hub located on the back of the ToF electronics box. This device receives power directly from the 120 VAC instrument power supply and is plugged into a programmable socket for remote control.

TPS voltage controls are accessed via web browser on the Windows PC (Fig. C.1). Voltage set points are defined on the Windows PC (found in C:\tofwerk\tps). The TPS is responsible for protecting the high voltage CIMS electronics when it is alerted to any issues with the turbomolecular pumps (hereafter, turbo pumps) by entering an “interlock” state. This state shuts down all CIMS voltages until the problem

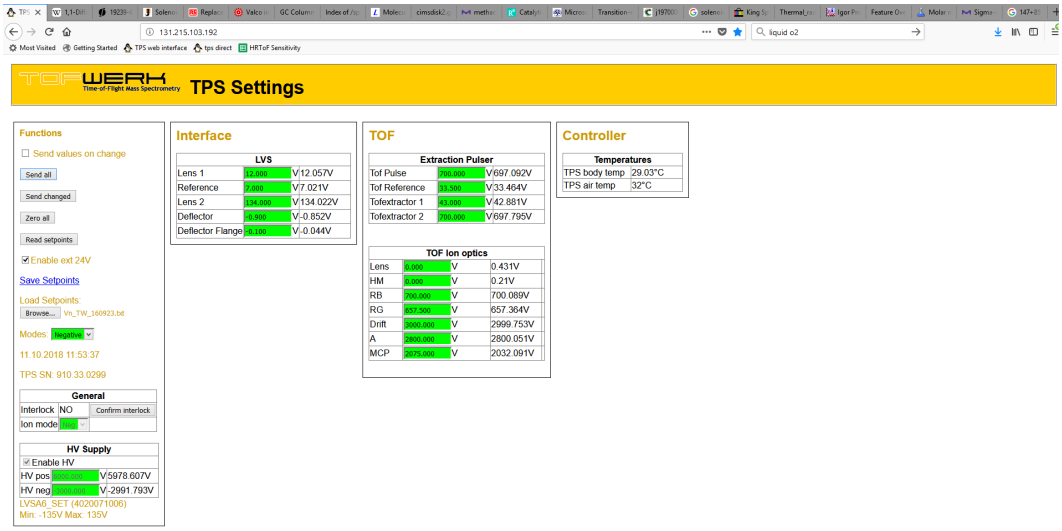

Figure C.1: TPS web browser interface.

is resolved. The interlock signal is relayed through a 2-pin molex connection that branches off from the turbo pump data cables.

C.2.1.3 Vacuum systems

Turbo pumps (Twistorr 304FS)
Agilent Technologies, Inc.
5301 Stevens Creek Blvd.
Santa Clara, CA 95051
www.agilent.com
Tel: +1 877-424-4536

Scroll pumps (nXDS 20i)
Edwards Vacuum, LLC
1735 Technology Drive, Ste 430
San Jose, CA 95110
www.edwardsvacuum.com
Tel: +1 800-848-9800

Ion gauges (972 DualMag™)
MKS Instruments, Inc.
2 Tech Drive, Ste 201
Andover, MA 01810

www.mksinst.com
Tel: +1 800-227-8766

The mass spectrometer is pumped down using a series of three turbo pumps (TwisTorr 304 FS, Agilent) which are remotely controlled and monitored through an RS485 serial connection on a Diamond Systems Hercules SBC, which located in the ToF electronics box. The three turbo pumps are connected to a power strip located in the instrument rack which draws power directly from the 120 VAC instrument power supply. Pressure within the mass spectrometer is monitored using two cold cathode ion gauges which communicate with the Hercules SBC. These ion gauges monitor the hexapole and time-of-flight (ToF) regions of the vacuum chamber.

During field operation, two scroll pumps (nXDS 20i, Edwards Vacuum, LLC) are co-located with the instrument in a separate weatherproofed enclosure. One scroll pump is used back up the three turbo pumps, while the other pumps on the flow tube (FT) and ion mixing region. The pumps are connected to the 120 VAC instrument power supply and can be remotely controlled by the Hercules computer via an RS232 serial connection.

Two normally-closed solenoid valves controlled by the Hercules SBC lie between each scroll pump and their respective connections on the mass spectrometer. This allows for separate evacuation and venting of the mass spectrometer and flow tube. A manual valve also exists between the turbo pumps and its scroll pump. It is closed during transport in case of solenoid valve failure.

C.2.1.4 MS data acquisition

14-bit Digitizer (ADQ 1600):
Teledyne SP Devices
765 Sycamore Drive
Milpitas, CA 95035
spdevices.com
Tel: +1 415-533-1341

Data is recorded at 10 Hz by a 14-bit digitizer (ADQ 1600, Teledyne Technologies). The ADQ uses +12 VDC power which is stepped down and converted directly from a 120 VAC programmable socket on the instrument power supply and acts as a link between the mass spectrometer and ToF data acquisition (ToFDAQ) software installed on the Windows PC (via USB 3.0).

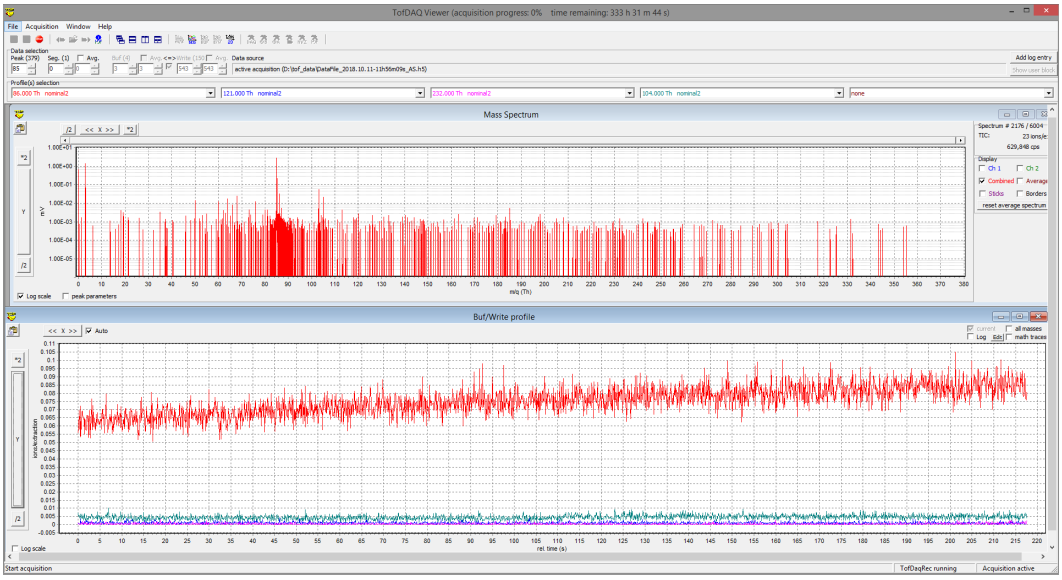

Figure C.2: TofDAQ software interface.

ToFDAQ is supplied by Tofwerk. A screenshot of the TofDAQ software interface is seen above (Fig. C.2). TofDAQ outputs a new H5 data file approximately every 10 minutes. This file format is then later converted into Matlab formatted data (.mat) using a series of Matlab functions located on the Windows PC.

C.2.1.5 ToF electronics box

The ToF electronics box provides power, communication, and/or network connections to all instrument components. It receives 120 VAC from the main instrument power supply, which is then converted to +28 VDC, +24 VDC, +/-15 VDC, +12 VDC and +5 VDC which are used as power or digital signal lines. Data and network connections are controlled by a Hercules III SBC (Diamond Systems). The front and back panels of the ToF Electronics Box can be seen below.

C.2.1.6 Gas handling and calibration

The gas box is responsible for controlling all non-GC gas flows and monitoring pressures and temperatures in the flow tube through a Diamond Systems Athena III SBC. The Athena is connected to the local instrument network through an Ethernet hub located on the back of the ToF electronics box. The gas box receives power from the ToF Electronics Box through a 10-pin Bendix circular connector.

The gas box also contains a heated calibration system (hot cal; Fig. C.4) held at a constant temperature (50 ^{o}C) using a Watlow PM6 temperature controller. This hot

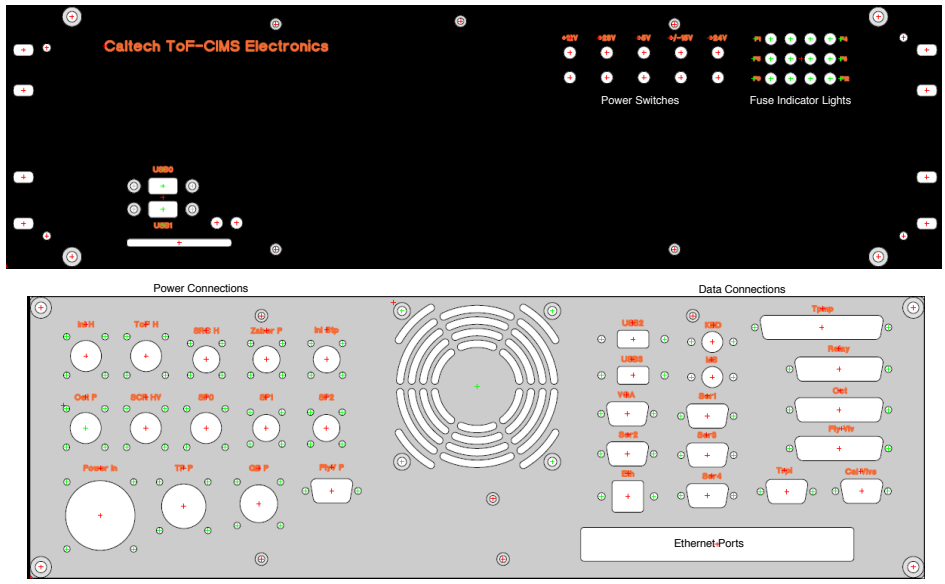

Figure C.3: Front (top) and back (bottom) panel of the ToF electronics box.

cal system is composed of three channels that contain separate calibration gases. These gases, typically held within permeation tubes, are then sent from the hot cal to a separate calibration valve box (also controlled by the gas box), which sends the gas to the flow tube, GC or exhaust. The gas box is also configured to control a cold calibration system (cold cal). However, a cold cal system has not yet been designed for this instrument.

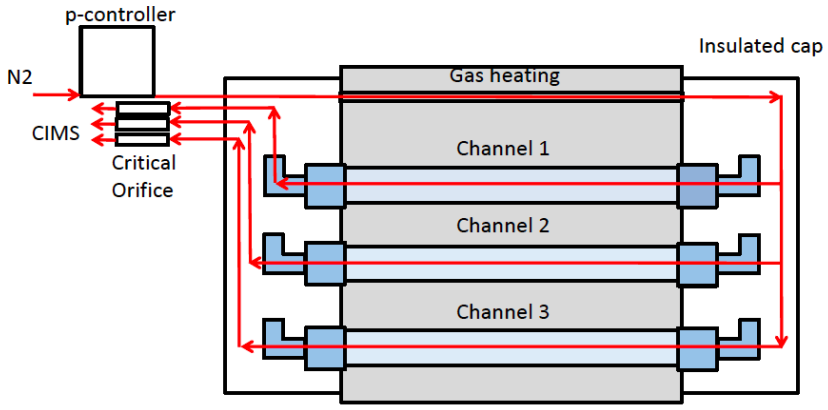

Figure C.4: Design of heated calibration system.

C.2.2 GC control box

The GC control box receives 120 VAC directly from the instrument power supply, after which the voltages are stepped down to +24 VDC, +/-15 VDC, and +5 VDC

to power its various components. Within the control box is a Diamond Systems Athena III SBC which is responsible for controlling and monitoring all GC flows, pressures, and temperatures and is connected to the local instrument network through an Ethernet hub located on the back of the ToF electronics box.

GC sample collection and elution are controlled by automated solenoid valves which are activated by two NResearch CoolDrive®driver circuits. The GC temperature is controlled by a Watlow Series F4 ramping controller together with resistance heaters (≈400 W) and three resistance temperature detectors (RTDs, F3102, Omega) which are attached to the GC itself. A spare temperature controller is also present in this box (Watlow PM6) though it currently does not have any specific use.

Details regarding the GC column box can be found in Sect. C.4

C.2.3 Power systems

The instrument requires two 120 VAC, 20A circuits. One circuit is dedicated to the uninterruptible power supply (UPS) and the enclosure AC units. The second circuit is dedicated solely to the inlet blower.

C.2.3.1 Uninterruptible power supply

USP (Online RT Series)
Orion Power Systems, Inc.
3811 University Blvd. W, Ste 3
Jacksonville, FL 32217
www.orionpowersystems.com/
Tel: +1 877-385-1654

The UPS receives approximately 24000 W to power all instrument components with the exception of the blower and the enclosure A/C units. The UPS contains one programmable circuits, which can be toggled remotely using its RS232 serial connection to the Hercules. The outlets on this circuit are typically connected to the ADQ and TPS.

C.2.4 Field-specific components

C.2.4.1 Inlet and blower

Regenerative Blower
The Spencer Turbine Company - Vortex
600 Day Hill Road

Windsor, CT 06095
www.spencerturbine.com/
Tel: +1 860-688-8361
Email: servicesdept@spencer-air.com

The instrument samples air from a custom Teflon-coated glass inlet (Fig. C.5), which measures 3.81 cm I.D. x 76.2 cm long. Air is drawn through the inlet at a high flow rate (~2000 slm) using a regenerative blower (Vortex) that is connected to the end of the glass tube. The instrument can sample a small fraction of this flow from four ports which are positioned perpendicular to the main flow in order to discriminate against large particles and other debris. Three of these ports draw air into either the CIMS, the GC, or the ambient zeroing plate. The fourth port is currently not in use.

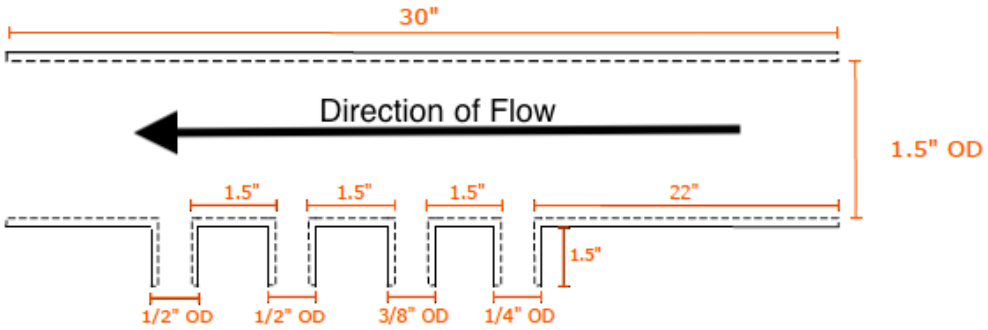

Figure C.5: Diagram of instrument inlet.

C.2.4.2 Zeno weather station

Coastal Environmental Systems - Zeno 3200
820 First Avenue South
Seattle, WA 98134
www.coastalenvironmental.com
Tel: +1 206-682-6048
Email: Support@CoastalEnvironmental.com

A Zeno 3200 weather station is typically co-located with the instrument during field campaigns and consists of commercial weather sensors for temperature and humidity (Rotronic HC2-S3), rain (ETI Model ES-1), barometric pressure (Setra Model 270), solar radiation (Li-Cor LI-200SZ), and wind speed and wind direction (Young Co. 03002 Wind Sentry). Sensors are connected to a datalogger which

continuously outputs values as a comma-delimited string at 1 Hz and sends them to the Hercules computer using an RS232 serial connection. The datalogger contains its own battery which is plugged in directly to the instrument power supply.

C.2.4.3 Sonic anemometers

Campbell Scientific, Inc. - Model CSAT3
815 West 1800 North
Logan, UT 84321
www.campbellsci.com/
Tel: +1 435-227-9100
Email: info@campbellsci.com

If conditions are appropriate, two three-dimensional ultrasonic anemometers can be used with this instrument to measure wind speeds along three non-orthogonal sonic axes at 10 Hz sampling frequency. These speeds are then transformed in real time to the wind velocity components u, v, and w. The Wennberg CSAT3 sonic anemometer contains its own electronics box which is plugged in directly to the instrument power supply. It communicates with the Hercules via a RS232 serial connection.

C.2.5 Instrument enclosure

T-Slotted Frames
80/20, Inc.
1701 County Rd 400 East
Columbia City, IN 46725
8020.net
Tel: +1 844-802-0932

Enclosure Paneling (Thermolite)
Edwards Vacuum, LLC
3255 Penn Street
Hatfield, PA 19440
www.laminatorsinc.com/
Tel: +1 877-663-4277

HVAC units (Blade Series)
Ice Qube, Inc.
141 Wilson Avenue
Greensburg, PA 15601

www.iceqube.com
Tel: +1 724-837-7600
Email: service@iceqube.com

The instrument enclosure measures 1.1 m x 1.7 m x 0.9 m (W x H x D). The total weight of this rack when fully assembled is approximately 275 kg. In the field, the aluminum rack (80/20, Inc.) is weatherproofed by attaching Thermolite insulated paneling (Laminators, Inc.) and weather stripping. In addition, the enclosure is equipped with two HVAC units (Ice Qube IQ1700B and IQ2700B, Blade series, cooling power = 478 and 791 W, respectively) to remove heat produced by the instrument electronics.

C.3 Instrument plumbing

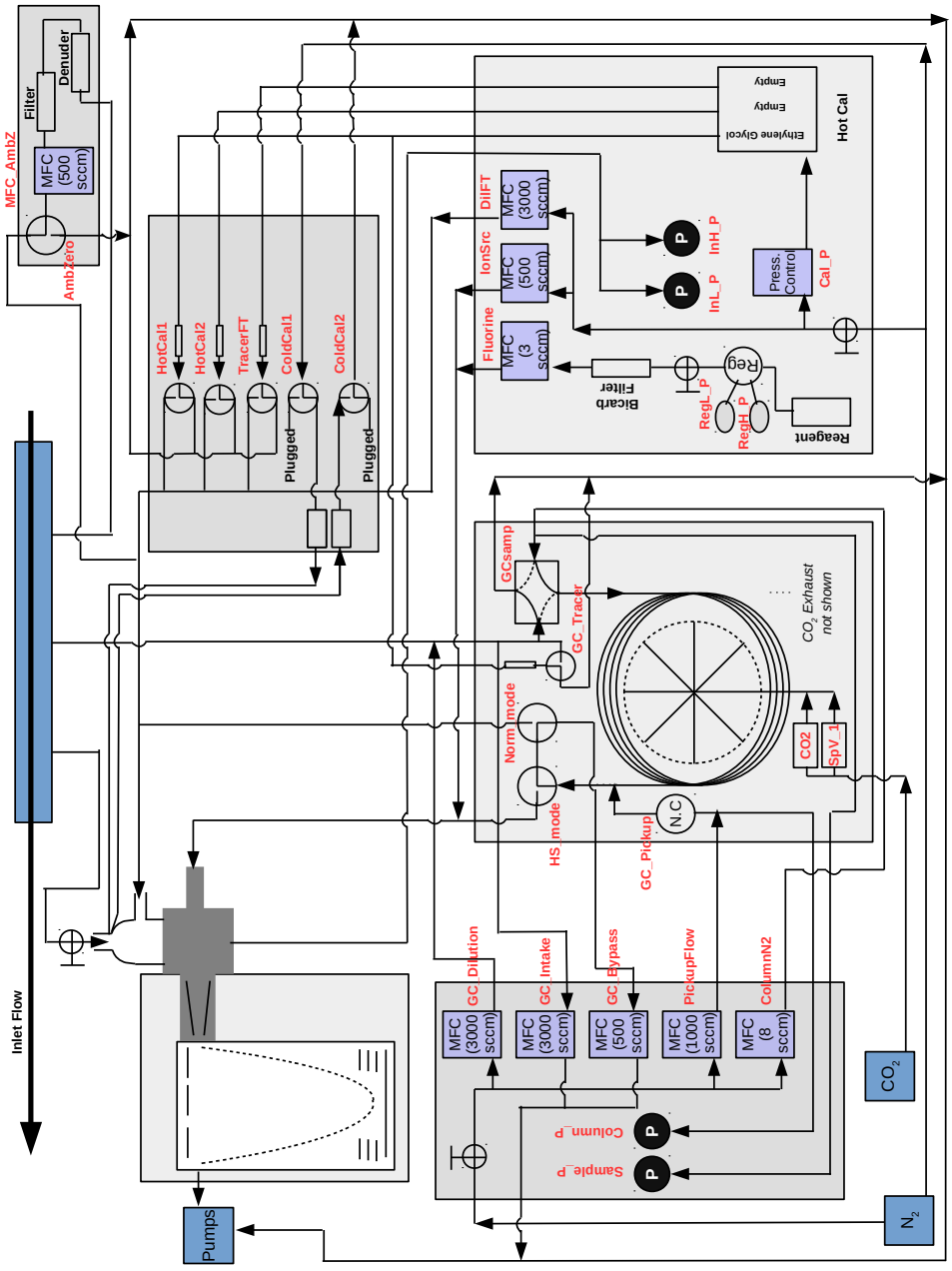

Figure C.6: Detailed schematic of instrument plumbing (as 2017). Valves are drawn in their default states.

C.4 GC column box

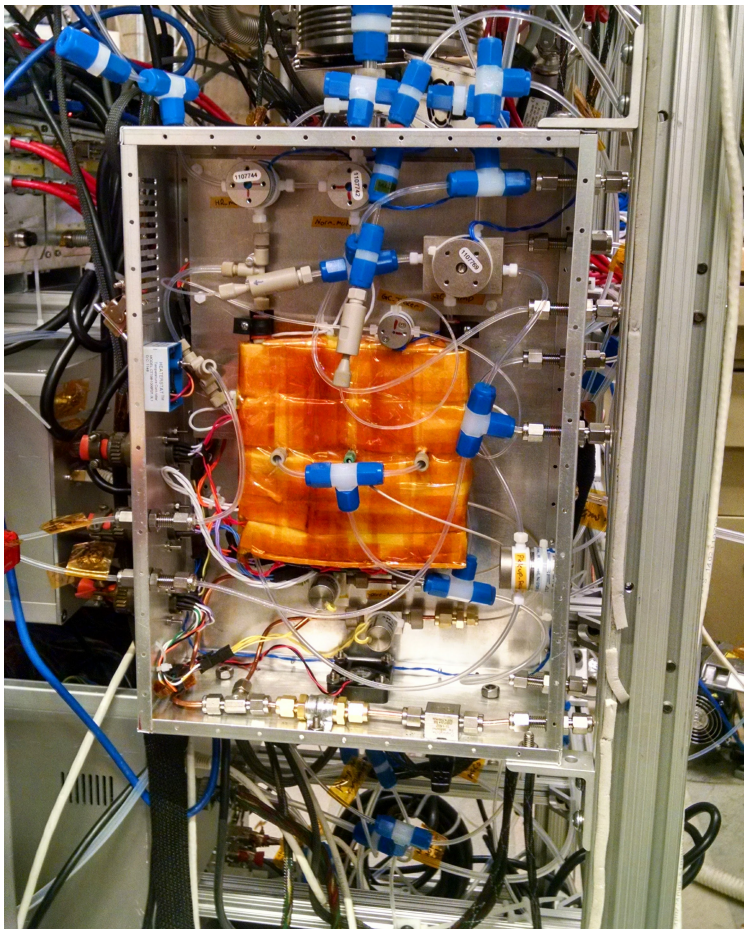

Figure C.7: Picture of the GC column box in the instrument rack.

The GC column box (Fig. C.8) houses the GC column assembly and all GC-related valves, heaters, temperature sensors, and gas lines. The GC is made up of a short (1 m) megabore column (RTX-1701, Restek) encased between two aluminum plates, each measuring 130 mm × 130 mm × 5 mm (total mass = 466 g). Liquid CO_2 used to cool the GC and enters directly into the center of the GC plates before flowing along eight radial grooves (Fig. C.9). The movement of the CO_2 from the center to the outside of the plate establishes a temperature gradient in the same direction while the symmetry of the design enables the entire column to remain at a similar temperature, in spite of this gradient.

The column box is connected to the GC control box with two 14 pin and one 10 pin Bendix circular connectors to allow communication between the GCAthena2 and the GC valves, heaters and RTDs, respectively. An overview of the GC plumbing is shown in Figure C.10.

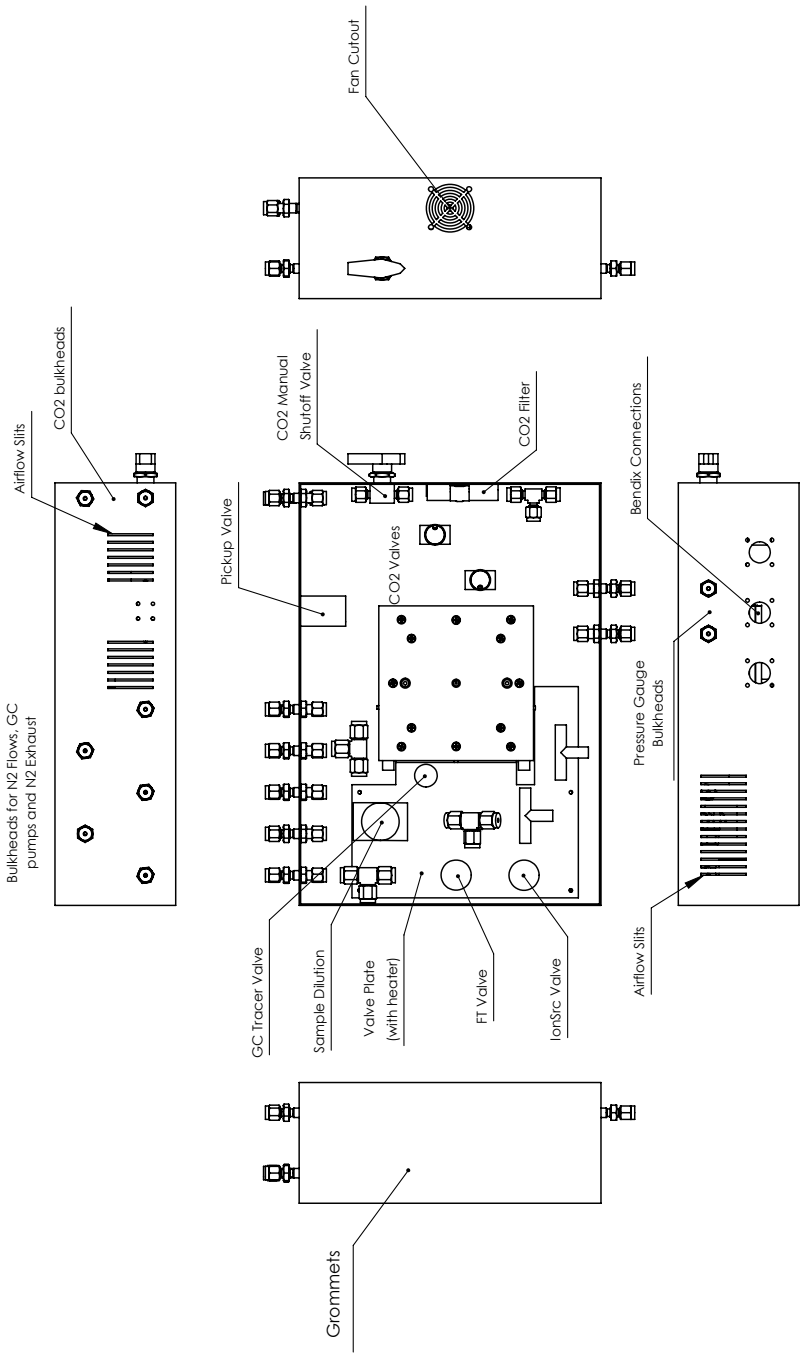

Figure C.8: Schematic of the GC column box.

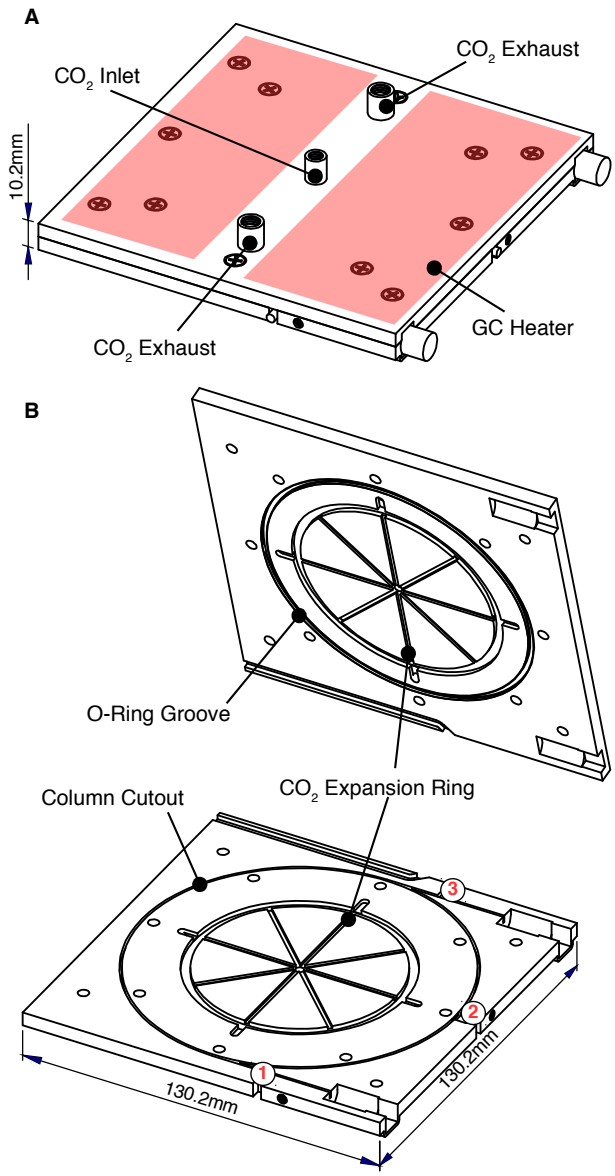

Figure C.9: Schematic of the GC cryotrap and heating unit. Figure taken from Vasquez et al. (2018). Column sits in a groove machined into one plate, providing good thermal contact. CO_2 enters from the center of both plates and expands in the eight radial spokes before exiting through four exhaust ports. Heaters are adhered to the outside of the GC assembly; two of these heaters are shown above in red. The temperature is measured at three locations near the column: (1) near the inlet of the column, (2) on the column ring, and (3) near the outlet of the column.

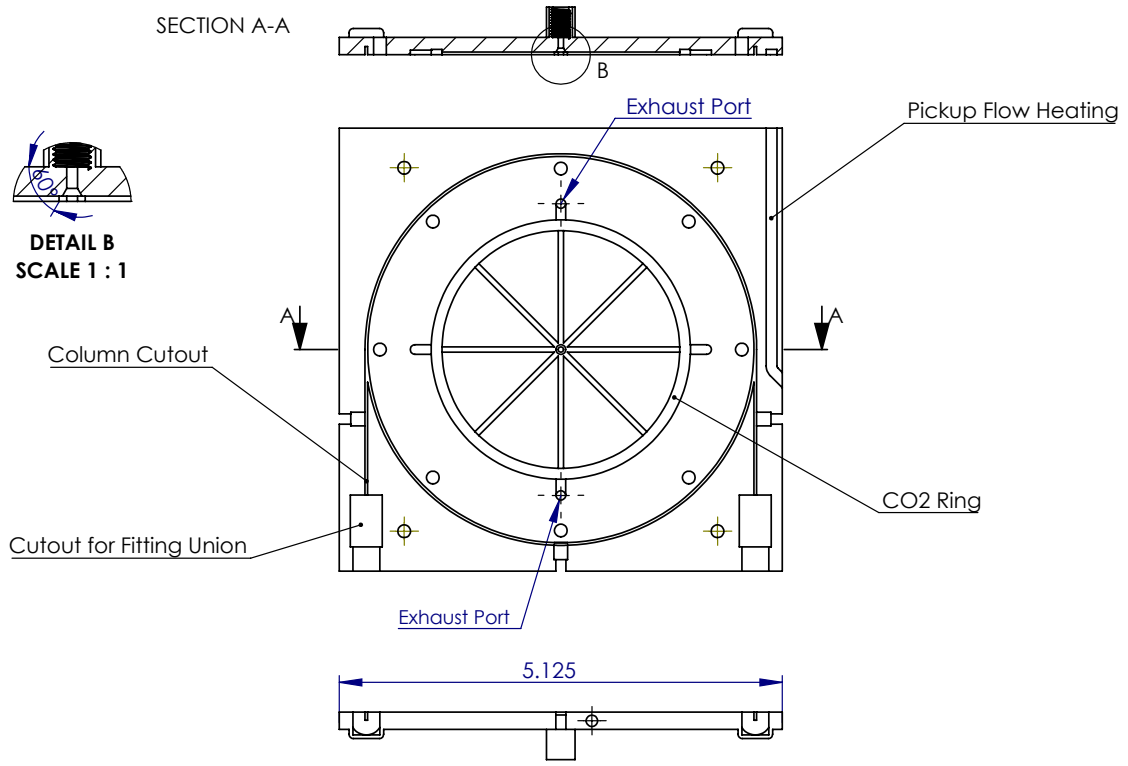

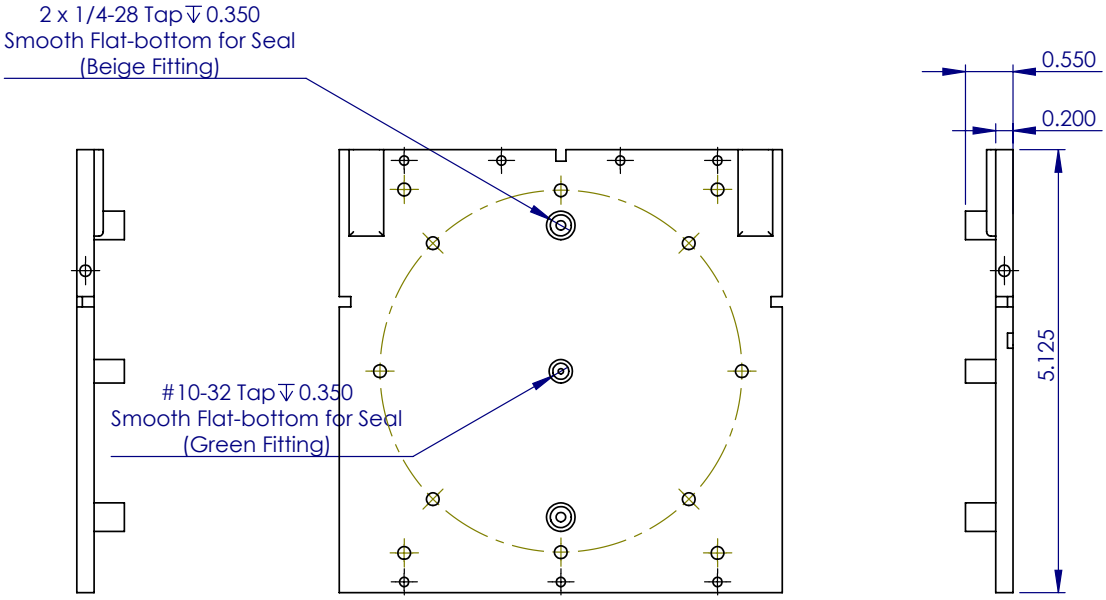

		DIMENSIONS ARE IN INCHES TOLERANCES: FRACTIONAL ± ANGULAR: MACH ± BEND ± TWO PLACE DECIMAL ± THREE PLACE DECIMAL ±		NAME	DATE
			DRAWN		
			CHECKED		
			ENG APPR.		
			MFG APPR.		
			Q.A.		
		MATERIAL Aluminum	COMMENTS:		
NEXT ASSY	USED ON	FINISH			
APPLICATION		DO NOT SCALE DRAWING			

Caltech

GC_Plate_Bottom

SIZE	DWG. NO.	REV.
A		
SCALE: 1:2	WEIGHT:	SHEET 1 OF 2

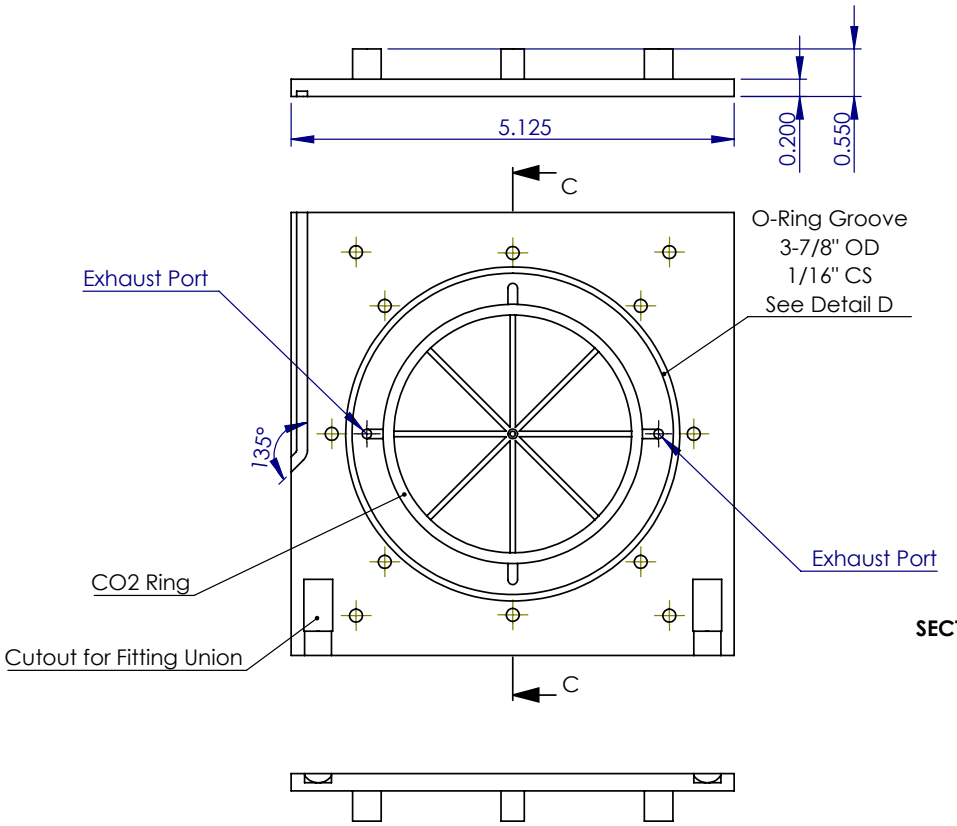

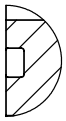

DETAIL D
SCALE 2 : 1

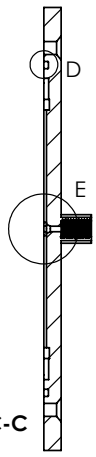

SECTION C-C

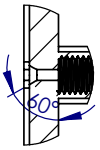

DETAIL E
SCALE 1 : 1

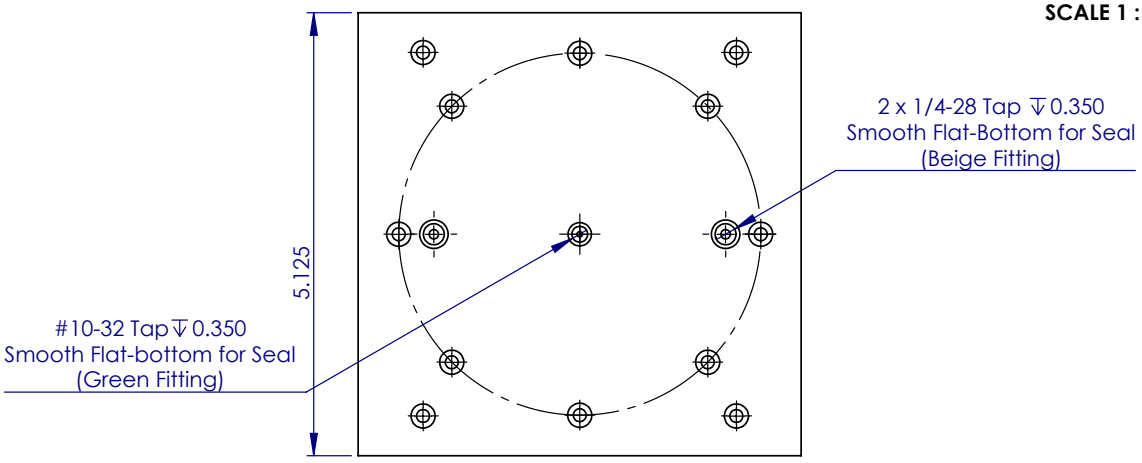

		DIMENSIONS ARE IN INCHES TOLERANCES: FRACTIONAL ± ANGULAR: MACH ± BEND ± TWO PLACE DECIMAL ± THREE PLACE DECIMAL ±		NAME	DATE
			DRAWN		
			CHECKED		
			ENG APPR.		
			MFG APPR.		
			Q.A.		
		MATERIAL Aluminum	COMMENTS:		
NEXT ASSY	USED ON	FINISH			
APPLICATION		DO NOT SCALE DRAWING			

Caltech

GC_Plate_Top

SIZE	DWG. NO.	REV.
A		
SCALE:1:2	WEIGHT:	SHEET 2 OF 2

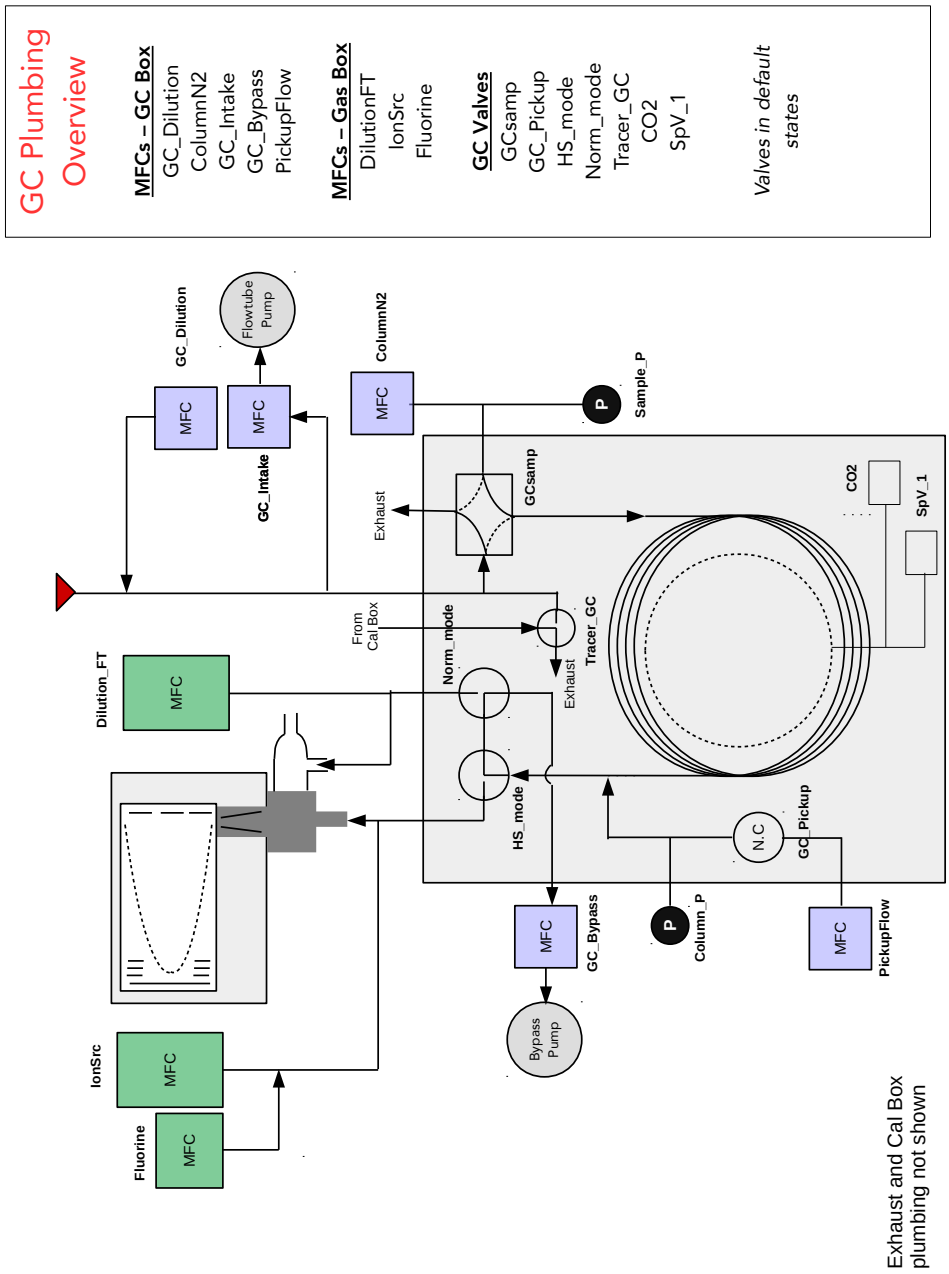

Figure C.10: GC plumbing overview for the 1 meter column.

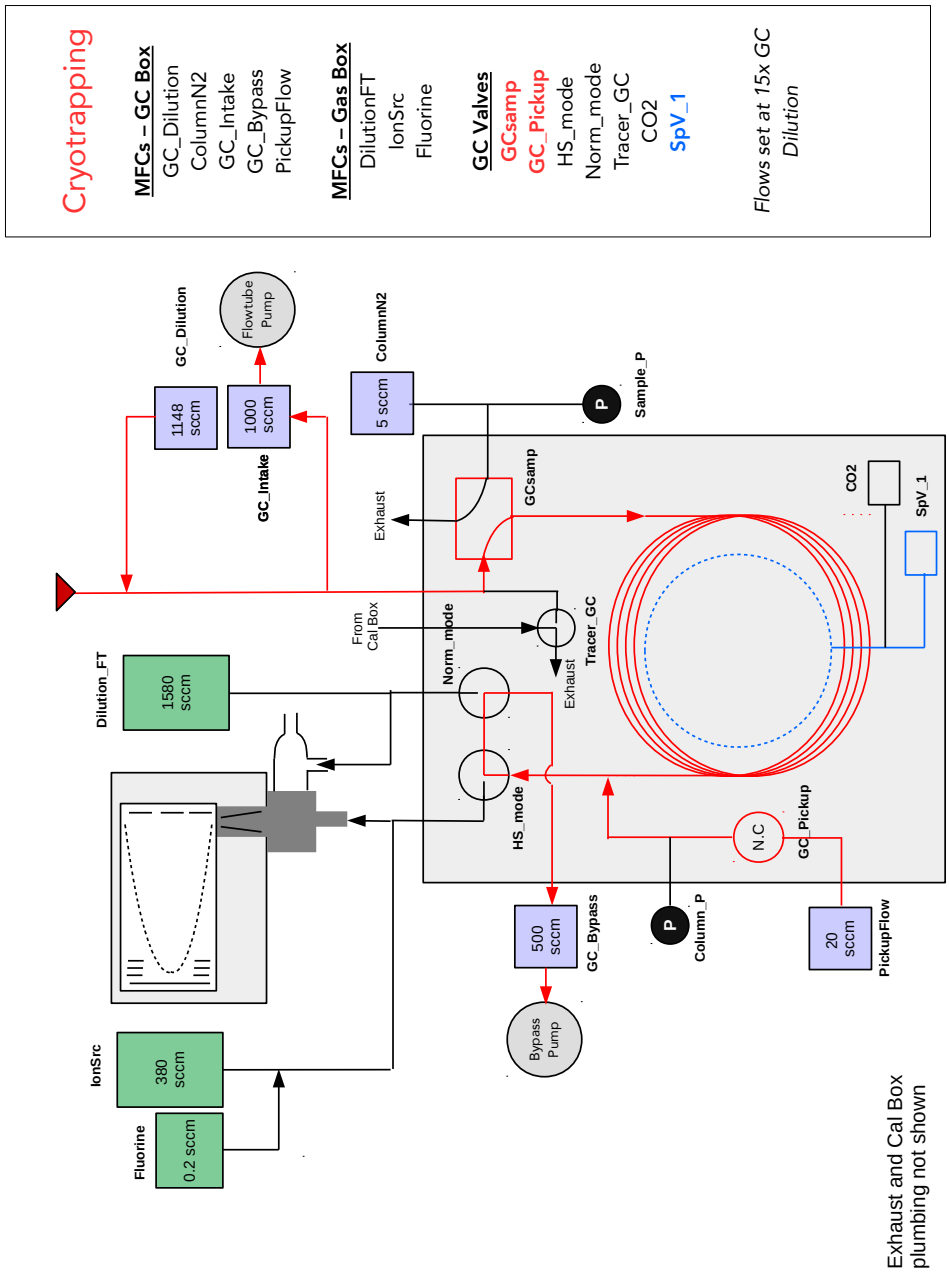

Figure C.11: GC plumbing overview for the 1 meter column. The flow path and valves activated during cyrotrapping is highlighted in red. The active CO_2 valve is highlighted in blue.

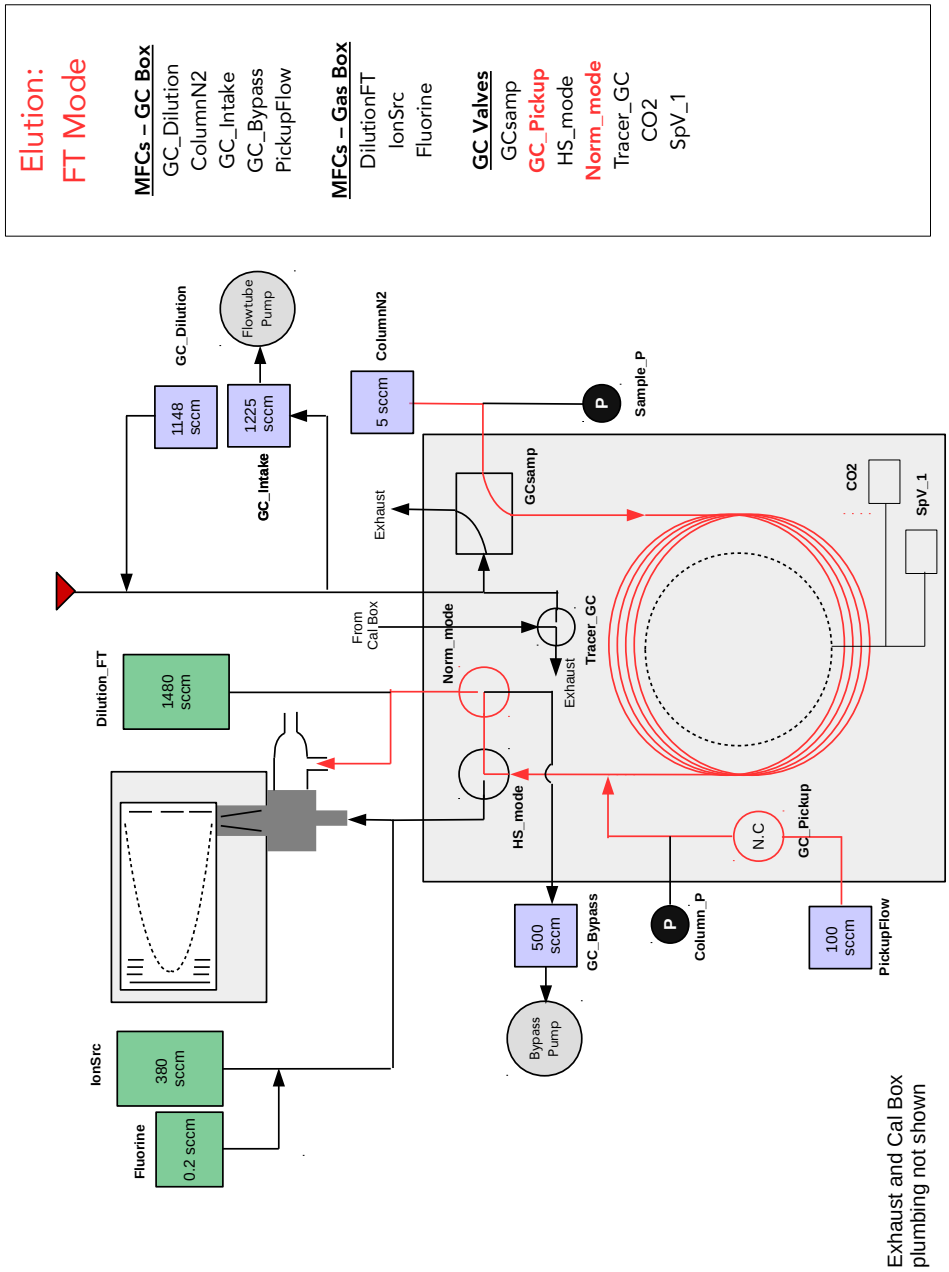

Figure C.12: GC plumbing overview for the 1 meter column. The flow path and valves activated during elution into the flow tube is highlighted in red.

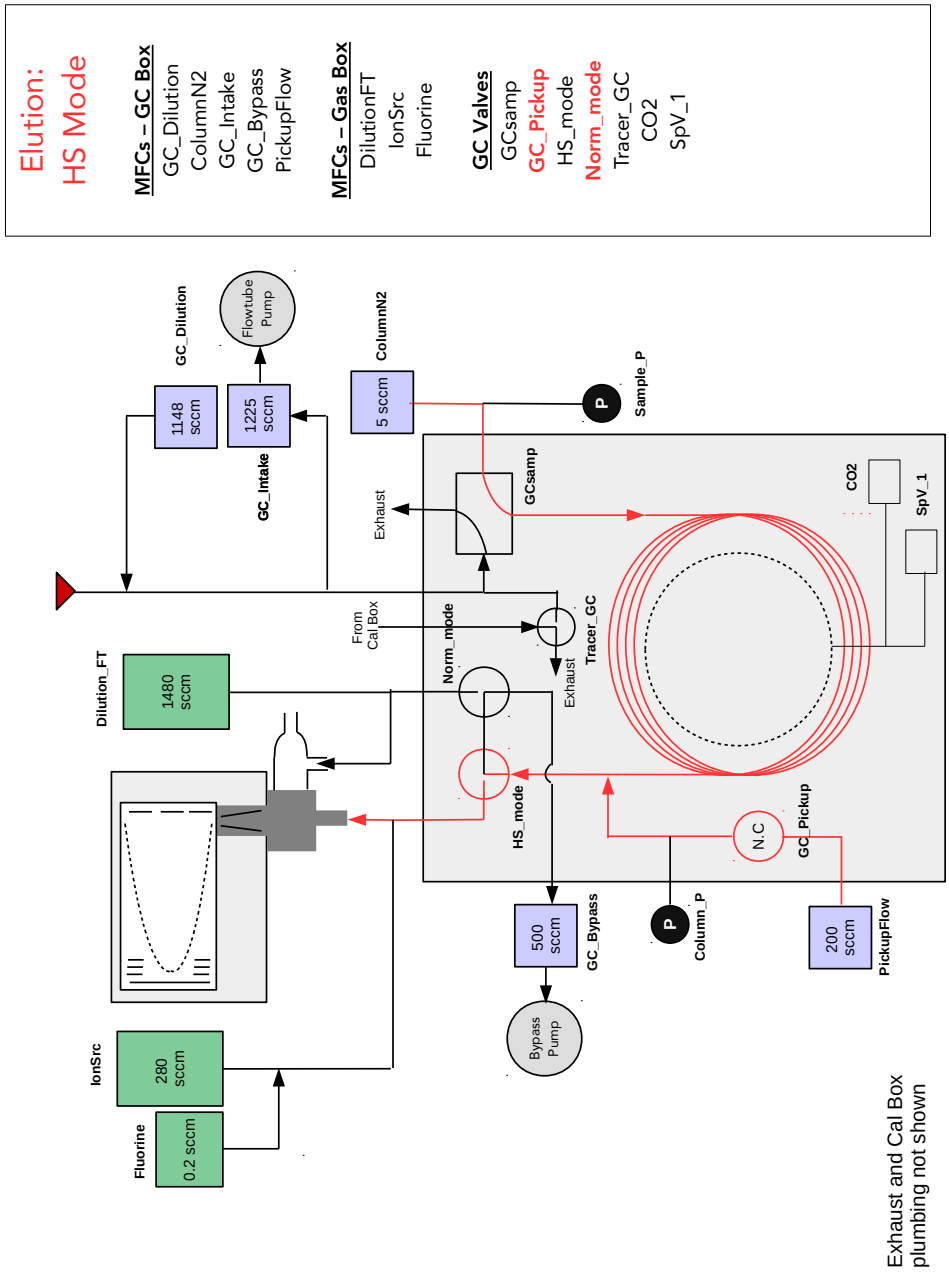

Figure C.13: GC plumbing overview for the 1 meter column. The flow path and valves activated during elution into the ion source is highlighted in red.

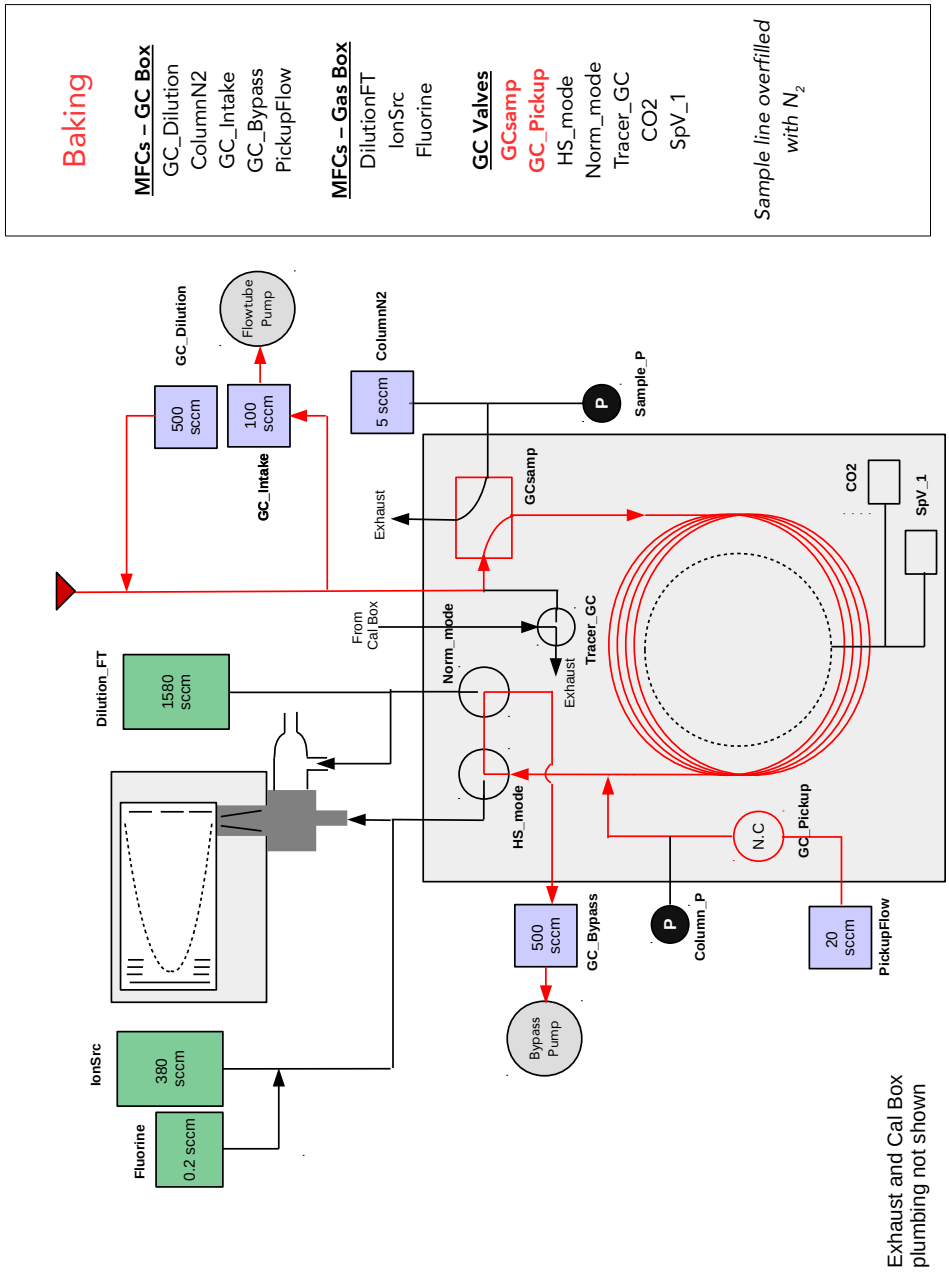

Figure C.14: GC plumbing overview for the 1 meter column. The flow path and valves activated during the GC baking period is highlighted in red.

C.5 Instrument software

C.5.1 Software overview

Devices that make up the instrument are either monitored and/or controlled with Diamond Systems single-board computers (SBCs) present in the Electronics Box (GCHerc), gas box (GCAthena1), or GC control box (GCAthena2). All computers are on the same network and display readbacks on software installed on the GCHerc QNX operating system. This software continuously acquires data from the various components of the instrument over serial, analog, digital, and network connections. Data is saved as binary telemetry data at either 1 Hz or 10 Hz (See Sect. C.5.2).

The GCHerc QNX operating system is accessed through a virtual machine installed on the Windows PC (GCwinVM). Software is initialized through a 'doit' script located in the /home/GCToF directory. Presently, a bug is present in the VM preventing the various readback screens from being displayed properly on the VM itself. Therefore, to access this software, you can SSH into GCwinVM (using software such as PuTTY on Windows PC or the built-in terminal in macOS; IP address (Lab): 131.215.103.242), go to /home/GCToF and type `./doit -sa`.

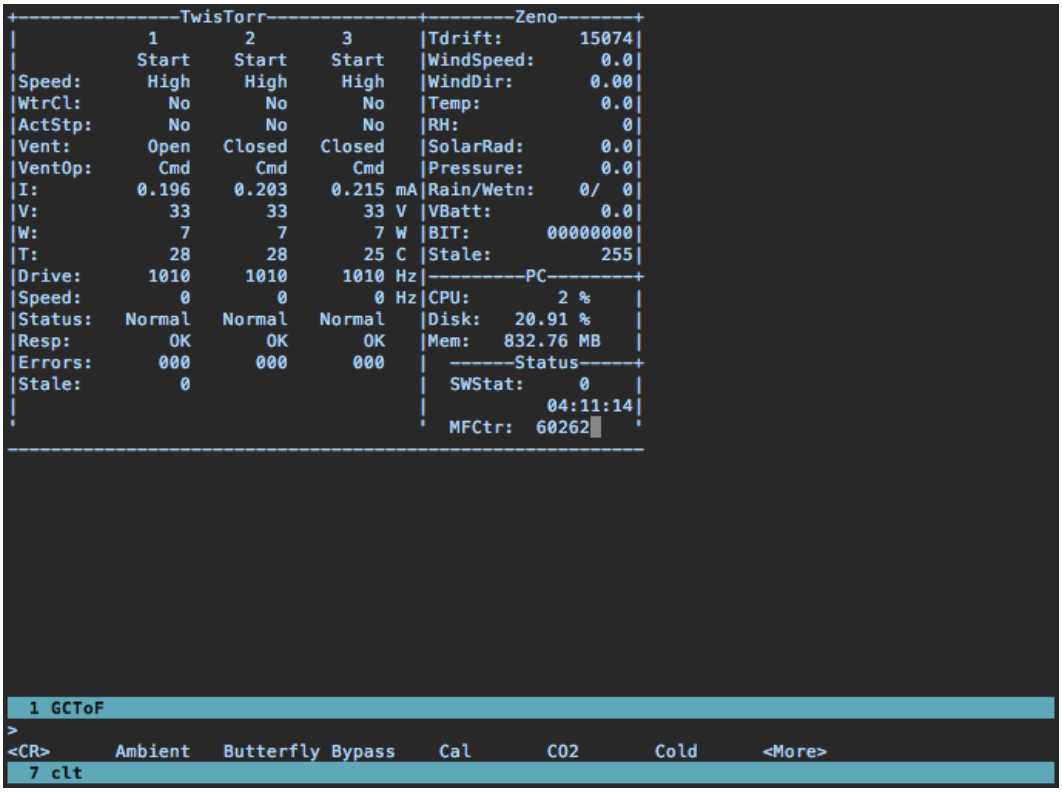

Figure C.15: QNX software interface.

When the software is initialized, it begins to continuously acquire device readbacks. Data is organized in a series of tables displayed on several screens, an example of which can be seen in Figure C.15. To switch between these screens, type `Ctrl + A` + space. Software commands (See Sect. C.5.3) can be typed while on any of these screens.

C.5.2 Telemetry data

The following table lists selected parameters that are continuously acquired by the software. Though the QNX software collects data that is not listed here, the following were included due to their importance in determining instrument health and assessing ambient conditions.

Table C.1: 1 Hz Telemetry Data.

Name	Unit	Description
SWStat	integer	Bit-mapped status word indicating change in GCToF.tma state
Zeno_Tdrift	s	Time difference between Zeno datalogger and GCHerc
Zeno_WindSpeed	m s^{-1}	Young Co. 03002 Wind Sentry; Wind speed reported by Zeno datalogger
Zeno_WindDir	degree	Young Co. 03002 Wind Sentry; Wind direction reported by Zeno datalogger
Zeno_Temp	^{o}C	Rotronic HC2-S3; Temperature reported by Zeno datalogger
Zeno_RH	%	Rotronic HC2-S3; Relative humidity reported by Zeno datalogger
Zeno_SolarRadiance	W m^{-2}	Li-Cor LI-200SZ; Solar radiance reported by Zeno datalogger
Zeno_Press	hPA	Setra 270; Barometric pressure reported by Zeno datalogger
Zeno_Rain	integer	ETI Model ES-1; Incidence of rain reported by Zeno datalogger
Zeno_VBatt	V	Battery voltage of Zeno datalogger battery
Zeno_BIT	integer	Error codes as described in Zeno manual
Zeno_Stale	s	Time since last reply from Zeno datalogger

Table C.1 Continued: 1 Hz Telemetry Data

Name	Unit	Description
RegH_P	psi	Reagent bottle pressure reading
RegH_L	psi	Reagent gas line pressure reading
InL_P	mbar	flow tube low pressure reading
InH_P	mbar	flow tube high pressure reading
FT_T1	V	Temperature sensor #1 of ion mixing region
FT_T2	V	Temperature sensor #2 of ion mixing region
CalP_SP	mbar	Hot calibration gas pressure set point
CalP	mbar	Hot calibration gas pressure read back
HotCalT_SP	^{o}C	Hot calibration system temperature set point
HotCalT	^{o}C	Hot calibration system temperature read back
Sample_P	mbar	Pressure at head of GC column
Column_P	mbar	Pressure at tail of GC column
GC_T_SP	^{o}C	GC column temperature set point
GC_T	^{o}C	GC column temperature read back #1
GCF4_T2	^{o}C	GC column temperature read back #2
GCF4_T3	^{o}C	GC column temperature read back #3
GCWatlow_F4_Op	integer	Bit-mapped status word indicating start of GC temperature profile
GCWatlow_stale	s	Time since last reply from GC temperature controllers
Fluorine_SP	sccm	Reagent gas flow controller set point
Fluorine	sccm	Reagent gas flow controller read back
IonSrc_SP	sccm	Ion source dilution flow controller set point
IonSrc	sccm	Ion source dilution flow controller read back
DilFT_SP	sccm	flow tube dilution flow controller set point
DilFT	sccm	flow tube dilution flow controller read back
MFC_Sp2_SP	sccm	Ambient zero flow controller set point
MFC_Sp2	sccm	Ambient zero flow controller read back
GBHoriba_stale	s	Time since last reply from gas box mass flow controllers
ColumN2_SP	sccm	GC carrier gas flow controller set point
ColumN2	sccm	GC carrier gas flow controller read back

Table C.1 Continued: 1 Hz Telemetry Data

Name	Unit	Description
GC_Intake_SP	sccm	GC sample intake flow controller set point
GC_Intake	sccm	GC sample intake flow controller read back
PickupFlow_SP	sccm	GC effluent pickup flow controller set point
PickupFlow	sccm	GC effluent pickup flow controller read back
GC_Dilution_SP	sccm	GC sample dilution flow controller set point
GC_Dilution	sccm	GC sample dilution flow controller read back
GC_Bypass_SP	sccm	GC bypass pump flow controller set point
GC_Bypass	sccm	GC column flow rate read back
GCHoriba_stale	s	Time since last reply from GC mass flow controllers
A1_DS_A	integer	Bit-mapped status word indicating switching of gas box-controlled valves
A2_DS_A	integer	Bit-mapped status word indicating switching of GC-controlled valves
A2_DS_B	integer	Bit-mapped status word indicating switching of CO_2 valves

Table C.2: 10 Hz Telemetry Data.

Name	Unit	Description
Hex_P	mbar	Hexapole pressure
ToF_P	mbar	ToF region pressure
IG_stale	s	Time since last reply from ion gauges
Sonic1_U	m s^{-1}	Wind speed of orthogonal wind component U reported by CSAT3 sonic anemometer
Sonic1_V	m s^{-1}	Wind speed of orthogonal wind component V reported by CSAT3 sonic anemometer
Sonic1_W	m s^{-1}	Wind speed of orthogonal wind component W reported by CSAT3 sonic anemometer
Sonic1_C	m s^{-1}	Speed of sound reported by CSAT3 sonic anemometer
Sonic1_stale	s	Time since last reply from CSAT3 sonic anemometer

Table C.2 Continued: 10 Hz Telemetry Data.

Name	Unit	Description
Sonic2_U	m s^{-1}	Wind speed of orthogonal wind component U reported by additional sonic anemometer
Sonic2_V	m s^{-1}	Wind speed of orthogonal wind component V reported by additional sonic anemometer
Sonic2_W	m s^{-1}	Wind speed of orthogonal wind component W reported by additional sonic anemometer
Sonic2_C	m s^{-1}	Speed of sound reported by additional sonic anemometer
Sonic2_stale	s	Time since last reply from additional sonic anemometer

C.5.3 doit command tree

This is a full description of useful commands that are accepted by the data acquisition software. Not all possible commands are listed here. The letters which are capitalized must be typed. The others will be finished by command completion.

Ambient zero valve

Off: Sends scrubbed ambient air to exhaust

On: Sends scrubbed ambient air to flow tube

COLD cal

1

Off: Overfills flow tube with dry nitrogen

On: Stops overfilling flow tube with dry nitrogen

2

Off: Does not pump on sample inlet

On: Pump on sample inlet

COLUm n2 pickup flow valve

Off: Turns GC pickup valve off

`On`: Turns GC pickup valve off

`CO2 flow valve`

`Off`: Turns high flow CO_2 valve off

`On`: Turns high flow CO_2 valve off

`Exit`: Exits out of doit software, but leaves everything running as is

`Gc` (space)

`Sample dilution`

`Off`: Sends ambient GC sample to exhaust

`On`: Sends ambient GC sample to column

`Tracer flow to`

`Ft`

`Off`: Sends hot cal tracer gas to exhaust

`On`: Sends hot cal tracer gas to flow tube

`Gc`

`Off`: Sends hot cal tracer gas to exhaust

`On`: Sends hot cal tracer gas to GC

`Gcwatlow`

`F4`

`Profile`

`STart file number`: Starts GC profile of specified file number

`Terminate`: Terminates GC profile

`Set gc`

`Column temperature`: Sets GC column temperature set point to specified value

`HIgh sensitivity mode`

`Off`: Directs GC effluent to bypass pump or flow tube depending on configuration of downstream valve

`On`: Directs GC effluent to ion source

NOrmal GC mode

Off: Directs GC effluent to bypass pump

On: Directs GC effluent to flow tube

Quit: Kills all processes, sets instrument to idle and exits out of doit software. Note: Quit does not close the zaber (actuator that allows airflow into the mass spectrometer). As described in later sections, standard protocol requires that the user sets the zaber position to zero (no airflow into the mass spectrometer) before quitting the software.

Set

Ft

Dilution flow: Sets flow tube dilution flow to specified value

Ion source dilution flow: Sets ion source dilution flow to specified value

Reagent flow: Sets reagent gas flow to specified value

Gc

Bypass flow: Sets GC bypass pump flow to specified value

Column n2 flow: Sets GC carrier gas flow to specified value

Dilution flow: Sets GC sample dilution flow to specified value

Intake flow: Sets GC intake pump flow to specified value

Pickup flow: Sets GC effluent pickup flow to specified value

Oct

Amp: Sets octopole amp voltage to specified value

Bias: Sets octopole bias voltage to specified value

Spare

2 flow: Sets ambient zero gas flow to specified value

SPare valve

A2_1

Off: Turns low flow CO_2 valve off

On: Turns low flow CO_2 valve on

SWstatus

Data loop

Flux

Gc start: Algorithm that alternates between direct CIMS sampling and GC-CIMS sampling (Field use only)

Only start: Algorithm that only performs direct CIMS sampling (Field use only)

Gc

Blank: Algorithm that collects blank GC run (Field use only)

Only: Algorithm that only performs GC sampling (Field use only)

Labgccims: Algorithm for high sensitivity GC experiments performed in the laboratory

LabgccimsFt: Algorithm for flow tube GC experiments performed in the laboratory

Watercal_lab: Algorithm to perform automated water calibration on a compound. The water calibration set up is not covered in this documentation.

StAndby: Stops any algorithm running; sets instrument to idle flows and temperatures

StOp: Stops any algorithm running; flows, valves and temperatures remain as is

TWistorr

A

STArt: Starts turbo pump A

SOft start

No: Does not start turbo pump A via soft start

Yes: Starts turbo pump A via soft start

STOp: Stops turbo pump A

Vent

Closed: Turns Blower on

Open: Turns Blower off

B

STArt: Starts turbo pump B

SOft start

No: Does not start turbo pump B via soft start

Yes: Starts turbo pump B via soft start

STOp: Stops turbo pump B

Vent

Closed: Opens solenoid valve connecting flow tube to vacuum pump

Open: Closes solenoid valve connecting flow tube to vacuum pump

C

STArt: Starts turbo pump C

SOft start

No: Does not start turbo pump C via soft start

Yes: Starts turbo pump C via soft start

STOp: Stops turbo pump C

Vent

Closed: Opens solenoid valve connecting turbo pumps to vacuum pump

Open: Closes solenoid valve connecting turbo pumps to vacuum pump

Ups socket 1

Off: Turns off power to devices connected to UPS socket 1

On: Turns on power to devices connected to UPS socket 1

Zaber

Move

All drives

Absolute: Move all zabers to specified position

`Drive`

`1`

`Absolute`: Move zaber 1 to specified position

`2`

`Absolute`: Move zaber 2 to specified position

Additional notes:

To safely shut down an individual computer, quit QNX, then type: `sudo on -f /net/[Computer Name]/ shutdown`. To shut down all computers, quit QNX, then type: `sudo ./shutdown_flight_gc.sh`.

C.6 Instrument automation

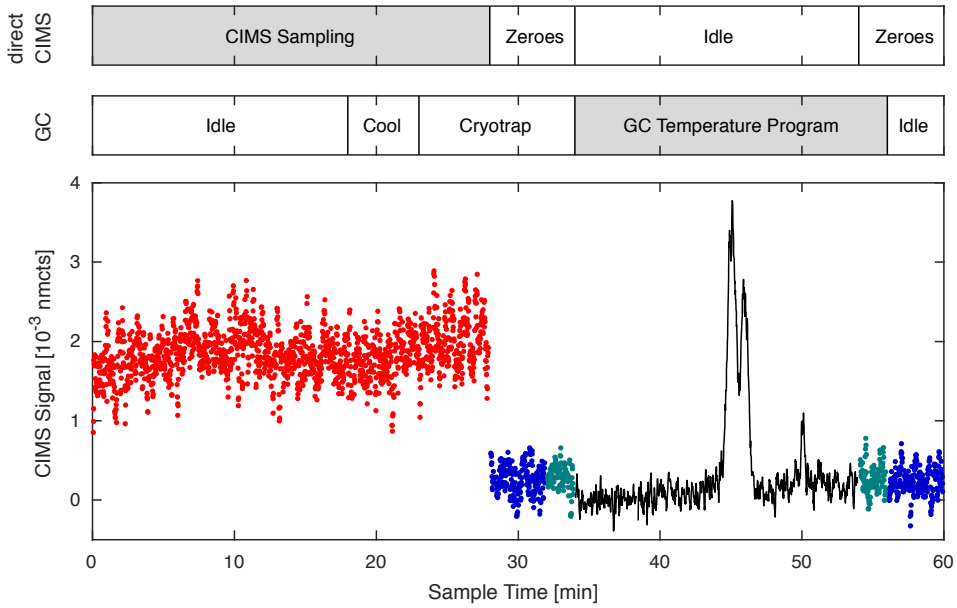

Figure C.16: A typical GC-CIMS sampling routine. Figure taken from Vasquez et al. (2018). Data is shown for *m/z* 232 and was collected during the 2017 field study in Pasadena, CA. Automation cycle has a period of 1 h in which the first half is dedicated to direct CIMS measurements (red), and the latter half measures compound signals that have undergone chromatographic separation (black). The two sampling modes are separated by a zeroing period comprised of a 4 min ambient zero (blue) and a 2 min dry zero (green). Most GC processes occur in the background during direct sampling, so as not to interrupt data collection.

The instrument automation source code can be found in /home/GCToF/src/TM. Automated data acquisition is defined in two files: flows.tma and GCToF.tma.

Flows.tma defines the instrument flows and temperatures for each instrument mode, while GCToF.tma determines the order and timing of each state and defines individual sampling routines (`SWStatus`). Each TMA file is also further separated into different partitions, controlling flows and temperatures specifically for the gas box and GC. Only one state can be active in each partition at a given time, but many partitions are allowed to be operating simultaneously.

A typical GC-CIMS sampling routine is shown in Figure C.16. While in the field, data acquisition occurs during a 1 hour cycle (`data loop labgccims`) in which the first half is dedicated to direct CIMS measurements and the second half measures compound signals that have undergone chromatographic separation. The two measurement modes are interlaced with two types of zeros: A dry nitrogen zero that is most similar to the GC measurements and can assess the health of the instrument over the course of a campaign, and an ambient zero that captures background signals that are adjusted for the water-dependent sensitivity of the compounds measured during direct CIMS sampling.

You can download the current TMA files by using using WinSCP (Windows) or you can SSH into GCwinVM (macOS/Linux) to transfer files from the VM to a personal computer. Best practices require that changes to these files should be done on your personal computer before re-uploading and distributing the files among the GCHerc and two GCAthena computers.

To upload and distribute the files:

1. Transfer files from personal computer to your personal folder located in GCwinVM (e.g. /home/kvasquez/). Make sure files are renamed to flows.tma and GCToF.tma before proceeding.
2. Change current directory to /home/GCToF/src/TM and backup the old tma files by renaming them, using the format (GCToF_tma.YYYYMMDD).
3. Copy the files from your personal directory to /home/GCToF/src/TM.
4. If the doit script is still running, open another terminal to quit the software before proceeding.
5. Once you have quit the doit script, return to /home/GCToF/src/TM and type `make`, then `distribute`. If properly compiled, terminal should output `Successfully distributed to node(s) GCwinVM GCHerc GCAthena1 GCAthena2`.

6. Restart the doit script and test new/updated algorithm.

If you want to create a new sampling routine, you also have to edit the following files: `GCToF.sws`, `SWData.cmd` and `SWData.h`. Simply follow the format of the last line, then make and distribute as directed above.

C.7 Daily operation

This section includes procedures for the day-to-day operation of this instrument. These procedures are applicable regardless of whether the instrument is in lab or in the field.

C.7.1 Instrument start-up

1. Set the CIMS flow tube dilution, ion source dilution, and reagent gas flows. Typical operating flows are as follows:

   FT dilution flow: 1580 sccm

   FT Ion Source dilution flow: 380 sccm

   FT reagent flow: 0.2 sccm

2. SLOWLY open the fluorine needle valve on the front of the gas box (black, round knob). Stop turning valve when the reagent flow read back jumps to 2-3 sccm. Wait until the reagent gas line equilibrates and the flow read back matches the set point. Open valve a little more. Repeat until the reagent flow no longer changes when valve is turned.

3. Ramp octopole amp voltage in 0.2 V increments until setpoint reads 0.9 V. Note: Setting the octopole amperage directly to 0.9 V may cause the fuse to blow.

4. Set octopole voltage bias to 0.1 volts.

5. On web browser, go to the TPS Web Interface tab. If a tab is not there, go to C:\tofwerk\TofDAQ on the instrument Windows PC and run `tps2locator.exe`. Copy the outputted IP address to the web browser.

6. Verify that a file is listed under the `Load Setpoints` section, `Interlock` is set to NO and `Ion Mode` is Negative. Then click `Send All` and wait for voltages to reach the set points. If a file is not listed under `Load Setpoints`, click `Browse...` and select the most recent file created in C:\tofwerk\tps

7. Go back to the QNX software and move the zaber to its fully open position (Typical value: 21000).

8. Verify that `InL_P` is around 35 ± 0.3 mbar. Adjust FT dilution flow as necessary to match this pressure.

9. Open TofDAQ and hit the green start button near the upper left hand corner to begin data acqusition. Then, on the Mass Spectrum window select `Log Scale` and check that reagent peak is present at *m/z* 85. If not, see Sect. C.10

After following the above procedure, the instrument should be taking a dry nitrogen background (dry zero). To begin sampling from the chamber or ambient air with the CIMS, turn on the cold cal 1 valve to stop overfilling the flow tube with nitrogen, as well as the cold cal 2 valve to begin pumping on the sample line.

To use the GC, several TMA scripts that have been developed (See Sect C.5.3). For manual GC operation (via command line) follow the procedure below:

1. Set GC flows. These flows are used to dilute the sample by 15x. You must calculate the flows needed for other GC dilutions assuming an intake flow of 1000 sccm and a bypass flow of ≈ 220 sccm.

   GC intake flow: 1225 sccm

   GC dilution flow: 1148 sccm

   GC column N2 flow: 5 sccm

   GC pickup flow: 20 sccm

   GC bypass flow: 500 sccm

2. Ensure that the flow readbacks match the above set points, with the exception of GC bypass which should read ≈ 25 sccm. After, check that the GC pickup valve is on and all other GC valves are off.

3. To cool the column, type `GCwatlow f4 set column temperature` and enter the trapping set point for this run. Then, turn on the two CO_2 valves and wait for the column temperature to match the set point.

4. To trap, turn off the CO_2 valve (leave the Spare A2_1 valve on) and set the GC intake flow to 1000 sccm. Then, turn the GC sample valve on, turning it off after the desired trapping time has elapsed (typically 5–10 minutes).

5. After trapping, wait 1 minute before sending the GC effluent into the mass spectrometer. If sending the effluent to the ion source, proceed with the following instructions:

   a) Turn off cold cal 1 and 2,

   b) Set GC pickup flow to 200 sccm,

   c) Set FT dilution flow to 1480 sccm,

   d) Set ion source dilution flow to 280 sccm,

   e) Turn off spare a2_1 valve,

   f) Turn on high sensitivity mode valve.

6. If sending to the flow tube:

   a) Turn off cold cal 1 and 2,

   b) set GC pickup flow to 100 sccm,

   c) set FT dilution flow to 1480 sccm,

   d) Turn off spare a2_1 valve,

   e) Turn on normal GC mode valve.

7. When you are ready to begin eluting, type `GCWatlow F4 profile start` and choose the appropriate file number (1 through 3) that has been pre-programmed into the Watlow. To change these Watlow profiles, refer to the Watlow F4 manual.

C.7.2 Instrument shutdown

Once an experiment is completed, the instrument should be switched to its idle state before extracting the data.

1. Press the stop icon on TofDAQ to halt data acquisition process. Then, close the program.

2. Using QNX software, close the zaber and stop any algorithms that are running (`SWStatus data loop stop`).

3. Put the instrument in its idle flow state by typing `SWStatus data loop standby` in the command line and verify that the flows are as follows and that all valves are off except for the GC pickup valve (in this flow configuration, `InL_P` should read around 4-5 mbar).

Fluorine: 0 sccm

IonSrc: 50 sccm

DilFT: 50 sccm

Column N2: 5 sccm

GC_Intake: 50 sccm

PickupFlow: 20 sccm

GC_Dilution: 100 sccm

GC_Bypass: 500 sccm (setpoint); ≈25 sccm (read back)

4. Set the octopole amp and bias to 0 V.
5. Go to TPS settings sand press `Zero All`. All voltage set points should turn blue.
6. Close the fluorine needle valve.

C.7.3 Data reduction

To extract the data and convert into a Matlab file format, perform the following steps:

1. On QNX, type `Quit`, then `Reduce` once the program has exited.
2. When prompted for `Run Type`, type `Data`.
3. When prompted for a description of this run, enter a single period (‘`.`’). Data reduction will then commence.
4. When reduce is finished, the window will display the following:

```
extract:  Extraction Complete
reduce:  No Analysis Defined
$ Memo Terminating
```

5. Restart instrument software by typing `./doit -sa`, and check that all flows and valves are still in their idle states.
6. On the Windows computer, go to D:\tof_data and create a new folder with the current date using the format YYYYMMDD.R, where R is the number of times the data has been processed. Move all Tofwerk files (H5 files) from D:\tof_data to this newly created folder.

7. Open Matlab and proceed with the following steps:

    a) Set Matlab directory to D:\tof_data.

    b) On the command window, type: `reproc_hrtof('d:\tof_data\YYYYMMDD.R', 'd:\tof_data', 'YYYYMMDD.R')`, where YYYYMMDD.R matches the folder name created earlier. Wait for the H5 files to finish processing.

8. In the meanwhile, open WinSCP program, connect to the GCwinVM IP address. Change the right screen to /home/GCToF/anal and the left screen to D:\tof_data. In /home/GCToF/anal, look for today's experiment folder whose name should follow the format YYMMDD.R. (Note: Folder may be named with tomorrow's date). Refresh if folder is not there. Then, transfer this folder to D:\tof_data.

9. Once H5 files have finished processing in Matlab, type the following in the command window:

    ```
    close all; clear all;
    cd ..
    load('YYYYMMDD.R_hrtofrpk_l.mat')
    ```

    `cd YYMMDD.R` (this is the name of the folder that was moved in the previous step).

    ```
    csv2mat
    GCToFeng_1 = load('GCToFeng_1.mat');
    GCToFeng_10 = load('GCToFeng_10.mat');
    ```

10. Save Matlab workspace as 'YYYYMMDD.R_hrtofrpk_l.mat' in the D:\tof_data folder. (Click OK to replace file.)

11. On the Matlab command window, type `ssh_ft` and follow prompts to automatically back up the QNX data files onto the server.

12. Go back to WinSCP and open a new connection to cimsdisk2.gps.caltech.edu

    a) On the right screen, find directory /home/cims-SSH/cims_data/GCToF/data/anal/lab/2018/windows/rpk_v0.3. This folder should contain a 1 Hz and 10 Hz folder.

b) Change the directory of the left screen to D:\tof_data. Move the '*_hrtofrpk_l.mat' file to the 1 Hz folder and the '*_hrtofrpk_h_all.mat' to the 10 Hz folder.

C.8 Field operation

This section includes procedures for field set-up, instrument disassembly, and instructions for regularly backing up the data files. Once instrument is set up, you can operate it using instructions covered in Sect. C.7.

C.8.1 Power up & network configuration

1. Connect all cables and plumbing.
2. Once all cables and plumbing are connected and double checked, turn on UPS by long-pressing the leftmost button. Verify voltage is input and output is about 120 V.
3. Turn on Windows computer and monitor. Verify computer has an internet connection.
4. On Windows computer, open the VM player software and log in. Right click to open terminal.
5. Verify all computers are under the same network domain by editing their respective net.cfg files.
    - Note: In the field, it is best to assign static IP addresses to each computer.
6. After editing the config files, restart all computers (`sudo ./shutdown_flight_gc.sh`).
7. Restart the VM (`Player` → `power` → `Restart Guest`).
8. Re-login to VM and verify that changes were kept by changing the directory to /net/ and long list the directory contents to see if all computers are under the same domain.
9. Lastly, change Windows computer IP address, if static IP is being assigned.
    a) Right click Ethernet connection. Open `Network and Sharing`,
    b) On left hand side, click `Change adapter settings`,
    c) Right click on correct Ethernet connection and open `Properties`,

d) In the boxes below `This connection uses the following items`, find `Internet Protocol Version 4 (TCP/IP)`, left click and select `Properties` button.

e) Make the appropriate changes.

C.8.2 Edit time server settings

1. Sync Herc to time server by typing the following commands

   `sudo slay ntpd` (say yes to prompts)

   `sudo ntpdate [server ip]`

   `sudo ntpd` (restarts syncing to server)

2. Sync VM to time server by doing the following:

   Change the directory to /etc/

   Type: `sudo vi ntp.conf`

   Edit location of time server and save changes.

   Restart ntpd as in the above step

3. Sync Windows Computer to time server

   - Find the following file: C:\ProgramFIles\NTP\etc\ntp.conf,
   - Edit as administrator and ensure IP address of Herc is listed,
   - Run 'ProgramFiles\Meinberg\NetworkTimeProtocol\QuickNTPStatus' to ensure update is occurring.

C.8.3 Evacuate CIMS vacuum chamber

Note: Before evacuating the CIMS vacuum chamber, perform a leak test on the instrument. Leak testing procedures can be found in Sect. C.9.

1. Start up the QNX software. Presently, the VM software has a bug, so use PuTTY and SSH into the IP address assigned to the GCwinVM.

2. Turn on the Edwards nXDS pumps backing the turbos and the flow tube.

3. Open manual valve between the turbo pump solenoid valve and turbo pump exhaust port.

4. Open the solenoid valve for the turbo pump and wait until `ToF_P` and `Hex_P` are stable. The pressure should get to as low as 0.2 mbar.

5. Turn on three turbo pumps in soft start mode. Start by powering on the one with the highest load.

6. Wait for pressures to reach the following:

   `Hex_P` should be on the order of 1×10^{-6} mbar

   `ToF_P` should be on the order of 1×10^{-7} mbar

7. Pump down the flow tube by opening the flow tube solenoid valve. The flow tube pressure (InP_L) should be about 1.8 mbar with manual flow tube PFA valve closed and no gas flow. InP_L should be about 3 mbar if manual PFA valve is open, but there is no additional gas flow.

8. Leak test the instrument using Dust Off compressed gas. Follow procedures listed in Sect. C.9.

C.8.4 Optimize zaber position

If zaber was removed during transport, a new zaber position will have to be determined.

1. Set the instrument in its idle flow state.

2. Gradually begin to move the zaber until pressure recorded in `ToF_P` noticeably increases. Note the position of the zaber.

3. Continue opening the zaber until `ToF_P` returns back to its initial pressure. Note the position of the zaber.

4. Repeat step 2 and 3 while moving the zaber in the opposite direction.

5. To obtain the zaber postition by averaging the four recorded zaber positions.

C.8.5 Field data reduction and backup

When in the field, data should be reduced once per day. It is recommended that data reduction occurs late at night when the concentrations of compounds of interest are at their lowest and should not be performed at the same time each day, as to prevent gaps in data collection.

1. Reduce QNX data using steps specified in Sect. C.7.3, steps 1-3.
2. Restart TofDAQ and TMA algorithm as soon as the reduction is finished as to minimize instrument downtime.
3. Transfer H5 files and QNX csv files to a separate computer (A spare Windows computer that has all the Matlab scripts pre-installed). Processing the data on the same computer simultaneously with data collection can cause TofDAQ to crash.
4. On the spare computer, process the H5 files as normal and combine with the QNX data as discussed in Sect. C.7.3. Upload files to cimsdisk.
5. Back up the QNX and H5 files to cimsdisk manually using PuTTY (Windows) or terminal (MacOS) using the following instructions:
    - SSH into GCwinVM and go to /home/GCToF/anal,
    - Tar the QNX folder (`tar -cvf YYMMDD.R.tar YYMMDD.R`), then gzip it (`gzip YYMMDD.R.tar`),
    - Secure copy it to the appropriate folder in cimsdisk,
    - Then, go to /home/GCToF/raw/data and tar and gzip the appropriate file, as above,
    - Secure copy it to the approriate folder in cimsdisk,
    - Back up H5 files by using WinSCP to transfer them to the appropriate directory on cimsdisk.

C.8.6 Disassembly

1. Stop data acquisition and place instrument in idle state as normal.
2. Turn off blower and vent up flow tube (See Sect. C.9).
3. Once vented, increase FT dilution flow to 1500 sccm.
4. Turn off the turbo pumps, and wait for them to wind down.
5. Turn off turbo solenoid valve. Then, close manual valve between turbo pump exhaust and turbo pump solenoid valve.
6. If packing up to return to lab, shut down nxDS pumps. If packing to go to the field, close knob on house vacuum connection and disconnect vacuum tubing.

7. Open zaber slowly until turbos are fully shut off (e.g. move to 5000 → 10000 → 150000 → 21000) and wait until ion gauges reach atmospheric pressure (may take a couple hours).

8. Once the CIMS vacuum chamber is at atmospheric pressure, close zaber and wait to see if ion gauge readings remain stable (no leak apparent).

9. Set all GC and gas box flows to zero and verify that all GC and gas box valves are in their off position.

10. Close the manual nitrogen valves on front panels of GC and gas boxes and ensure that the fluorine needle valve on the front of the gas box is fully closed.

11. Quit QNX and shut down computers using the terminal. Then, toggle the switches for the two GCAthenas on the GC and gas boxes.

12. Power off the GC and electronics boxes using the switches located in the front of each box.

13. Shut down GCwinWM (Top left menu → `power shutdown guest`) followed by the Windows PC.

14. Shut down UPS (long-press rightmost button on UPS).

15. Begin removing all tubing and cabling.

C.8.7 Returning to lab

Once the instrument is back in the lab, set up the instrument as soon as possible so that the CIMS vacuum chamber is under atmospheric pressure for the minimal amount of time.

1. Follow steps from the Sect. C.8.1 and initiate the doit script.

2. Pump down the mass spectrometer

    a) Connect the flow tube and turbo pumps to the house vacuum.

    b) Open manual valve between turbo pump solenoid valve and turbo pump exhaust port.

    c) Open knob on the turbo pump house vacuum connection.

- Note: DO NOT do this if other instruments are already connected to the house vacuum. Consult with others to isolate the other instruments before proceeding with the above step.

d) Open the turbo pump solenoid valve and wait until `ToF_P` and `Hex_P` are stable. Pressure should read as low as 0.2 mbar.

3. Proceed with steps 5 and 6 from Sect. C.8.3

4. Pump down the flow tube by opening the corresponding knob on the house vacuum connection

   - DO NOT do this if other instruments are already connected to the house vacuum. Consult with others to isolate the other instruments before proceeding with the above step.

5. Open the FT solenoid valve and check the flow tube pressure. `InP_L` should be about 1.8 mbar with FT manual valve closed and no gas flow and 3 mbar if manual flow tube valve is open, but there is no additional gas flow.

6. Open manual flow tube valve (blue PFA valve located at the end of the flow tube) and set default idle flows. `InP_L` should be about 4 - 5 mbar.

C.9 Instrument maintenance

This section includes procedures for basic instrument maintenance.

Leak testing

Leak testing should be performed regularly, especially after new plumbing connections have been made. There are two general ways to leak test depending on the status of the instrument.

When the mass spectrometer is off (as during initial set up in the field), leak test by using flows and changes in pressure as specified in the procedure below. An excel sheet to calculate size of leaks can be found on the Windows PC.

1. Close off the flow tube frit by turning off cold cal 1 and 2 and closing the manual flow tube valve (blue PFA valve located at the end of the flow tube).

2. Set FT dilution to 0 and FT ion source dilution to 10 sccm.

- Note: In cases of a leaky flow controller, it might be necessary to vent up the flow tube and cap off the leaky line first before proceeding. The FT Dilution MFC has a tendency to leak.

3. Close FT solenoid valve and record change in pressure every 10 seconds for half a minute. Reopen the FT solenoid valve.

4. Repeat step 3, this time setting both the dilution and ion source flow controllers to zero (ensuring no flow into the flow tube) and shutting off the manual nitrogen valve in the front of the gas box.

5. Use the provided excel sheets to calculate leak rate in sccm. If leak is larger than 0.5 sccm, tighten fittings and repeat procedure until leak is sufficiently small.

Note: The flow tube and ion source are likely culprits of large leaks at this stage. The flow tube may have to be re-seated in its compression fitting and the ion source may have to be unscrewed from the mass spectrometer and have its O-ring assessed for damage.

When mass spectrometer is up and running, leak tests can be performed using Dust Off compressed gas as the CIMS is sensitive to its main component, difluoroethane (*m/z* 151). To do this, set up the instrument flows and start up TofDAQ as specified in the Sect C.7. Then, spray Dustoff around fittings and watch for sudden increases in the *m/z* 151 signal. Tighten fittings, as necessary and repeat until no noticeable leaks are found.

Venting up the flow tube

Venting up the flow tube may be required when reconfiguring the instrument plumbing or performing tasks such as unclogging the flow tube frit.

1. Ensure zaber is closed.

2. Set FT Dilution to 150 sccm and ion source dilution to 150 sccm.

3. Turn cold cal 1 ON and cold cal 2 OFF.

4. Close manual flow tube valve (blue PFA valve positioned at the end of flow tube).

5. Close the FT solenoid valve. The `InH_P` read back should begin climbing.

6. Create a vent in either the dilution or ion source lines (such as unscrewing the tubing from ion source) when InH_P reaches about 900 mbar. If vent is not created, flow tube will over pressurize.

To pump down the flow tube, close the vent line and immediately open the FT solenoid valve. Leak test instrument and verify that pressure (InL_P) returns to 3 - 4 mbar.

Measuring the flow tube frit flow

Measuring the frit flow may be required diagnosing any clogs. As such, it should also be done regularly when in the field.

1. Turn cold cal 1 ON and cold cal 2 OFF.
2. Close manual flow tube valve (blue PFA valve positioned at the end of flow tube).
3. Adjust FT dilution so that InL_P is approximately 35 mbar
4. Open manual flow tube valve and lower dilution flow until InL_P returns to 35 mbar.
5. This change in the dilution flow equals the frit flow. (Typical value: 180 sccm)

Recoating the flow tube frit

All glass surfaces and critical orifices are coated with Fluoropel in order to prevent analyte interactions with these surfaces. These coatings will have to be reapplied on occasion. Recoating the frit is perhaps the most common maintenance task that is required following return from a field campaign. Recoating glass surfaces is not presently covered in this documentation.

1. Vent up flow tube and remove frit.
2. Scrub off old coating off the frit with alkanox and brush.
3. Rinse very well with DI water and leave to dry.
4. Transfer Fluoropel into a squirt bottle.
5. Use squirt bottle to coat the inside and outside of the frit a few times, letting it air dry in between layers.

6. Dry in the oven using the following procedure:

    a) Place in oven when oven is cool and begin heating to 120^{o}C.

    b) Leave for 15 minutes at 120^{o}C.

    c) Allow oven to cool to at least 50^{o}C by leaving the oven door cracked.

7. Clear any blockages to frit hole by poking with a wire or needle.

8. Place back in instrument and pump down the flow tube.

9. Leak test the instrument.

File system management

Files on the Herc must be regularly tarred and deleted in order to allow for space for new reductions of the QNX data as QNX will stop recording the telemetry data once space fills up for no nodes are available. It is especially important to do this before and after a field campaign. You can check both the file system space and nodes available using `df -h` and `df -g`, respectively, which will output information as seen in the figures below.

If space is approaching 100% or 0 nodes are available, tar and/or remove data files from the file system. You can begin with raw data files located in /net/GCHerc/home/GCToF/raw/data after verifying that they have been backed up on cimsdisk and the file sizes are consistent. Once this data is cleared, you can do the same with /net/GCHerc/home/GCToF/anal.

```
$ df -h
/dev/hd0t179                30G       19G       11G      63%  /
/dev/cd0                     0         0         0     100%  (/fs/cd0/)
/dev/hd0                    40G       40G         0     100%
$ df -g
/dev/hd0t179   /
    Blocks: 31455220 total  11702083 avail   [1024-byte blocks]
    Files :  3931904 total   3714349 avail
    Type  : qnx6
    Flags : 00000000 []
    Option: sync=optional
```

Figure C.17: QNX outputs of `df -h` and `df -g`.

GC column replacement

Unless it has been damaged, a typical GC column should last for approximately a year with heavy use. If column does need to be replaced, use the following procedure.

Remove GC column box from the instrument rack:

1. Vent up the flow tube and set all GC flows to zero.
2. Shut off the GC nitrogen supply by turning the ball valve located on the front of the GC control box.
3. Gently shut down GCAthena2 using the terminal, then toggle the Athena power switch on the back of the GC control box.
4. Power off the GC control box using the switch on the front of the box.
5. Disconnect GC exhaust lines.
    a) Working quickly, close manual green valve for main exhaust located near the flow tube solenoid valve.
    b) Disconnect GC exhaust lines and cap off those fittings.
    c) Reopen green valve.
6. Disconnect tubing and cables that connect the GC column box to the GC control box, then remove the box from the rack.

Remove the GC from the column box and disassemble the GC plates:

1. Remove front panel of GC column box for easy access to the various electrical connections.
2. Disconnect tubing connected to the valves, breaking as few connections as possible, and disconnect the power cables for valves, heaters and RTDs.
3. Unscrew stand offs holding GC and valve plate to the box.
4. Carefully separate valve plate from GC and neatly remove tape and insulation wrapped around the GC plates.
5. Remove the screws holding the two plates together and separate the plates carefully using a flathead screwdriver. (Be careful of the RTDs, as they are quite fragile.)
6. Remove old column and O-ring.
7. Use the old column to cut the new column to approximately the same size.

Replace the column and reassemble GC:

1. Attach fittings to column and place back in the groove on the plate.
2. Place the O-ring, pickup tubing and RTDs in their appropriate places on the plate and screw the two plates back together.
3. Perform a quick leak test by capping one end of the column and attach another to a small flow controller (< 20 sccm) that is connected to a nitrogen supply. Set MFC at max flow and wait for its read back to read zero (This should take a few minutes). If read back does not return to baseline, open GC plates and assess the condition of the column and fittings.
4. If the GC is leak free, wrap the GC plates with the insulation and Kapton tape, being careful of the RTD and heater wires.
5. Reattach GC and valve plate to the column box and reconnect all plumbing and wires.
6. Before placing column box back in instrument rack, double check that the plates can hold the CO_2 pressure, the GC temperature gradient is minimal (less than 3^oC) at trapping temperatures, and that the heaters and RTD still work properly.
7. Reattach GC column box back to rack and reconnect all GC tubing and cables.
8. Power on GC control box (front panel switch) and toggle Athena 2 switch (on back panel).
9. Restart doit script and verify that GCAthena2 is connected.

C.10 Troubleshooting

Power outage

If there is a power outage, the UPS is available to provide instrument power for about 8 - 10 minutes to prevent damage to the instrument components and allow for a safe shutdown.

Diagnosis: On the UPS table in QNX, 'mode' is B, 'V_in' is 0, and values listed under 'Cap' (Capacity) and 'Rem' (Time Remaining) are decreasing. UPS will begin beeping.

Solution: Begin executing shutdown procedures until power issue is resolved. The shutdown procedures are as follows:

1. Stop data acquisition and close TofDAQ.
2. On QNX, close zaber, stop all data algorithms currently running and set all flows to zero before closing all solenoid valves.
    - If you can easily access instrument, be sure to also close the manual nitrogen valves on the GC and gas boxes, as well as the fluorine valve BEFORE setting the instrument flows to zero.
3. Set octopole amp and bias voltages to zero.
4. Zero all TPS voltages.
5. Turn off blower.
6. Turn off TPS and ADQ using the command `UPS socket 1 off`.
    - Note: Stop here if only a lowered power state is required due to situations such as instrument overheating.
7. Turn off turbo pumps. When turbos are wound down, close turbo solenoid valve.
8. Close FT solenoid valve. **Watch to ensure pressure is not increasing faster than known leak rate.**
9. Turn off nXDS pumps.
10. Turn off Herc and Athena computers (`sudo ./shutdown_flight.sh`).
    - If you can easily access instrument, you start powering off the boxes once the computers have shut down, beginning with the GC Control Box, then the GB Athena, then the Electronics Box.
11. Exit VM and shut down windows computer.

TPS interlock triggered

The TPS will automatically trigger the interlock to shuts down all power supplies if pressure of the CIMS vacuum chamber begins to climb.

Diagnosis: No ions on TofDAQ, TPS voltages zero, and `Interlock` (on TPS browser tab) is ON. Lights on the front of the TPS have turned red.

Solution:

1. Stop data acquisition, close the zaber, set octopole amp/bias to 0 V and set flows to idle.
2. Check to see if turbos are drawing current. If not, they may have thermally shut off. Check instrument to see if turbo fan is still on (Turbo B, in particular, can easily overheat).
3. If in the field, check to see if the nXDS pump that is backing the turbo is operational (these may shut off if they overheat).
4. Turn of TPS and ADQ (`UPS socket 1 off`).
5. If ToF pressure reads below 0.1 mbar, attempt to restart turbos.

No ions seen on TofDAQ

Diagnosis: On TofDAQ, ions/ext. read 18 or less. Reagent ion signal is not seen in Mass Spectrum window.

Solution:

1. The TPS interlock triggered. See above for troubleshooting procedure.
2. The fluorine valve is closed or the reagent gas has run out. Verify that fluorine valve is open and use `RegH_P` read back to check reagent bottle pressure.
3. The zaber is closed. Check current zaber position on QNX. If its position reads what it should be, verify that the zaber moves when QNX commands are typed. If it does not, check cable connections.
4. The octopole voltage is zero. Verify that the read back matches the set point on QNX. If it does not, it is likely its fuse has blown. Turn off octopole (via toggle switch) and unplug its power and data cables. Open octopole box and replace fuse.

Clogged flow tube frit

Diagnosis: When instrument is set up with typical sampling flows (e.g. FT dilution ≈ 1580 sccm; FT ion source = 380 sccm; manual FT valve is open), `InL_P` reads around 35 mbar. If pressure is lower than expected, verify diagnosis by measuring frit flow (See: Sect. C.9) and proceed with the steps below. If pressure is higher than expected, initiate leak checking procedures.

Solution:

1. Vent up the flow tube (See Sect. C.9) and remove the frit. Clean the frit by sticking a thin wire or needle through the hole at the end. When wire/needle easily moves through the hole, the clog is cleared.
2. Replace frit and pump down the flow tube.
3. Leak check instrument (See 'Leak Testing' in Sect. C.9)

Unresponsive GC/GB Athena computers

Diagnosis: On QNX, under the MFC readouts for either the GC or gas box, 'stale' reads greater than 0. In addition, under 'DSdaq', Athena1, and/or Athena2 read 'disconnected' or 'init.' This can be further verified by opening a new VM terminal. Go to the /net/ directory and list the directory contents. The computers that are not connected to the network will not be listed.

Solution:

1. Stop data acquisition.
2. Close zaber, turn off octopole amp and bias and zero all TPS voltages.
3. Quit QNX.
4. Toggle Athena switches (on back of respective boxes). Reboot may take a few minutes.
5. On the terminal, change directory to /net/ and list the directory contents. If the disconnected computer reappears on the list, restart the doit script and verify that computer reads connected under the `DSdaq` table. QNX may have to be restarted several times before Athena reconnects.

6. If the computer does not reconnect, plug in a monitor via the VGA ports located on either the GC or gas box and observe whether the software starts up. If it starts back normally, see previous step.

7. If the computer still does not start up properly, it may be a result of an unstable 5 V line. It may be best to power the disconnected Athena computer with an external power supply using the following procedure:

    a) Turn off Athena power via toggling switch. If Athena 1 is the issue, note that the gas box is powered entirely by the Electronics box. If power needs to be cut for safe handling, carefully remove the power cable that is located on the back of the box. If Athena 2 is the issue, power off entire GC control box by using the switch on the front panel of the box.

    b) Remove green connector from the Athena board and unscrew the two wires from the connector. Keep track of which terminal holds the +5 V line and which is the GND.

    c) Strip the cables from the external power source and use a voltmeter to verify which is positive and which is ground.

    d) Screw the two new wires from the external power source (**Be sure the external power source is unplugged**) into the green connector and plug it back into the Athena board.

    e) Secure old 5 V wires so that they cannot touch each other, any other connections in the box, or the box itself.

    f) Turn on the power to the box and plug in the external power supply.

    g) Repeat above steps to see if the computer is back on the network.

8. If the Athena computer is still unresponsive, replace with spare computer.

GC not cooling

Diagnosis: GC not reaching -20^{o}C in specified cooling time and/or temperature is increasing during trapping period.

Solution:

1. Determine whether the CO_2 cylinder is empty. Replace cylinder and see if problem is resolved.

2. If problem persists, it is possible that one of the CO_2 restrictors is clogged.

a) If in the field, switch instrument to a CIMS only data loop.

b) Identify which restrictor is causing the issue. In general, if the GC is having trouble reaching -20^{o}C, it is likely the restrictor attached to the CO_2 valve. If the GC is having trouble maintaining the temperature during trapping, it is likely the restrictor attached to the Spare A2_1 valve.

c) If clog is visible at either end of the restrictor, cut off a small portion of the affected piece of tubing. If clog is not visible or restrictor is kinked, replace the entire restrictor.

3. If GC is still not cooling after restrictors have been replaced, it is possible that one of the O-ring inside the CO_2 valves have failed. This will be obvious as CO_2 will be leaking from the valve when its switched on. Isolate which valve is causing the problem and either replace the O-ring or the entire valve.

Large GC temperature gradient

Diagnosis: GC temperature sensors are reading a temperature different greater than 3^{o}C when cooling and trapping.

Solution: Make sure the GC has been properly wrapped with the insulation and that non of the RTDs have slid out from in between the GC plates.

Shifting retention times of GC peaks

Diagnosis: GC peaks for specific compounds are not eluting at approximately the the same temperature each time (assuming same temperature profile was used).

Solution: It is possible that column media has degraded or was damaged by another compound and column must be replaced. See Sect. C.9 for instructions.

CO_2 cylinder empties too quickly

Diagnosis: A normal CO_2 cylinder should last for approximately 15-20 GCs depending on the length and inner diameters of the restrictors.

Solution: Lengthen either restrictor or replace with one that has a smaller inner diameter such that the GC cools quickly and maintains temperature, but uses the minimal amount of CO_2 possible.

***doit* script not starting**

Solution: It is likely that the Herc computer has run out of space. See Sect. C.9 on how to clear space. Once space is cleared, restart doit script.

Failed QNX reduction

Diagnosis: If failure occurs doing transfer between Herc and VM, the folder with current reduction date is not present in /home/GCToF/raw/data. If failure occurs during transfer extraction (conversion between binary files and csv format), then folder with current reduction date is not present in /home/GCToF/anal.

Solution: Most likely GCwinVM has run out of space or nodes. See Sect. C.9 on how to fix this problem. Then:

1. If failure occurs doing transfer between Herc and VM, transfer binary data from Herc computer (/net/GCHerc/home/GCToF/raw/data/YYMMDD.R) to GCwinVM (/home/GCToF/raw/data).

2. If failure occurs during transfer extraction, rerun extraction code in the /home/GCToF/ directory (`extract raw/data/YYMMDD.R GCToFengext`).

ssh_ft script failed

Diagnosis: Matlab error message appears that reads "It seems like this data has already been archived. I stop."

Solution:

1. Go to root → tmp. Look for file named 'tfp.txt'. If exists, delete it.

2. Using WinSCP, log into cimsdisk and change directory to /home/cims-SSH/cims_data/GCToF/data/notes1. If file exists with current date, delete it and rerun SSH_ft script.

3. If instrument is in the field, back up files manually (See Sect. C.8).

Tofwerks DAQ crashed or frozen

Solution:

1. Close TofDAQ.

2. Open Task Manager. Find Tofwerks in the list and end task.

3. Go to directory D:\tof_data and delete the corrupted file

4. Open TofDAQ again.

5. If still not working or if mass cal has shifted significantly (e.g. *m/z* 85 is instead near *m/z* 100),

    a) Go to C:\tof_werk\TofDAQ,

    b) Find TofDAQRec.ini file and rename to TofDAQRec_crash_[date].ini,

    c) Find TofDAQRec_jdc4.ini to TofDAQRec.ini.

6. If TofDAQ is *still* not working, disconnect and reconnect ADQ power, then try restarting the program again.

7. Note: Sometimes when ToFDAQ crashes, it changes the run time to only about 3 h (that is, ToFDAQ will automatically stop data acquisition after this time has elapsed). If this is the case, proceed with the following:

    a) Open ToFDAQ.

    b) Go to `Acquisition`, then click `Open DAQ Configuration`.

    c) Go to the tab named `Basic ToF Timing`.

    d) Under the `Run` field, enter a number that makes the run time (listed next to the field) change to something over 24 hours.

    e) Close the window and start data acquisition to verify changes.